UNIVERSIDADE DE LISBOA
FACULDADE DE CIÊNCIAS
DEPARTAMENTO DE FÍSICA

Investigation of Dynamic Functional Connectivity in Cerebral Small Vessel disease

Maria João Silva Lopes Palma

Mestrado Integrado em Engenharia Biomédica e Biofísica
Perfil em Biofísica Médica e Fisiologia de Sistemas

Dissertação orientada por:
Prof. Dr. Patrícia Figueiredo, Biomedical Engineering Lab (LaSEEB), Institute for Systems and Robotics | IST
Prof. Dr. Nuno Matela , Faculdade de Ciências da Universidade de Lisboa

2020

Preface

The work presented in this thesis was performed at the Laboratory of Evolutionary Systems and Biomedical Engineering (LaSEEB), a research lab of ISR-Lisboa at Instituto Superior Técnico, between September of 2019 and September of 2020, under the supervision of Prof. Patrícia Figueiredo and Prof. Nuno Matela.

Acknowledgments

Firstly, I would like to express all my gratitude to Prof. Patrícia Figueiredo, for providing me the opportunity to be a part of such an interesting project and welcoming into her research group LaSEEB, for the crucial and constant support through this year and at last for always being available to guide me during the entire process.

Also, I would like to thank Dr. Joana Cabral for providing me the key tips and expertise to complete this work.

I want to thank Joana Pinto, for the sympathy, and guidance throughout the ups and downs of this journey. It was very important to have the support of someone that have been through this before and know exactly how I am feeling.

To Prof. Nuno Matela thank you for advising me on my thesis project and for being one of the best teachers I ever had during these 5 years.

To my Parents, I would be forever thankful for being given the opportunity to complete my studies, for the unconditional support and for always believing in me.

Finally, to my sister and friends Raquel, Inês and Isabel thank you for encouraging me when I thought I was not capable and for giving me the confidence to overcome the obstacles that I found along the way. I could not forget Helena and Carla, the friends I made at FCUL, who made this journey a lot easier, I will take you for life.

This work was supported by Fundação para a Ciência e Tecnologia (FCT) through Grants PTDC/BBB-IMG/2137/2012 and UIDB/50009/2020.

Resumo

A doença dos pequenos vasos cerebrais ou *Small Vessel Disease* (SVD) é a principal causa de disfunção cognitiva em idosos e refere-se a um conjunto de processos patológicos e neurológicos que afetam os pequenos vasos do cérebro. As suas manifestações clínicas variam desde deficiências cognitivas, que podem levar a uma deterioração cognitiva progressiva e até demência, e incapacidades físicas, incluindo perda funcional em fases mais avançadas da doença. A neuroimagiologia é uma ferramenta essencial no diagnóstico e caracterização da SVD, em particular, a ressonância magnética funcional em repouso (rs-fMRI) já demonstrou potencial para fornecer biomarcadores da SVD, revelando interrupções da conectividade funcional (CF) em redes neuronais. No entanto, até o momento, apenas um estudo explorou as flutuações temporais da CF comumente observadas – a chamada conectividade funcional dinâmica (dFC). Em contraste com a CF, a dFC tem em consideração a natureza dinâmica da atividade cerebral, analisando-a em escalas de tempo mais rápidas de segundos a minutos. De facto, diversos estudos de dFC reportaram que esta abordagem pode fornecer uma maior compreensão das propriedades fundamentais das redes cerebrais e servir como um biomarcador de diversas doenças, uma vez que as alterações relacionadas com as mesmas nas propriedades dinâmicas da CF parecem ter origem neuronal.

Deste modo, neste trabalho, o objetivo foi investigar a dFC medida por rs-fMRI em dois grupos de pacientes com SVD – do tipo esporádico (sSVD) e arteriopatia cerebral autossómica dominante com enfartes subcorticais e leucoencefalopatia (CADASIL) - em comparação com um grupo saudável. Para tal, a dFC foi estimada entre pares de regiões do cérebro em cada tempo de repetição, TR, com o método de *Phase Coherence*. Neste método, os padrões de dFC para todos os pontos de tempo foram obtidos calculando o alinhamento de fase entre cada par de regiões do cérebro, estimando a fase do sinal de cada ponto de tempo, em cada uma das 90 regiões do cérebro, com a transformada de Hilbert. De seguida, os padrões de dFC ao longo do tempo e de todos os sujeitos foram analisados utilizando o método *Leading Eigenvector Dynamics Analysis* (LEiDA), que considera apenas o autovetor principal de cada padrão de dFC obtido, reduzindo deste modo a dimensionalidade dos dados. Este vetor captura a orientação principal das fases do sinal sobre todas as áreas, onde cada elemento do mesmo representa a projeção da fase do sinal em cada área do cérebro no autovetor principal.

Em seguida, o algoritmo k-médias foi aplicado a todos os autovetores principais de dFC para obter um número finito de estados de dFC, cada um representando um padrão dFC recorrente, para um k (número de estados) variável. Como este trabalho teve como objetivo explorar se existem estados de dFC que diferenciam pacientes SVD do grupo saudável, e não determinar o número ideal de estados de dFC, o número de estados foi variado de 2 a 20. Para cada k, examinámos as diferenças em termos de probabilidade de ocorrência, duração e perfis de transição dos estados de dFC entre o grupo de doentes e o grupo de controlos saudáveis. Adicionalmente, os estados de dFC foram correlacionados com sete redes neuronais de repouso comuns, nomeadamente a rede somatomotora, a rede de atenção ventral e dorsal, a rede visual, a rede frontoparietal, a rede límbica e a rede de modo padrão.

Posteriormente, a fim de determinar se as alterações nas propriedades de dFC, encontradas neste trabalho, poderiam ser potenciais biomarcadores de declínio cognitivo causadas pela SVD, foi realizado uma análise de correlação entre as pontuações dos testes neuropsicológicos em quatro domínios relevantes (função executiva, velocidade de processamento, memória de trabalho e memória de longo prazo) e as propriedades de dFC dos pacientes. Do mesmo modo, uma análise de correlação entre os mapas probabilísticos dos tratos de substância branca mais frequentemente lesionados destes pacientes e as propriedades de dFC foi, também, realizada com o objetivo de determinar se as alterações nas

propriedades de dFC, encontradas nos pacientes quando comparadas com o grupo saudável, poderiam estar correlacionadas com lesões estruturais dos mesmos.

Quando comparado com o grupo de controlos saudáveis, o grupo de doentes apresentou uma probabilidade de ocorrência significativamente maior num estado de dFC fracamente conectado, composto por áreas clinicamente relevantes. Este estado compreende áreas dos lobos frontais e parietais e está significativamente associado a redes neuronais envolvidas na integração de informações sensoriais e processos específicos para o controlo da atenção, nomeadamente a rede somatomotora, a rede de atenção ventral e dorsal. Estas mesmas redes foram anteriormente identificadas, em estudos de CF, como afetadas em pacientes com SVD, mas também em indivíduos com deficiências cognitivas e com doença de Alzheimer. Além disso, estudos de dFC em doenças relacionadas com a SVD, como a demência e a doença de Alzheimer, relataram que os pacientes também apresentaram maiores probabilidades de ocorrência em estados fracamente e esparsamente conectados, com ausência de fortes conexões positivas e negativas. Em particular, o único estudo de dFC em SVD também descobriu que os pacientes com SVD tiveram mais ocorrências num estado fracamente conectado nas regiões do domínio sensório-motor, quando comparado ao grupo saudável. Deste modo, podendo indicar que mudanças dinâmicas na CF nestas áreas podem ser particularmente importantes para esta doença.

É também importante ressaltar que as probabilidades de transição entre este estado fronto-parietal fracamente conectado para o estado de coerência global, fortemente conectado, foram significativamente correlacionadas com melhor desempenho no domínio cognitivo da velocidade de processamento. Estas descobertas estão de acordo com resultados anteriores de estudos de dFC em indivíduos com melhores e piores desempenhos cognitivos, onde indivíduos com melhores desempenhos cognitivos tiveram maior número de transições para este estado de coerência global. Da mesma forma, as probabilidades de transição do estado fortemente conectado para o estado fronto-parietal fracamente conectado, foram significativamente correlacionadas com um pior desempenho neste mesmo domínio cognitivo. De facto, défices na velocidade de processamento estão entre as primeiras e mais proeminentes manifestações cognitivas da SVD, com diversos estudos demonstrando associações entre o declínio na velocidade de processamento e medidas quantitativas de ressonância magnética. Assim, estudos futuros devem investigar com maior detalhe transições entre estes estados, de modo a determinar se alterações nesta propriedade de dFC podem ser biomarcadores do declínio cognitivo na SVD.

Em relação à análise dos mapas probabilísticos dos tratos de substância branca mais frequentemente lesionados nestes pacientes, embora nenhuma correlação significativa tenha sido encontrada com as alterações nas propriedades da dFC encontradas neste trabalho, é interessante notar que vários estudos têm relatado associações entre estas lesões e o declínio cognitivo. O facto de a substância branca ser organizada no cérebro por tratos, conectando regiões cerebrais funcionais entre si, espera-se que danos a esses tratos levem a défices funcionais. Efetivamente, dois dos tratos frequentemente lesionados nestes pacientes, conectando regiões frontais, foram anteriormente relacionados com um pior desempenho cognitivo na velocidade de processamento em pacientes com SVD e demência. É, portanto, tentador sugerir que estes mesmo tratos frequentemente lesionados nos pacientes com SVD aqui estudados, poderiam ter alguma influência no pior desempenho no teste da velocidade de processamento encontrado neste estudo, que foi correlacionado com uma maior probabilidade de transição para o estado fracamente conectado, composto por regiões do lobo frontal e parietal. A compreensão dessa relação poderia ajudar a prever em quais das regiões do cérebro a patologia da substância branca causaria maiores défices funcionais, permitindo uma prevenção e terapia precoce.

No geral, os nossos resultados fornecem um novo suporte de que a conectividade funcional dinâmica pode fornecer biomarcadores mais sensíveis da SVD e deste modo, futuras investigações deverão explorar o seu potencial para prever o declínio cognitivo relacionado com a mesma.

Palavras-chave: doença dos pequenos vasos, ressonância magnética funcional em repouso, conectividade funcional, *phase coherence*, *Leading Eigenvector Dynamics Analysis*, algoritmo k-médias, estados de dFC, redes neuronais de repouso, testes neuropsicológicos.

Abstract

Cerebral small vessel disease (SVD) is the leading contributor to cognitive dysfunction in the elderly and it refers to a set of pathological and neurological processes that affect the smallest vessels of the brain. Its clinical manifestations vary from cognitive impairments, which can lead to progressive cognitive deterioration and even dementia, and physical disabilities, including functional loss in more advanced stages. Neuroimaging is a crucial tool in the diagnosis and characterization of SVD; in particular, resting-state functional magnetic resonance imaging (rs-fMRI) has demonstrated potential to deliver sensitive biomarkers of SVD, by revealing disruptions in functional connectivity (FC) across brain networks. However, so far only one study has explored the commonly observed FC temporal fluctuations – so-called dynamic FC (dFC). Here we aim to further investigate dFC measured by rs-fMRI in two groups of patients with SVD – sporadic SVD (sSVD) and cerebral autosomal dominant arteriopathy with subcortical infarcts and leukoencephalopathy (CADASIL) – compared with a healthy control group.

For this purpose, dFC was estimated at each repetition time point, TR, using Phase Coherence between the BOLD signals in pairs of brain regions, and dFC patterns were then analysed over time and subjects using the Leading Eigenvector Dynamics Analysis (LEiDA) approach. Then, a finite number of dFC states, each representing a recurrent dFC pattern, was obtained by k-means clustering with varying k (number of clusters). For each k, we examined differences between SVD and healthy control groups in terms of the occurrence, duration and switching profiles of dFC states. Additionally, the correlations between each dFC state and seven common resting-state networks (RSNs) were computed.

SVD patients showed a significant higher probability of a weakly connected dFC state, consisting of clinically relevant areas, when compared with healthy controls. This state comprises frontal and parietal areas and is significantly associated with the somatomotor, dorsal attention and ventral attention RSNs, which are involved in the integration of sensory information and specific processes for attention control. Further, the fact that the state is weakly connected agrees with the only previous study on dFC in SVD. Overall, our findings contribute with novel support that dFC may provide sensitive biomarkers of SVD and should be further explored in terms of its potential to predictive cognitive decline.

Keywords: small vessel disease, resting-state functional magnetic resonance imaging, functional connectivity, phase coherence, dFC states, resting-state networks.

Contents

List of Tables

List of Figures

List of Abbreviations

AAL Automated Anatomical Labelling

AD Alzheimer's disease

ANTs Advanced Normalization Tools

ASD Autism Spectrum Disorder

BET Brain Extraction Tool

BOLD Blood Oxygenation Level Dependent

CAA Cerebral Amyloid Angiopathy

CADASIL Cerebral Autosomal Dominant Arteriopathy With Subcortical Infarcts and Leukoencephalopathy

CBF Cerebral Blood Flow

CBV Cerebral Blood Volume

CEN Central-Executive Network

CI Cognitive Impairment

CSF Cerebrospinal Fluid

CT Computed Tomography

DAN Dorsal Attention Network

DLB Dementia with Lewy bodies

DMN Default Mode Network

EEG Electroencephalography

FC Functional Connectivity

FIX FMRIB's ICA-based Xoiseifier FLAME

FLAIR Fluid-Attenuated Inversion Recovery

fMRI Functional Magnetic Resonance Imaging

FWHM Full Width Half Maximum

GCP Good Cognitive Performance

GLM General Linear Model

HC Healthy Control

HRF Hemodynamic Response Function

IC Independent Component

ICA Independent Component Analysis

JHU-ICBM Johns Hopkins University International Consortium for Brain Mapping

LPM Lesion Probability Map

MCFLIRT Motion Correction FMRIB's Linear Registration Tool

MCI Mild Cognitive Impairment

MEG Magnetoencephalography

MELODIC Multivariate Exploratory Linear Optimized Decomposition into Independent Components

MNI Montreal Neurological Institute

MPRAGE Magnetization-Prepared Rapid Gradient Echo

MRI Magnetic Resonance Imaging

PCA Principal Component Analysis

PCP Poor Cognitive Performance

PD Parkinson's Disease

PET Positron Emission Tomography

PS Phase Synchronization

ROI Region of Interest

ROIs Regions of Interests

rs-fMRI Resting-state fMRI

RSN Resting-State Network

SIVD Subcortical Ischemic Vascular Disease

SMN Sensorimotor Network

SNR Signal-to-Noise Ratio

SVD Small Vessel Disease

SZ Schizophrenia

TE Echo Time

TI Inversion Time

TR Repetition Time

VAN Ventral Attention Network

WAIS-III Wechsler Adult Intelligence Scale

WM White Matter

WMHs White Matter Hyperintensities

WML White Matter Lesion

WMLL White Matter Lesion Load

WTC Wavelet Transform Coherence

Chapter 1
Introduction

This Master's Thesis proposes to investigate changes in dynamic functional connectivity (dFC) using measures of resting-state functional magnetic resonance imaging (rs-fMRI) in two groups of patients with cerebral small vessel disease (SVD) – sporadic SVD and cerebral autosomal dominant arteriopathy with subcortical infarcts and leukoencephalopathy (CADASIL) – compared with a healthy control group. Furthermore, we aim to determine whether these alterations could be associated with the disease and its cognitive deterioration. Hence whether they could provide a valuable clinical biomarker to predict disease progression.

This chapter starts by describing the motivation behind this study, followed by a brief overview of functional magnetic resonance imaging (fMRI), section 1.2. In section 1.3, a state of the art review of studies regarding dFC in SVD and related diseases. The last two sections, 1.4 and 1.5, present the main objectives of this work and an outline of the following chapters.

1.1 Motivation

1.1.1 Small Vessel Disease (SVD)

Cerebral small vessel disease (SVD) refers to a set of pathological and neurological processes that affect the smallest vessels of the brain, including small arteries, arterioles, venules, and capillaries, which are essential to maintain cerebral blood flow. It is also associated to different clinical manifestations and neuroimaging features caused by structural changes of vascular and brain parenchyma, including neuronal apoptosis, diffuse axonal injury, demyelination, and loss of oligodendrocytes. [1,2]

As a result, SVD is recognized to be the most important vascular contributor to dementia and has a crucial role in stroke and ageing. [3,4] Its clinical manifestations vary from cognitive impairments, which can lead to progressive cognitive deterioration and even dementia, and physical disabilities, including functional loss in more advanced stages. [1,5] However, these clinical symptoms have been reported to be significantly heterogeneous among patients with a similar radiological degree of SVD-associated features on brain imaging. [3]

Despite the advances in structural and functional neuroimaging, which are essential to the understanding of this disease and thus to a possibility of prevention and treatment, its pathophysiologic mechanisms are not yet clear as in vivo assessment of the smallest blood vessels is not yet possible in humans with conventional imaging techniques. Yet, many radiological biomarkers of SVD can be detected, including white matter hyperintensities (WMHs), lacunes, enlarged perivascular spaces, microbleeds, recent small subcortical infarcts and brain atrophy. [1,3]

As there are different types of SVD there are many proposed classifications, one can be based on cerebrovascular pathologic changes, which classifies SVD in six subtypes [4]:

- Type 1: Arteriolosclerosis (or age-related and vascular risk-factor-related small vessel diseases);
- Type 2: Sporadic and Hereditary cerebral amyloid angiopathy;

- Type 3: Inherited or genetic small vessel diseases;
- Type 4: Inflammatory and immunologically mediated small vessel diseases;
- Type 5: Venous collagenosis;
- Type 6: Other small vessel diseases.

Whereby the most frequent forms of SVD are type 1 and type 2. The first type, Arteriolosclerosis, it is also referred to as cerebral small vascular atherosclerosis, hypertensive SVD, age-related or vascular risk factor related SVD and relates to common vascular risk factors, such as elderly, hypertension, Diabetes mellitus and others. [1,2] This type of SVD is described by arteriolar wall thickening, mainly as a result of collagen, plasma proteins and inflammatory cells deposits in the vessel wall, loss of smooth muscle cells involved in the regulation of arterial pressure and blood flow, and leakage of plasma proteins into the perivascular tissue. As a result, the small vessels become elongated and inflexible and therefore unable to perform autoregulation, causing a reduced cerebral blood flow (CBF) and chronic cerebral hypoperfusion. [3]

As for the second type, Cerebral Amyloid Angiopathy (CAA), it is caused by progressive deposits of amyloid protein in the walls of small-to-medium-sized arteries and arterioles, mainly on the region of the hippocampus and cortex, leading to vessel dysfunction and brain parenchymal injury. [2] It is also observed vessel wall thickening, loss of smooth muscle cells, fibroid necrosis and exudation of blood breakdown products into perivascular tissue. [3] Besides, CAA is also the main cause of lobar intracerebral haemorrhage, which leads to stroke and relates to cognitive impairment. In addition, it also occurs in rare genetically transmitted diseases, such as Down's syndrome. [1,4]

Regarding the genetic form of SVD it refers to the pathophysiology of hereditary forms of SVD. Hereditary SVD is caused by mutations in different genes involving structural or signalling components of vascular cells, some of these include CADASIL (cerebral autosomal dominant arteriopathy with subcortical ischaemic strokes and leukoencephalopathy) and Fabry's disease, which are among the most prominent. [4,6] However there is still controversy on the brain mechanisms, as some believe that the deposition of globotriaosylceramide (Gb3) leads to altered vascular reactivity, resulting in increased blood flow and metabolic vulnerability in the deep white matter. [1] CADASIL is the most common monogenic condition resulting in SVD, it is due to mutations of the NOTCH3 gene on chromosome 19, which codes for a cell signalling receptor in the vascular smooth muscle cells. This results in irregular production of cysteine residues in the signalling protein, leading to abnormal signal transduction and impaired smooth muscle maturation and differentiation. [1] Fabry's disease is a hereditary disease, in a X-linked manner, and it is caused by a mutation in lysosomal GLA (galactosidase alpha) gene resulting in the absence or deficiency in lysosomal GLA activity. There is an accumulation of glycolipids in the lysosomes, a membrane-bound cell organelle that contains digestive enzymes, leading to lysosomal and cell dysfunction. Consequently, it is observed tissue ischemia and fibrosis. [6]

As for inflammatory and immunologically mediated small vessel diseases, there are a different set of rare diseases described by the presence of inflammatory cells in the vessel walls. Venous collagenosis is characterized by increased thickness of the veins and venules by collagen deposits, which can result in narrowed lumen and occlusion. Other types of SVD include post-radiation angiopathy which is a side effect of cerebral irradiation therapy, after months or years, and affects the small vessels of the white matter, resulting in fibrinoid necrosis, thickening of the wall by deposits of hyaline material, narrowed lumen and thrombotic occlusion. Also included in this group are the non-amyloid changes observed in the capillaries and basal membrane in Alzheimer's disease patients.[4]

1.1.2 Neuroimaging in SVD

Neuroimaging is a crucial tool in the diagnosis and characterization of SVD, since parenchymal lesions caused by small vessel changes are imaging features commonly seen in this disease. [1,2] SVD patients may undergo brain imaging by computed tomography (CT), which can detect ischemic strokes, haemorrhages and brain atrophy and might also reveal white matter changes. However, magnetic resonance imaging (MRI) is the preferred neuroimaging modality to study this disease due to its higher sensitivity and specificity for detecting pathological changes. [7] A number of different MRI methods, including fluid-attenuated inversion recovery (FLAIR), T2-weighted, T1-weighted, gradient echo/ T2*/susceptibility-weighted sequences and diffusion tensor imaging (DWI) has already been shown to provide a wide spectrum of structural changes associated with SVD.[2]

As previously mentioned, the main imaging features of SVD visible on MRI include white matter hyperintensities (WMH), recent small subcortical infarcts, lacunes, brain atrophy, enlarged perivascular spaces, cortical microinfarcts and cerebral microbleeds, which are briefly described in Table 1.1. [8] Moreover, most of these lesions are referred to as "silent" lesions due to their subtle clinical manifestations, on the contrary of small subcortical infarcts which cause stroke symptoms. [5]

Table 1.1 - Summary of SVD markers: SVD is associated with a broad range of tissue alterations detectable with MRI (highlighted by yellow arrows). Images adapted from [3].

Imaging marker		Description
Small subcortical infarcts	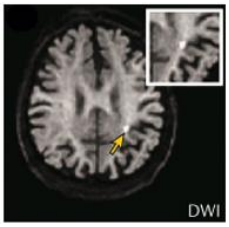	Neuroimaging evidence of recent infarction in the territory of one perforating arteriole. With imaging features or clinical symptoms consistent with a lesion occurring in the previous few weeks. [2] Are visible on DWI, as small hyperintensities, and lesions < 5 mm are detectable only with high resolution imaging.[3]
White matter hyperintensities	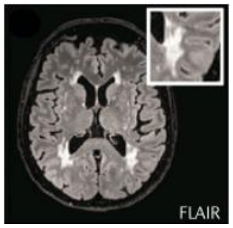	White matter lesions appear on MRI commonly as symmetric diffused areas distributed throughout the brain with a preference for the periventricular and deep white matter. They appear hyperintense on T2-weighted and fluid-attenuated inversion recovery images and hypodense on CT. [4,1]
Lacunes	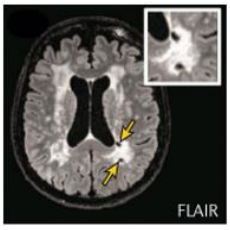	Lacunes are small cerebrospinal fluid (CSF)-containing cavities located in the deep grey or white matter, between 3 mm and about 15 mm in diameter. [2,8] They are thought to result from acute, small subcortical infarcts or haemorrhages in the territory of a single perforating artery. [3]
Brain atrophy	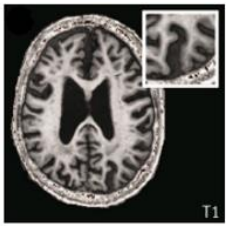	Cortical or subcortical brain volume loss that is not related to a specific macroscopic injury such as trauma or infarction on imaging. [2,3]

Enlarged perivascular spaces	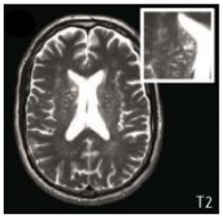	Perivascular spaces surround the small deep perforating arterioles as they pass through the deep grey and white matter. These spaces are visible on T2-weighted or T1-weighted MRI because they contain increased fluid of similar signal to CSF. They appear round or linear shape depending on the image orientation. [3,8]
Cortical microinfarcts	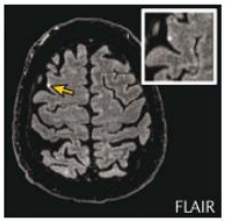	Small ischemic lesions with 50 μm and few millimetres that are detected on high-resolution structural MRI and DWI. [3]
Cerebral microbleeds	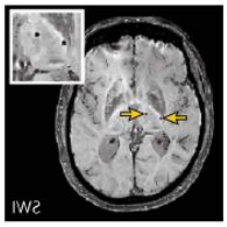	Small (generally 2-10 mm in diameter), round or ovoid areas of hypointensity on T2* or susceptibility-weighted imaging. Microbleeds are associated with lacunar stroke and white matter hyperintensities. They are consistent with blood cell leakage into brain tissue. [3,8]

Both conventional CT and MRI can detect morphologic lesions and indicate the extent and severity of SVD, but they cannot detect functional or cognitive consequences of the underlying pathological changes. In addition, several SVD patients with common imaging features seen on SVD are asymptomatic while others are not and therefore, there is an increased interest to investigate beyond basic structural imaging in SVD as these structural changes may not fully explain the variance in this disease and a measure of functional deficit may thus be a more accurate correlate of symptom burden, as well as underlying pathophysiological mechanisms. [7,9] Functional imaging techniques, such as fMRI, which measures brain activity through changes in blood flow and oxygenation levels, and positron emission tomography (PET), which makes use of radiotracers to provide images of metabolism, can help to understand the functional effects of SVD. [7,10] Regarding PET studies, changes in cerebral glucose metabolism can be assessed using fluorodeoxyglucose (FDG)-PET, and it has already shown differences in patterns of hypometabolism between Alzheimer's disease patients and vascular cognitive syndromes. Moreover, fMRI studies, which analyse correlated blood oxygenation level dependent (BOLD) signal fluctuations, has been used to evaluate how SVD patients respond to certain tasks, such as motor or visual tasks, and found impaired BOLD responses when compared to healthy controls. Also, rs-fMRI has been able to extract networks of connected activity during rest by using, for example, cortical regions as seeds to determine their connectivity to other regions, and it has found differences in the pattern of rs-fMRI activation in patients with SVD when compared to healthy controls. [9,10]

1.2 Functional Magnetic Resonance Imaging

Functional Magnetic Resonance Imaging (fMRI) has expanded enormously since the mid-1990s, becoming a standard tool to measure brain activity and connectivity, both in health and in disease. There are two experimental designs used in fMRI: task-based and resting-state. Several studies used the task-based paradigm investigating the differential neuronal responses to various forms of stimuli and activity during task performance. However, rs-fMRI has been increasingly applied among clinicians and researchers in the neuroscience community as it has been recognized that spontaneous/intrinsic brain activity is a fundamental aspect of normal brain function. [12,13]

1.2.1 The BOLD signal

The most widely used fMRI technique for functional brain mapping is based on a phenomenon called the blood oxygenation level dependent (BOLD) effect, which is considered an indirect measure of neuronal activity, reflecting changes in local cerebral blood flow (CBF) and blood oxygenation, that are coupled to underlying neuronal activity by a mechanism called neurovascular coupling. [13,14]

The theory is that active brain areas consume more oxygen that inactive areas, therefore an increase in local neural activity leads to a rise in metabolic rate of oxygen (CMRO2) consumption. To overcompensate the oxygen demand from the cells, a hemodynamic response is observed, in which local vasodilation leads to increased local cerebral blood flow (CBF), cerebral blood volume (CBV) and blood oxygenation. An important aspect of this mechanism is that CBF increases to a greater extent than the increase in CMRO2, leading to a relative surplus of oxygenated hemoglobin (oxyhemoglobin) in the activated region [14,15].

The BOLD fMRI signal lies in the different magnetic properties of deoxy- and oxy- hemoglobin. Deoxyhemoglobin is paramagnetic relative to brain tissue, therefore capillaries and veins containing blood partially deoxygenated cause local distortion of the magnetic field and consequent local signal decrease. Whereas oxyhemoglobin is diamagnetic, thus vessels containing oxygenated arterial blood cause little or no distortion to the magnetic field in the surrounding tissue. Upon neuronal activation, the oversupply of oxyhemoglobin causes an increase in the oxy-/deoxy-hemoglobin ratio and thus an increase in the MRI signal when compared to that of the surrounding tissue [14,15].

It should be noted that this response, commonly known as haemodynamic response, is much slower that the neural activity, with an intrinsic delay before regional vasodilation occurs and flow increases. This mechanism is represented by the hemodynamic response function (HRF), which has a time course of several seconds after the increase in activity. Thus, the HRF can describe the BOLD response to neuronal activity. [12]

Therefore, the magnitude of the BOLD signal is an indirect measure of neuronal activity and a complex function of metabolism (CMRO2), CBF and CBV (see fig.1.1). As a result, the BOLD signal must be interpreted as a relative measure of neuronal activity. The resultant indirect determination of brain function is typically represented as a statistical map which reflects regional activity. [12,13]

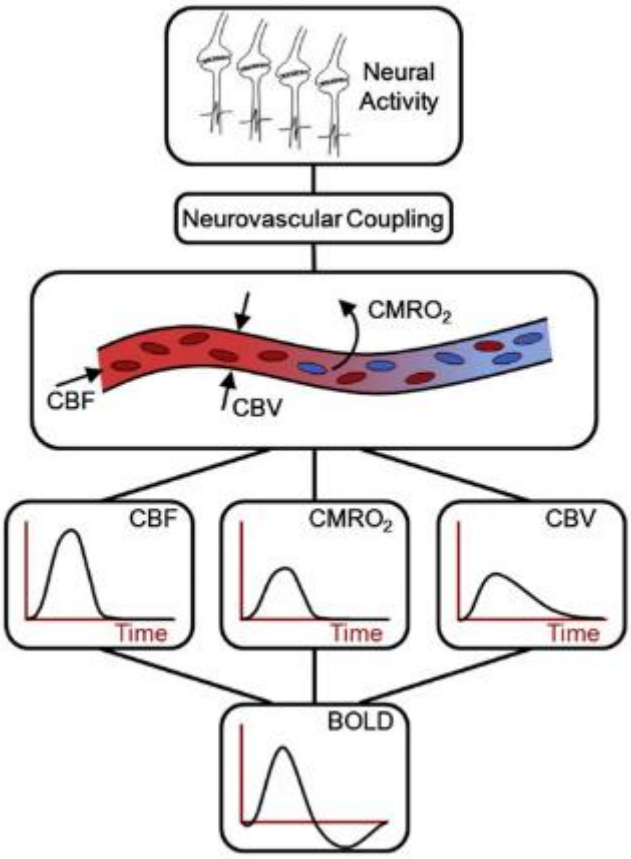

Figure 1.1- Scheme of the relation between neuronal activity and the associated BOLD signal. (Adapted from [23])

1.2.2 Functional Connectivity in Resting-state fMRI

Brain function arises from a complex interaction between brain regions, forming multiple complex brain networks. Developments on functional neuroimaging has allowed the detection of these connections enabling a better understanding of the functional neuroanatomy of specific brain functions. [3,16]

Network integrity can be assessed using functional connectivity, which refers to correlated activity between functionally related brain regions, using BOLD fMRI. [1,17] In the early stages of fMRI, the study of brain activation was done using external stimuli, by designing task-based paradigms. However, in the late 90's, the study of the brain function at rest has gained more attention as it requires less effort from the patients and due to the facility in data acquisition and identifying the functional areas in different patient's populations. [18] rs-fMRI focuses on spontaneous low frequency fluctuations (< 0.1 Hz) in the BOLD signal, reflecting the baseline activity of the brain. During these experiments, subjects are usually asked to lay still and quiet, under resting conditions, with their eyes closed and to not think of anything in specific, during the acquisition time. Then, spontaneous modulations in the BOLD signal are recorded and analysed. [19,20] In 1995, Biswal and colleagues [21] were the first to present functional significance of these fluctuations, finding a high correlation between the left somatosensory cortex and regions associated with motor function, suggesting ongoing FC between these regions during rest.

Through functional connectivity analysis of rs-fMRI data it has been possible to identify different resting-state networks (RSNs), which consist of anatomically separated, but functionally linked brain regions that show a high level of ongoing functional connectivity during rest. [22] These studies have been able to bring new insights into normal brain activity and to a variety of neurological and psychiatric disorders, as the spatial extent and connectivity strength of these networks depends upon the physiologic and pathologic conditions of patients. [17]

The most common RSNs identified by Smith and colleagues [24] derived from thousands of different activation conditions and across more than 1600 journal articles, are represented in Figure 1.2.

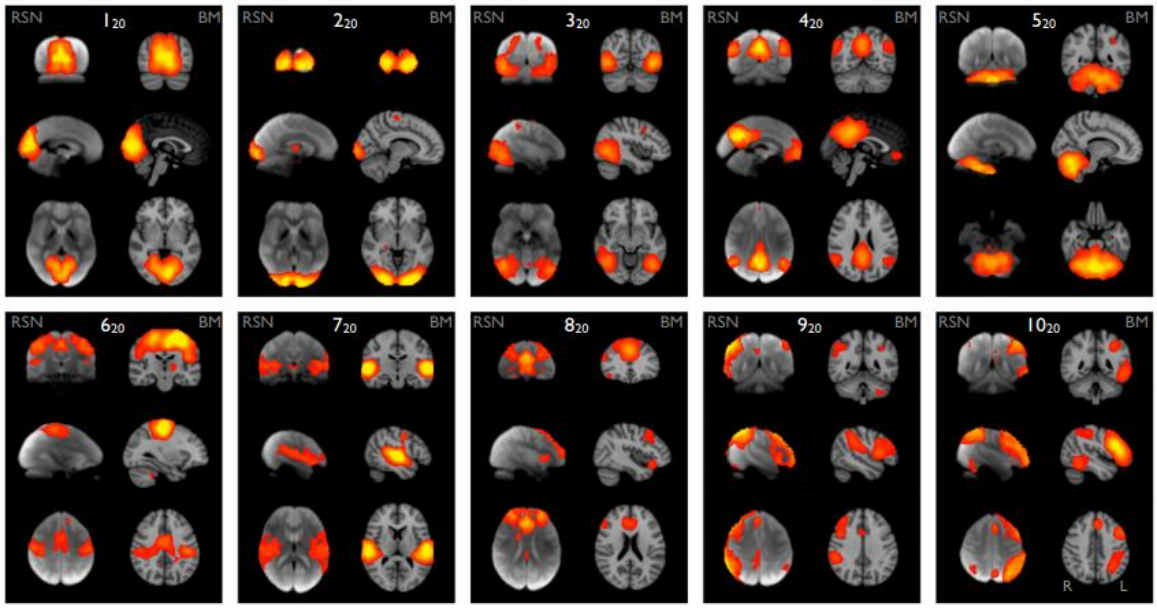

Figure 1.2- Resting state networks identified by Smith et al [24].From left to right, top to bottom: visual medial, visual occipital, visual lateral, DMN, cerebellum, sensorimotor, auditory, executive control, right frontoparietal, left frontoparietal.

Of special interest is the so-called default mode network (DMN), which consists of functionally linked posterior cingulate cortex/precuneus, medial frontal and inferior parietal regions. This network is task-negative, showing an elevated level of neuronal activity during rest, in comparison to when (cognitive) tasks are performed. In contrast with the DMN, the remaining RSNs - occipital visual, medial visual, lateral visual, cerebellum, sensorimotor, auditory, executive control and frontoparietal - are task-positive, being linked for example to cognitive processes and processing of external sensory inputs. [22] Furthermore, other significant RSNs have been identified over the past years, such as dorsal and ventral attention networks [25] and salience network [26]. The structural and functional description of all these networks is described in table 1.2 based on findings from different studies.

Table 1.2 - Structural and functional description of the most common resting-state networks reported in the literature.

Resting-State Networks	**Anatomical Structures**	**Function**
Visual	Medial, occipital pole, and lateral visual areas. [27]	Visual behaviour domain. The occipital pole and lateral visual maps are associated with paradigms cognition–language–orthography and cognition–space. [27]
DMN	Medial parietal (precuneus and posterior cingulate), bilateral inferior–lateral–	Involved in introspection and active episodic memory, becomes deactivated during specific goal-directed behaviour. [23]

	parietal and ventromedial frontal cortex. [27]	
Cerebellum	Cerebellum [27]	Corresponds to action–execution and perception–somesthesis– pain domains. [27]
Sensorimotor	Supplementary motor area, sensorimotor cortex, and secondary somatosensory cortex. [27]	Detection and processing of sensory input and preparation and execution of motor functions. [23]
Auditory	Superior temporal gyrus, Heschl's gyrus, and posterior insular. It includes primary and association auditory cortices. [27]	Associated with action–execution–speech, cognition–language–speech, and perception–audition paradigms. [27]
Executive Control	Medial–frontal areas, including anterior cingulate and paracingulate.[27]	Involved in executive control and working memory function, as well as action–inhibition, emotion, and perception–somesthesis–pain. [23,27]
Frontoparietal	Middle frontal gyrus, posterior parietal córtex. [23]	Implicated with several cognition and language paradigms. Also related to perception, somesthesis and pain processes. [27]
Dorsal attention	Superior parietal and superior frontal areas, including intraparietal sulcus and frontal eye-fields. [23]	Active when attention is overtly or covertly oriented in space. [25]
Ventral attention	Temporoparietal junction and the ventral frontal cortex. [25]	Responds when behaviorally relevant stimuli occur unexpectedly. [25]
Salience network	Dorsal anterior cingulate cortex and bilateral insulae. [23]	Responds to behaviorally salient events: the orientation toward salient emotional stimuli, conflict monitoring, information integration, and response selection. [23, 25]

1.2.2.1 Functional connectivity analysis in resting-state fMRI

There are several methods to process and to extract the relevant functional information from rs-fMRI data. The most common methods aiming to examine the existence and extent of functional connections between brain regions, are represented in figure 1, and include: seed-based correlation, regional homogeneity (ReHo), amplitude of low frequency fluctuations (ALFF), principal component analysis (PCA), independent component analysis, clustering, and graph theory. [12, 22]

Seed-based correlation analysis was first applied to rs-fMRI by Biswal and colleagues [21] and it is considered the most straightforward way to examine the functional connections of a particular brain region. This method entails selecting *a priori* defined region-of-interest (ROI), the seed region, which may be a single voxel or a region containing multiple voxels, and correlating the average BOLD time course of voxels within this ROI with the time courses of all other voxels in the brain. [12, 27] Thus, resulting in a functional connectivity map that provides a clear view of which regions are functionally connected to the seed region. [22]

In contrast to seed-based analysis, which aims to detect long-distance connections between a seed region and other brain structures, regional homogeneity (ReHo) analysis purposes to investigate connectivity at a more local level based on the assumption that neuronal activity is expressed in terms of a cluster instead of isolated voxels. Hence, this method uses Kendall's coefficient of concordance to measure the synchronization between the time-series of each voxel and that of its nearest neighbours to assess the extent of synchronization. Such computation can be performed on a previously defined ROI or ReHo can be calculated for all brain voxels. [12, 28]

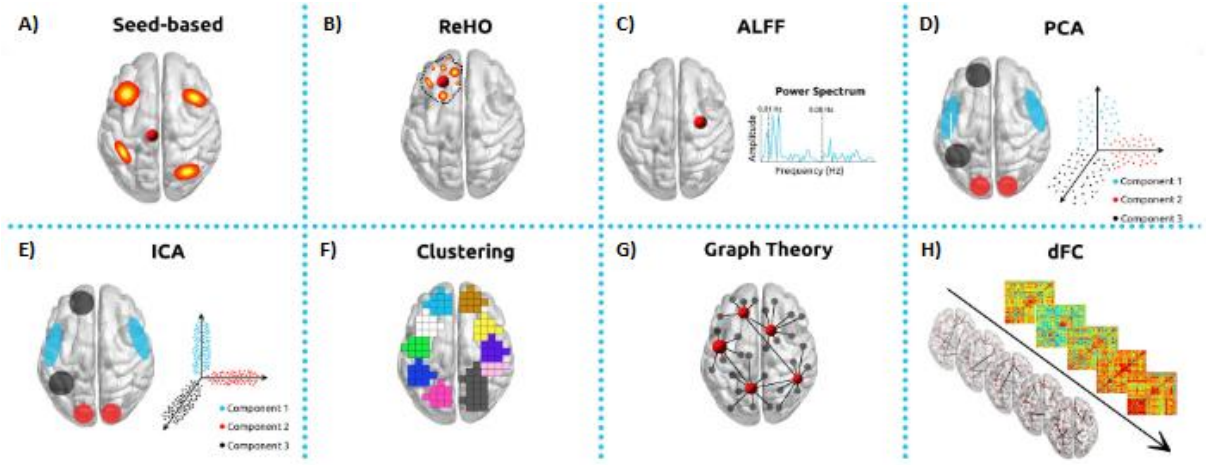

Figure 1.3- Commonly used analysis methods in functional MRI studies. Seed-based correlations (A), Regional homogeneity (ReHo, B), Amplitude of Low Frequency Fluctuations (ALFF, C), Principal Component Analysis (PCA, D), Independent Component Analysis (ICA, E), Clustering (F), Graph Theory (G), or dynamic Functional Connectivity (dFC, H). Figure adapted from [12].

Another method is ALFF which measures the signal amplitude magnitude of local spontaneous activity on a voxel by voxel basis. As the BOLD signal consists in low frequency fluctuations because of the slow timescale of the HRF, its power spectrum can be obtained by computing the Fourier transform of the time series in a voxel, to determine how much of the power is in the low frequency range, normally between 0.01 and 0.1 Hz, which can then be compared between subjects. [13, 29]

Principal component analysis is based on finding a set of orthogonal axes (independent components) that can maximize the explained variance of the data and separate the relevant information from the noise. The efficacy of PCA is strongly dependent on assumptions of linearity, orthogonality of principal components, and high SNR. [12]

The most frequent method used is ICA, an extension of PCA, which separates individual elements into their underlying components, and models the fMRI data set as a constant number of spatially or temporally independent components, which then are linearly mixed. Therefore, ICA maps are generated using spatial or temporal independent components, however temporal ICA has the disadvantage over spatial ICA of its high computational demands and necessity of relying on fewer points.[10] Compared with seed-based methods, ICA has the advantage of requiring few *a priori* assumptions but does compel the user to manually select the important components and distinguish noise from physiologic signals. Some studies have aimed to automate this process and use ICA as a method for identifying noise within the BOLD signal. [27]

As for the clustering method, it is based on the grouping of datapoints into a sub-group that show a high level of similarity and different sub-sets that show a low level of similarity. The main goal is to maximize the level of similarity between datapoints, grouping connected points into non-

overlapping sub-clusters. [22] When analysing rs-fMRI data, one may want to group a collection of voxels or ROIs on the basis of similarities in their BOLD time courses by using some distance metric, such as a Pearson correlation, reflecting functional connections between brain regions. [22, 27] Clustering algorithms assigned all voxels to one of the several clusters on the basis of their distances from the cluster centers, which are calculated from an average of their members. Then the algorithm iterates to update memberships and cluster centers until convergence is achieved. [22]

Graph theory is an increasingly prominent tool that allowed the possibility to examine the overall structure of the brain networks, showing the formation of multiple resting-state networks and of one integrative complex network linking all brain areas and sub-networks together into one complex system. [22] This approach models the brain as a network comprised of nodes, voxels or regions, and edges, connections between nodes (e.g., time-series correlations). This whole-brain network is mathematically modelled as graph and, consequently, graph-theory metrics can be used to study the topological properties of such network. [12] Properties of interest include the average path length, a measure of global connectivity of the network, clustering coefficient, which provides information about the level of local neighbourhood clustering within a graph, the level of modularity, that describes to which extent groups of nodes in the graph are connected to the members of their own group, indicating the formation of sub-networks within the full network, among others. [22, 27] All together, these graph values provide insights about functional integration, segregation, resilience or organization of the network as whole or of its individual nodes. [12]

All these methods above assumed that FC is stationary over a full resting state scan, i.e., that the underlying connections do not change over time. However, considering the dynamic nature of brain activity, a novel approach, dynamic functional connectivity (dFC) introduced by Chang & Glover [30], considers the temporal fluctuations of functional connections in faster timescales of seconds to minutes. [31, 32] The study of dFC can be implemented using different methodologies [33, 34, 35], therefore the next section will be focused on an overview of these methodologies and the advances made throughout the years.

1.2.3 Dynamic Functional Connectivity

In contrast with conventional static FC obtained from the correlation across an entire time series, dFC analyses brain activity within short segments of time series. Indeed, several studies regarding dFC reported that this approach can provide a greater insight into fundamental properties of brain networks and serve as a disease biomarker, since disease related alterations in the dynamic properties of FC seem to have a neural origin. [31, 36]

However, while many studies focusing on the analysis of rs-fMRI on much shorter time scales than before demonstrated that FC fluctuates over time, others have difficulties determining if the dynamic changes observed were attributed to neural activity or could be related to physiological changes, such as respiration or heart rate fluctuations, or even noise associated, for example, to head motion. [37] Therefore, to perform a dFC analysis it is crucial to go through several steps of pre-processing, such as motion correction, slice timing correction, spatial smoothing and specially physiological noise correction, which can strongly influence FC estimates. [38]

There are a set of different approaches to study resting-state dynamic functional connectivity (rs-dFC), however two main categories can be highlighted: time-domain analysis and time-frequency joint mapping. As for time domain analysis, the methods used are often the same as the ones used in static analysis such as correlation between signals in different brain regions, but using a sliding window moved across the time series as it is considered the simples approach. In contrast, time-frequency

methods allow to quantity correlations between BOLD signals in different brain areas as a function of both time and frequency. [32, 39]

1.2.3.1 Sliding window analysis

Sliding window analysis is commonly used to study dynamics in resting-state FC due to its analytical simplicity and easy implementation, whereby the fMRI data are segmented into windows and functional interconnections between brain areas are assessed within each window, as shown in figure 1.4 [32, 36] This analysis depends on the selection of the window length, which is then shifted in time, by a chosen step, until it reaches the end part of the timecourses. The data points within that window are used to calculate the FC metric of interest. Thus, resulting in a quantification of the time varying behaviour of a chosen metric over the duration of the scan. [31, 39]

So, a crucial parameter is the choice of window length, which ideally should be large enough to allow robust estimation of FC and to resolve the lowest frequencies of interest in the signal but small enough to detect potentially interesting transients. In this way, it is essential to compromise between time resolution and estimation accuracy, as smaller window suffers from a possibly deceptive FC calculation due to the limited number of samples, introducing spurious fluctuations and increasing sensitivity to noise, while a larger window would interfere on the detection of the temporal variations of interest. Several studies suggested that a window length of 30-60s would be sufficient for detecting dFC changes. [31, 36]

Furthermore, the step of window shifting, which is the number of time lags by which the sliding window is shifted, defining the amount of overlap between successive windows, is usually selected as on time lag (1 TR). [31, 32] Another critical parameter regarding the sliding window approach is the choice of FC metric used to calculate the statistical interdependencies between the time-series within each window, commonly, Pearson linear correlation and the covariance matrix are two of the metrics used for quantifying rs-dFC. Each window's result can be considered a discrete correlation state and clustering of these states may measure transient cognitive states which the brain is moving through. [32, 38]

However, other methods can be implemented in a sliding-window approach, for example Independent Component Analysis (ICA), which is a data-driven approach usually used to estimate networks from the entire spatio-temporal dataset, has been applied [40] to estimate dFC on a sliding window basis by detecting a set of independent components (ICs) for each window. Obtaining spatial maps of resting-state networks over time. [31]

Moreover, some studies focused on local functional interactions between spatially adjacent regions rather than focusing on global connectivity between spatially separated brain regions. The most common measure used to quantify localized brain connectivity is regional homogeneity (ReHo), which measures the synchronization between the time-series of each voxel and that of its nearest neighbours based on a pre-defined region of interest (ROI). [12] This method can also be implemented on a sliding window basis to study the dynamic behaviour of regional FC. A study [35] characterized the temporal fluctuation of local FC by calculating ReHo inside a short time window, showing an association between local FC dynamics and global brain function.

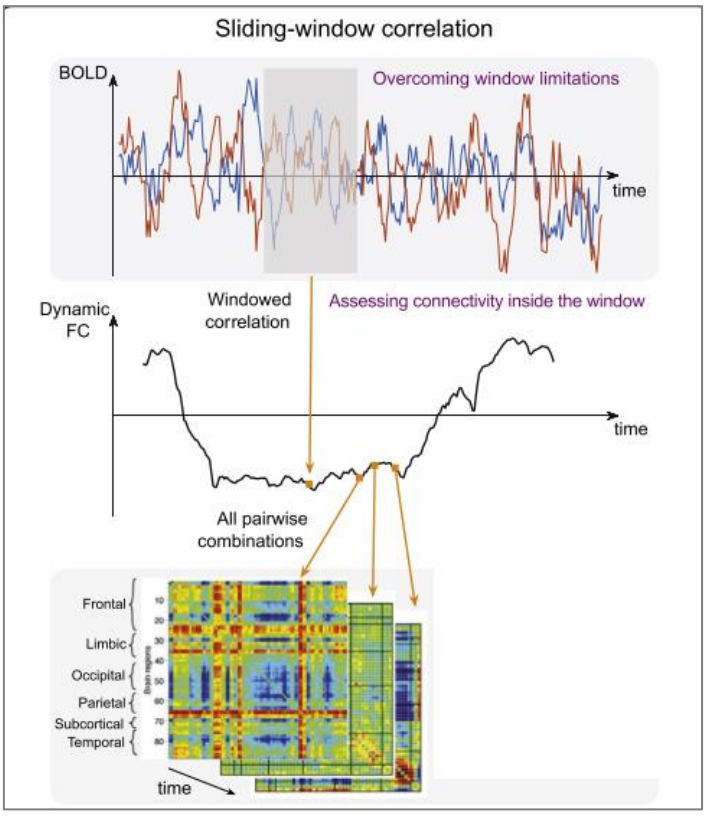

Figure 1.4- Sliding window methodology. On the top are represented two time-courses from two different ROIs and the window where the Pearson Correlation coefficient is computed. On the centre is the result of the correlation across all windows. In the bottom are represented the dFC matrices across time, which is the result of the correlation across all windows (centre image) for all pairs of ROIs. Figure adapted from [39].

1.2.3.2 Time-frequency analysis

Another method which overcomes some of the limitations of sliding-window analysis is time frequency analysis, which can be applied to estimate the coherence and phase lag between two time-series as a function of both time and frequency. Time-frequency coherence analysis can be implemented with the wavelet transform coherence (WTC), which is based on the continuous wavelet transform that decomposes a single time series into time frequency space by successively convolving the time series with scaled and translated version of a wavelet transform. [30, 31]

Wavelet transform allows to vary the scale of the wavelet according with the natural time scale of the frequencies in the signal, meaning that higher frequencies or faster changes are analysed in shorter time windows and in accordance lower frequencies are analysed with longer time windows. Thus, providing information of the coherence across multiple time scales, for example enabling the characterization of the dominant frequencies at which regions or networks display coherence or the extent to which magnitude and phase relationships between two brain regions fluctuate over time within a given band. However, the main challenge of this analysis is regarding the large amount of information produced when scaling the analysis to multiple subjects and brain regions and which can be overcome by, for example, summarizing the output along several potentially relevant dimensions. [31]

1.2.3.3 Phase coherence

Another method used to measure dFC and which increases temporal resolution is instantaneous phase synchronization (PS) or phase coherence (PC). PC compares two signals by first separating their instantaneous amplitude from instantaneous phase information and then compare only phase time series. This is performed usually with Hilbert transform, which converts the real signal into its complex analytic version. This tool is mostly used in magnetoencephalography (MEG) or electroencephalography (EEG) research rather than studies with fMRI, however using instantaneous phase as a measure of functional connectivity has several advantages, one of them is that there is no need for time-windowed averaging as PC instantly identifies full temporal dynamics and also the fact that PC is a nonlinear measure, being more appropriate to identify complex dynamic processes in the brain. Further, PC is computationally faster than temporal correlation, since with one transform, we obtain the phase value for each time point for the whole brain. [35]

Therefore, some studies [34, 41, 42] have explored the dynamics of the complex phase of the BOLD signal during rest. On these studies the BOLD signal is first bandpass filtered, and the phase alignment between each pair of brain regions is then computed by estimating the BOLD phases, θ(n,t), using the Hilbert transform, for each BOLD regional time courses. As previously mentioned, with Hilbert transform, the real signal, $x(t)$, is converted into the analytic signal, $x_a(t)$: [35]

$$x_a(t) = x(t) + jH[x(t)] \quad (1.1)$$

where $H[\cdot]$ represents the Hilbert transform and j the imaginary unit. Considering $x(t)$ a narrowband signal, it can be written as the product of an amplitude-modulated low-pass signal, $a(t)$, and a sinusoidal carrier, $\theta(t)$:

$$x(t) = a(t)\cos[\theta(t)] \quad (1.2)$$

Using the Bedrosian's theorem, the Hilbert transform of $x(t)$ can be rewritten with the equation (1.1):

$$H[x(t)] = a(t)\sin[\theta(t)] \quad (1.3)$$

Thus, the analytic signal $x_a(t)$ becomes represented by $x_a(t) = a(t)\cos[\theta(t)] + j[a(t)\sin(\theta(t))]$, where the $\sin[\theta(t)]$ represents the imaginary part of the analytic phase and $\cos[\theta(t)]$ its real part. Then, by the Euler's formula:

$$x_a(t) = a(t)e^{j\theta(t)} \quad (1.4)$$

where *a(t)* represents the instantaneous amplitude and $\theta(t)$ the instantaneous phase. After the estimation of the phase of the BOLD signals in each brain area, *n*, $\theta(n,t)$, the phase coherence between brain areas *n* and *p*, at time *t*, $PC(n,p,t)$, is obtained by:

$$dFC(n,p,t) = \cos[\theta(n,t) - \theta(p,t)] \quad (1.5)$$

Therefore, it is possible to obtain a whole-brain pattern of BOLD phase coherence, dFC matrix, with size NxN, where N is the number of brain areas, at each single time point t. Using the cosine function, two areas n and p with temporarily aligned BOLD signals, meaning with no phase difference, will have a value $dFC(n,p,t) = \cos(0) = 1$ and on the other hand, $dFC(n,p,t) = 0$ when the BOLD signals are orthogonal. [34, 41]

1.2.4 Dynamic Functional Connectivity States

After the estimation of all the dynamic FC matrices, using one of the methods mentioned above, decomposition of these dFC patterns into a limited set of connectivity states may be performed, using a matrix factorization technique such as k-means clustering, principal component analysis (PCA), dictionary learning or other. [39]

K-means clustering is one of the most common methods of factorization of dFC patterns and was introduced by Allen and colleagues [43]. It consists of grouping data into subsets (clusters) such that parameters of the same cluster are more similar to one another than they are to those of different clusters. This algorithm divides n samples in observation space, which in this case are all the dFC matrices of all participants, into k clusters (states), where each sample belongs to the nearest cluster according to its distance from the cluster centroid. However, in this method it is required a predefine number of clusters k, thus being sensitive to the initial values, which may lead to different results and affect the interpretation of the states. [12, 39]

Principal component analysis (PCA) is a data-driven method without requirement of prior information, and which converts a number of possibly correlated variables into a set of linearly uncorrelated variables, called principal components. It has been used to investigate dynamic brain connectivity patterns by ranking and extracting the principal components of the dynamic whole brain functional connectivity with higher variability across time and subjects. Unlike clustering this method allows a temporal overlap between connectivity building blocks, as at every time point the connectivity pattern is now given by a combination of states, each one with a different contribution. [39, 44]

As for dictionary learning, states are seen as building blocks of the connectivity patterns with different temporal contributions. This matrix factorization method describes each dFC matrix as a linear combination of a subset of dFC states, thus imposing a certain degree of temporal sparsity. [45]

After obtaining the dFC states, measurements such as the number of occurrences, the mean time spent on each state, or the switching behaviour between states, can be assessed. [39]

1.3 State of the art

As SVD is thought to be among the main causes of vascular cognitive impairment (CI), a condition that includes vascular dementia and mild CI caused by cerebrovascular disease, a significant amount of studies has been focused on investigating its mechanisms and its relationship with cognitive performance. Moreover, an early diagnosis is essential, as risk factors such as hypertension, smoking, diabetes and others must be controlled and, which when achieved in time may prevent the development and progression of CI. This involves several cognitive domains, in particular executive function, processing speed and attention. [17]

For this reason, for the state of the art of this thesis, all dFC studies of CI were considered, not only in the case of SVD. These studies are listed in Table 2, including a brief description of their main methods and results.

Some researchers, using rs-fMRI in SVD patients, suggested that these cognitive symptoms may be caused by the disruption and disconnection of the frontal-subcortical pathway. [46] Thus, there has been an increased interest in studying intrinsic network connectivity such as default mode network (DMN), which consists of the ventromedial prefrontal cortex and posterior cingulate cortex, and central-executive network (CEN), which includes the dorsolateral prefrontal cortex and lateral posterior parietal cortex, of these patients. While the first contributes to both episodic memory and visual imagery, the second plays a crucial role in executive attention, working memory, problem solving and others. [47]

Schaefer and colleagues [48] investigated changes of FC in early small vessel disease and reported reduced connectivity in frontoparietal networks which were closely related to white matter lesions and typical neuropsychological deficits related to SVD. In addition, others revealed that SVD patients with cognitive impairments presented lower FC of the DMN with the anterior cingulate cortex, as well as with temporal and frontal regions. [17] Also, a study with CADASIL patients also demonstrated abnormalities between intrinsic frontoparietal functional networks, associated with cognitive measures, particularly measures of executive ability and speed. [49]

Meanwhile, these previous studies employed static rs-FC which may be limited because of the assumption of spatial and temporal stationarity of functional interactions throughout the resting-state. To date, only one study [49] focused on the dynamic functional connectivity in patients with cerebral small vessel disease and its association with cognitive impairments. However, this approach, which takes into account the fluctuations in FC, has been implement in neuroscience research and successfully identified numerous dynamic FC biomarkers for many brain disorders [7], including Alzheimer's disease[49][50], Dementia with Lewy bodies (DLB)[50], Parkinson's disease[51][52], Schizophrenia and autism[53]. Moreover, this approach has also been used to study the relationship between the switching behaviour of resting-state activity and cognitive performance in healthy older adults. [34] In addiction, studying how specific psychoactive compounds modulate the relative stability of functional networks over time can provide insights into its behaviour in healthy and disease subjects. [41]

Generally, most of these studies used a sliding time-window to calculate dFC matrices, resulting in a specific representation of the connectivity in each time segment. After, to identify the reoccurring patterns of connectivity, usually data-driven clustering (k-means) is applied to all FC matrices of all participants. These reoccurring patterns represent states of functional connectivity, which individuals shift between during the scan. [53]

Table 1.3 - State of the art of Dynamic Functional Connectivity studies of CI.

Citation	Condition	Population	Data	Analysis Methods	Results
[49] Fu et al, **2019**	**Alzheimer's disease (AD)** and **Subcortical ischemic vascular disease (SIVD)**	**T= 76** (Controls and patients were matched by number and age) -HC=38 -AD=19 -SIVD=19	**Acquisition:** 3T scanner **rs-fMRI data:** -TR = 460 and 2000 ms (scanned with different head coils) -TE = 29 ms -Total acquisition time of 5 min	**Sliding window and K-means clustering** Number of states=4	**SIVD** and **AD** patients spent **more time** and had **more occurrences** in **weakly connected dFC states**, and the opposite was observed in strongly connected states. It was also revealed a correlation with **cognitive performance**, patients that **spent more time** in **strongly connected states** would have **better performance** in **attention** and **processing speed** and patients with **less occurrences** in with **weakly connected states** would have **better language performance.**
[50] Schumachet al, **2019**	**Dementia with Lewy bodies (DLB)** and **Alzheimer's disease (AD)**	**T= 102** (with over 60 years of age) -HC = 31 -DLB= 31 -AD=29	**Acquisition:** 3T scanner **rs-fMRI data:** -TR=3000 ms -TE=40 ms -Total acquisition time of 6 min	**Sliding window and K-means clustering** Number of states=3	**DLB** and **AD** patients **spent less time** and **had less occurrences** in the **strongly connected state**. In particular, DLB spent more time and had more occurrences in a specific weakly connected state. In addition, the **distribution of states** in the AD and DLB groups was more **out of balance** compared to controls.
[51] Díez-Cirarda et al, **2018**	**Parkinson's disease** (with mild cognitive impairment (**PD-MCI**) and with normal cognition (**PD-NC**)	**T=61** (age between 45 and 75) -PD=35 -HC=26	**Acquisition:** 3T scanner **rs-fMRI data:** -TR= 2100 ms -TE= 16 ms -Total acquisition time of 7.4 min	**Sliding window and K-means clustering** Number of states=2	**PD-MCI** patients **spent less time** in the **weakly connected state** and had a **higher number of transactions** between states, when compared to HC. **PD-NC** patients didn't reveal significant differences on the dFC features between states when compared with the HC or PD-MCI groups.
[41] Lord et al, **2019**	Subjects injected with either **psilocybin** (tryptamine psychedelic found in "magic	**T=9** -at least 21 years of age -no personal or family history of a major psychiatric disorder	**Acquisition:** 3T scanner **rs-fMRI data:** -TR= 3000 ms -TE= 35 ms -Total acquisition	**Phase coherence (Leading Eigenvector Dynamics Analysis (LEiDA)** and **K-**	Two main states were altered after the injection of psilocybin: one of the **non-global state** that correlated with the frontoparietal network which showed a **reduction** in the **probability of occurrences** and **transition** and the **state of**

	mushrooms") or **placebo**	-no substance dependence	time of 12 min	**means clustering** Number of states=7	**global coherence** showed an **increase** in the **probability of occurrence** and the **time spent** on this state.
[34] Cabral et al, **2017**	Healthy older adults with overall **good** (GCP) or **poor cognitive performance** (PCP)	**T=98** (with minimum of 50 years old) GCP=55 PCP=43 (Differences between groups with respect to **socio-demographic** and **cognitive measures**)	**Acquisition:** 1.5T scanner **rs-fMRI data:** -TR= 2000 ms -TE = 30 ms	**Phase coherence (Leading Eigenvector Dynamics Analysis (LeiDA)** and **K-means clustering** Number of states=5	**GCP** spent **more time** and had **more occurrences** in the **state of global BOLD coherence** when compared to PCP. In addition, **GCP** present a more **stable switching profile**, meaning that the FC states lasted longer whereas **PCP** had **less stable switching behaviour**, meaning that FC states lasted shorter. Thus, **FC switching measures** may serve as **novel indicators** of cognitive reserve.
[52] Fiorenzato et al, **2019**	**Parkinson's disease** (PD)	**T=153** PD=118 which were divided as: -normal cognition (NC)= 52 -mild cognitive impairment (MCI)= 46 -dementia (PDD)= 20 HC=35	**Acquisition:** 1.5T scanner **rs-fMRI data:** -TR= 1939.4ms -TE= 45ms -Total acquisition time of 8 min	**Sliding window and K-means clustering** Number of states=2	**PD patients** with **major cognitive alterations** stayed **longer** in the state of sparsely within-network functional connectivity, making **fewer transitions** and **spending less time** in the **strongly interconnected state.** Moreover, an **increase** in the **time spen**t in a dFC state with **weakly connected patterns** was associated with **worse cognitive performance** and an **increase** in the **number of occurrences** in each state was associated with **poorer cognitive function.**
[53] Rabany et al, **2019**	**Schizophrenia** (SZ) and **autism spectrum disorder** (ASD)	**T= 100** young adults (age 18–35) SZ=33 ASD=33 HC=34	**Acquisition:** 3T scanner **rs-fMRI data:** -TR=475 ms -TE=30 ms	**Sliding window and K-means clustering** Number of states=4	**SZ** and **ASD** spent **an increased** portion of the **time** in a state of **weak intra-network connectivity**, and a **decreased** portion of the **time** in the state of **strong connectivity**. When **SZ** participants transitioned into the state of **strongest connectivity**, they **switched** states very **rapidly**, while ASD and HC participants stayed in this state for a longer duration. More **severe symptoms** were associated with **fewer transitions** between states.

1.4 Objectives

The aim of this study was to investigate dynamic functional connectivity (dFC) measured by rs-fMRI in two groups of patients with SVD – sporadic SVD (sSVD) and cerebral autosomal dominant arteriopathy with subcortical infarcts and leukoencephalopathy (CADASIL) – compared with a healthy control group.

In this project, changes in dFC using measures of rs-fMRI were investigated in SVD patients and healthy controls to determine whether these alterations could be associated with the disease and associated cognitive deterioration and hence whether they could provide a valuable clinical biomarker to predict disease progression. For this purpose, not only changes in dFC in patients compared to controls were investigated, but also if the association between the dFC features and the patient's neuropsychological evaluations could add new insights on how rs-fMRI might provide information about functional alterations caused by SVD. To accomplish the main goals of this Thesis, the following steps were carried out:

1. Pre-process the rs-fMRI data collected from the groups of patients and healthy controls. Although pre-processing of these data was performed previously by another member of the project NeuroPhysIm, additional pre-processing steps were performed in this Thesis to better suit the proposed dFC study.

2. Estimate dFC throughout the methodology presented on section 1.2.3.3. In particular, we parcellated the brain using the Automated Anatomical Labelling (AAL) atlas and compute dFC using Phase Coherence between pairs of brain regions. We then applied Leading Eigenvector Dynamics Analysis (LEiDA), which considers only the leading eigenvector of the dFC matrix at each timepoint, instead of the whole matrix, allowing a big reduction in dimensionality and being able to explain the majority of the variance of the BOLD phase coherence.

3. Identify dFC states using a k-means clustering algorithm, being the inputs the leading eigenvectors. Therefore, a predefined number of centroids, k, which represent each one of the k FC states were obtained.

4. Perform statistical group comparisons of dFC features between healthy controls and SVD patients.

5. Characterize the dFC states, in particular by exploring the most relevant dFC states and a comparison with resting-state networks defined in the literature.

6. Investigate correlations between dFC features and the cognitive scores on four relevant cognitive domains (executive function, processing-speed, working-memory and long-term memory), to determine if the dFC analysis can provide additional relevant information on the disease.

7. Investigate correlations between dFC features and the probabilistic maps of the most frequently lesioned white matter tracts of SVD patients and the total lesion load on each patient, in order to determine if this dFC behaviour of these patients could be correlated with structural lesions.

1.5 Thesis Outline

This dissertation is organized in 4 main chapters. The first and current chapter constitutes an introduction to the work, comprising a motivation for the study, the theoretical concepts behind this study, a literature review focusing on previous studies, directly or indirectly related to the present work, and the objectives here proposed to be accomplished. Afterwards, chapter 2 starts with a description of the participants involved in this study and the acquired fMRI data, the tract-specific white matter lesion load, the pre-processing and the methods to extract the dFC states in the fMRI data. The methodology used to explore the number of states will also be presented along with the characterization of the dFC states in terms of dynamical proprieties and their correlation with known resting-state networks, with neurophysiological tests and with SVD lesion maps.

Afterwards, results obtained throughout this dissertation will be displayed in chapter 3, starting by exploring the dFC states obtained with k-means clustering algorithm, the most different dFC states found between group comparisons and further investigating these relevant states, section 3.5 comprises the results of the correlation between the RSN and the relevant dFC states, followed by the description of the switching profile in patients and controls, the dFC features correlation with neurophysiological tests and with SVD white matter lesion maps. The results will be discussed and interpreted within chapter 3.

At last, chapter 4 provides the main conclusions of this study, along with its comparison with findings from previous studies, followed by the main limitations and suggestions regarding future work.

Chapter 2

Materials and Methods

2.1 Imaging data

2.1.1 Data acquisition

Imaging data were gathered in the scope of the project NeuroPhysIm at Hospital da Luz between 2015 and 2017, on a 3T Siemens Verio MRI system. The participants taking part of this project comprised of 3 groups: 11 (9 females and 2 males) sporadic SVD (sSVD) patients, 6 (4 females and 2 males) CADASIL patients, and 12 (6 females and 6 males) healthy controls (HC), making a total of 29 individuals. The ages of the groups were ranged between 37 and 66 years (mean=52.1±7 years old) for the sSVD group, 34 and 61 years (47.2±11 years old) for the CADASIL group, and between 37 and 59 years (52±6 years old) for the HC group. The patient's diagnosis was defined through clinical and neuropsychological evaluation by neurologists and neuropsychologists at Hospital Egas Moniz.

The MRI data were composed by both T1-weighted and T2-weighted structural images, where T1-weighted images were collected using a MPRAGE sequence and T2-weighted images were collected using a fluid attenuation and inversion recovery (FLAIR) sequence, with the parameters indicated in table 2.1. Resting-state BOLD fMRI images were collected using a gradient-echo Echo-planar imaging (EPI) sequence with parameters represented in 2.1. During resting-state fMRI acquisition, the subjects were instructed to keep their eyes closed without falling asleep and with the least possible movement, with a duration of ~6.5 min.

Table 2.1 - MRI acquisition parameters.

	T1-weighted (MPRAGE)	**T2-weighted (FLAIR)**	**BOLD rs-fMRI**
TR (ms)	2250	8500	2500
TE (ms)	2.26	97	30
Flip Angle	9°	150°	90°
Voxel size (x,y,z) [mm^3]	1x1x1	0.69x0.69x3	3.5x3.5x3
Image size (x,y,z)	240x256x144	256x320x47	64x64x40
Field of View [mm^3]	240x256x144	179x224x155	224x224x120

2.1.2 Data analysis

2.1.2.1 rs-fMRI pre-processing

The fMRI data had been previously pre-processed by another member of the project NeuroPhysIm, however an additional pre-processing step, ICA clean-up, was performed in this work to better suit the proposed dFC study. The following steps of pre-processing were performed using the FSL tools: [54]

(i) Distortion correction, using a B0 field mapping approach (https://fsl.fmrib.ox.ac.uk/fsl/fslwiki/FUGUE), in order to reduce EPI distortions due to magnetic field inhomogeneities.

(i) Removal of non-brain tissues using FMRIB Software Library (FSL)'s brain extraction tool (BET). [55]

(ii) Head motion correction using the Motion Correction FMRIB's Linear Registration Tool (MCFLIRT). This tool applies rigid-body transformations to align the different volumes with the middle one, so that there is a consistent spatial correspondence between the voxels and the anatomical areas over time. MCFLIRT estimates 6 motion parameters (3 translations and 3 rotations) for each volume in respect to the reference. [56]

(iii) Spatial smoothing using the SUSAN tool (https://fsl.fmrib.ox.ac.uk/fsl/fslwiki/SUSAN), with a Gaussian kernel of 5 mm of full-width at half-maximum (FWHM).

(iv) Nuisance regression of motion parameters and outliers. The detection of motion outliers, i.e., time points most significantly affected by rapid and large motion, was performed using the FSLMotionOutliers tool (https://fsl.fmrib.ox.ac.uk/fsl/fslwiki/FSLMotionOutliers). A confound matrix is generated, consisting of zeros (in the positions of non-outliers) and ones (in the positions of outliers). Both the 6 motion correction parameters and the outlier's confound matrix entered were used as nuisance regressors in a GLM, which was then fitted to the data using FSL's tool FLIRT in FEAT (https://fsl.fmrib.ox.ac.uk/fsl/fslwiki/FEAT). [57]

As one major problem with rs-fMRI is the presence of noise-related nuisance fluctuations that are difficult to distinguish from the signal of interest,[58] an additional pre-processing step was performed in order to further clean-up the signal using ICA.

(v) ICA-based denoising has proven to be a successful technique for separating noise from signal sources. [58]

First, a single-subject ICA decomposition was performed using the FSL tool Multivariate Exploratory Linear Optimized Decomposition into Independent Components (MELODIC, https://fsl.fmrib.ox.ac.uk/fsl/fslwiki/MELODIC [59]), to find subject-specific effects. The 4D data for each subject is decomposed into multiple components each described by a single 3D spatial map and an associated time course. Then, identification of each component as being of interest, purely reflecting BOLD signal, or artefactual was performed using an automatic component classifier, FMRIB's ICA-based Xnoiseifier, (FIX, https://fsl.fmrib.ox.ac.uk/fsl/fslwiki/ FIX), as hand-classification of artefactual components is time-consuming, operator dependent and requires expert knowledge.

FIX aims to remove components that account for multiple types of noise, thus for each resulting component, FIX generated a large number of distinct spatial and temporal features, each describing different aspects of that component. The set of features is then fed into a multi-level classifier that was trained in expert-hand-labelled data available in FSL and applied to the data. [60] As noise components share some variance with components containing signal of interest, the performance of the classifier was manually evaluated for each subject to avoid losing signal of interest. [61] This was done through the investigation of each component's spatial, temporal and spectral characteristics. The IC's classified as signal would have s the spatial map predominantly composed by low number of relatively large clusters and clusters on the grey matter, the temporal features would be fairly regular, without sudden abrupt changes, and the power spectra would largely show power at low frequency. Afterwards, the last step o ICA-based denoising consists of removing the noise components from the original data, also using FIX.

2.1.2.2 Co-registration and lesion segmentation

The registration of the images from the functional (original) space to the standard space, was performed in a two-stage process by another member of the project of NeuroPhysIm. First, the functional

images were registered to the structural space, through boundary- based registration (BBR, https://fsl.fmrib.ox.ac.uk/fsl/fslwiki/FLIRT_BBR), which is the most suitable for registration between the echo-planar imaging (EPI) and structural spaces and relies on intensity differences across boundaries and uses the white matter boundaries derived from the structural images segmentation. Second, consisted in the registration from the structural to standard space, using the Montreal Neurological Institute (MNI-152, 2mm) template. This second step was performed using Advanced Normalization Tools (ANTs), which involves two steps: a linear registration in which datasets are roughly aligned, and a non-linear registration, that accounts for the alignment of boundaries and internal structures by warping the data. Finally, the registration from the functional space to the standard space was performed, through the transformation matrices obtained, by applying consecutive transformations through the concatenation of the respective transformation.

For the purpose of this study, the structural image of each subject was parcellated into 90 cortical and subcortical non-overlapping ROIs, according to the AAL atlas. [62] Afterwards, these ROIs were co-registered to the patient's functional space and the pre-processed BOLD data was averaged within each ROI. The following steps were performed using MATLAB R2016b (The Math- Works Inc., Natick, MA, USA).

Moreover, the quantification of White Matter Lesion Load (WMLL), which are detected as WM hyperintensities (WMH) on MRI Fluid Attenuation Inversion Recovery (FLAIR) images, was previously determined in the context of another master's thesis [63], by manually creating masks in FLAIR images. The lesion volume was calculated using fslmaths (https: //fsl.fmrib.ox.ac.uk/fsl/fslwiki/Fslutils) and the values were normalized through the division of each subject lesion volume by the respective brain volume resulting directly from SIENAX (https://fsl.fmrib.ox.ac.uk/fsl/fslwiki/SIENA), a tool of FSL. Then, the lesion map generated from FLAIR images was co-registered to Magnetization Prepared Rapid Gradient Echo (MPRAGE) data of each subject, using FLIRT from FSL (https://fsl.fmrib.ox.ac.uk/ fsl/fslwiki/FLIRT), and normalized to Montreal Neurological Institute (MNI) 2mm standard space using Ants - Advanced Normalization Tools (http://stnava.github.io/ANTs). Then the lesion probability map (LPM) was generated by averaging the binarized normalized lesion maps within SVD patients, figure 2.1.

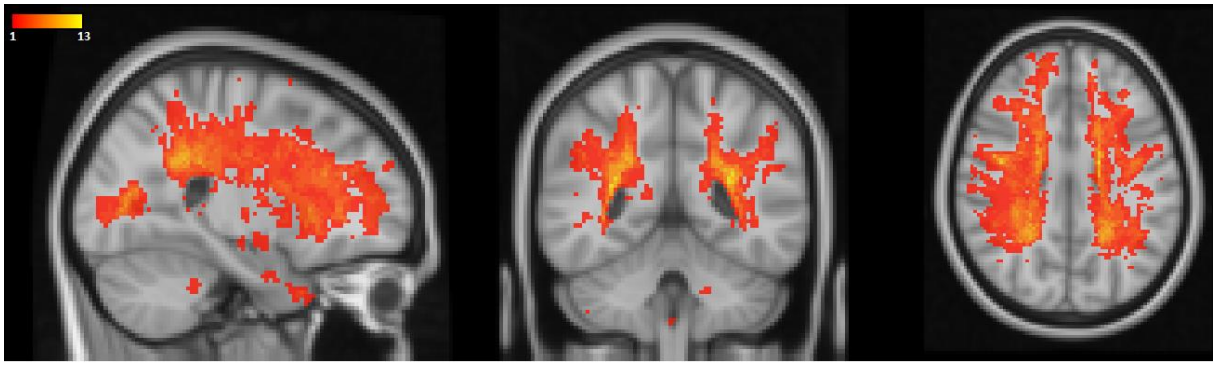

Figure 2.1- Sum of the patients WML binary maps, represented with a hot colormap, along the 3 anatomical planes (sagittal, coronal and axial) in the standard MNI152 space.

For the present study, tract-specific WML probability was calculated for each subject. The Johns Hopkins University International Consortium for Brain Mapping probabilistic fiber tract atlas (JHU-ICBM-tracts) [64], which includes 20 major WM tracts of the human brain, was used to create 11 ROIs of the WM tracts, figure 2.2, whereas symmetric tracts where added, using fslmaths. Then, the WM lesions probability on each ROI was calculated from the binary lesion maps of each subject, using fslmeants (https: //fsl.fmrib.ox.ac.uk/fsl/fslwiki/Fslutils), using the ROI as a mask and counting the

voxels on the binary lesion map that were equal to one (meaning that had lesion) and dividing by all the voxels in that ROI. This way the lesion probability was obtained for each of the 11 ROIs for each patient. Also, the total lesion load of each subject was obtained by counting the number of voxels on the binary mask which were different than zero using fslstats (https: //fsl.fmrib.ox.ac.uk/fsl/fslwiki/Fslutils).

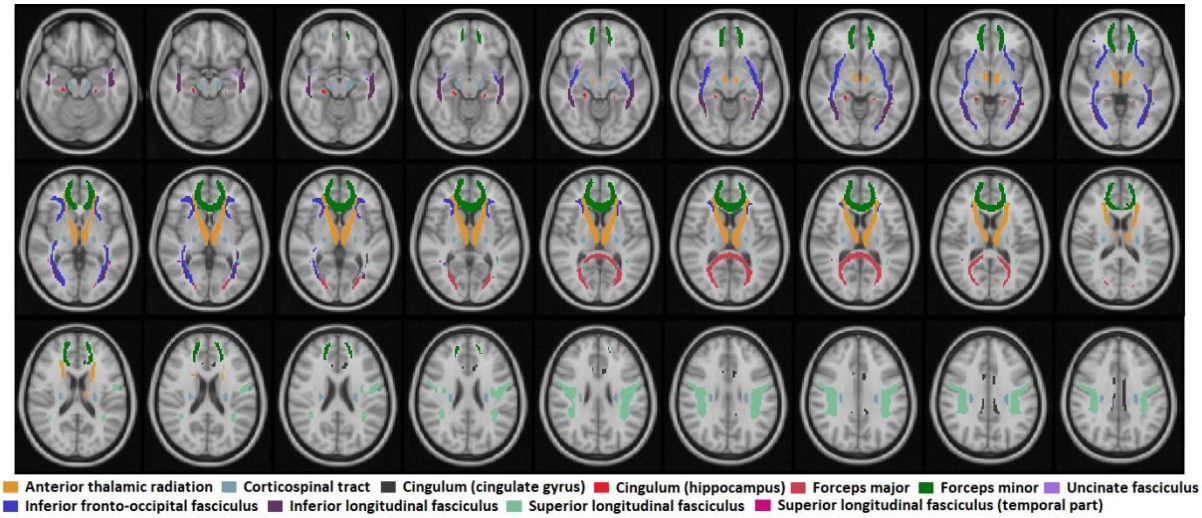

Figure 2.2- Maps of the 11 white matter tract ROIs obtained from the JHU-ICBM-tracts atlas in the standard MNI152 space (axial slices).

2.1.2.3 dFC estimation: Leading Eigenvector Dynamics Analysis (LEiDA)

For the estimation of the dFC matrices, the PC method, which was previously presented on section 1.2.3.3, was used. The first step consisted in applying a second-order Butterworth band-pass filter in the range 0.01 - 0.1 Hz and then the Hilbert transform was applied to the filtered BOLD signal of each ROI, n, and the phase of each time point, θ(n, t), was estimated. In fig. 2.3A, we can see a representation of the BOLD phases in all N=90 regions of the AAL space, at a single time point t, placed at the center of gravity of each brain area, also the same BOLD phases are plotted in the complex plane. After that, the PC is obtained for each pair of ROIs, n and p, using the equation [34, 41, 42]:

$$dFC(n,p,t) = \cos\left[\theta(n,t) - \theta(p,t)\right]$$

Hence, obtaining the dFC patterns for all time points. Afterwards, to characterize the evolution of the dFC patterns over time and identify those that reoccur over time, the most common approach is to compare the dFC matrices obtained at each time point, however, since matrices are symmetric, comparison is usually performed between the upper triangular elements of the matrices. Still, an alternative method is to apply Leading Eigenvector Dynamics Analysis (LEiDA), proposed by Cabral and colleagues [34, 41, 42], which considers only the leading eigenvector $V_1(t)$ of each dFC(t) (i.e., the one associated with the largest magnitude eigenvalue). The leading eigenvector, $V_1(t)$, is a Nx1 vector that captures the main orientation of BOLD phases over all areas, where each element in $V_1(t)$ represents the projection of the BOLD phase in each brain area into the leading eigenvector (Fig. 2.3C). This way, a reduction of the dimensionality of the data, when compared to considering all upper triangular elements of dFC matrices, from N(N-1)/2 to N can be achieved, while still explaining most of its variance. [34, 41] When all elements of $V_1(t)$ have the same sign, it means that all BOLD phases are pointing in the same direction with respect to the orientation determined by $V_1(t)$, exhibiting a strong coherence. In this case, a global mode is governing the BOLD signals. [34, 42] If instead, all the elements of the eigenvector have different signs, meaning positive and negative signs, the BOLD signals follow

different directions with respect to the leading eigenvector, this way dividing the brain into two clusters according to their BOLD phase relationship. [42] In addition, the magnitude of each element in $V_1(t)$ indicates the "strength" with which brain areas belong to the communities in which they are placed. [65]

In order to cluster all the samples of dFC states into a reduced number of recurrent patterns, the k-means clustering algorithm was applied to all the dFC leading eigenvectors across all subjects, dividing them into a predefined number of clusters, k, each representing a recurrent dFC pattern (see fig 2.3D). Although there is not a consensus regarding the number of dFC states revealed by fMRI, this generally falls between 7 and 17 depending on the selected criteria. [42] As this work aimed to explore whether there are dFC states that differentiate SVD patients from controls, and not to determine the optimal number of dFC states, the k-means clustering was run with a number of clusters, k, ranging from 2 and 20, using the cosine distance as the distance metric for minimization (although squared euclidean distance, L1-norm and correlation distance metrics were also tried and did not make a difference in observed results). For each k, examined how each dFC state changed between groups. Further, the k-means algorithm was run 1000 times, to increase chances of escaping local minima, and the best result (that where the distance of each cluster point to its centroid was minimum) was chosen.

As shown in figure 2.3E, each dFC state can be represented in cortical space, where each element of V1 is characterized as a sphere placed at the centre of gravity of the corresponding brain area and its colour is scaled according to the value of the corresponding eigenvector element. Yellow-to-Red spheres represent the positive values of V_1, corresponding to brain areas following the global mode. To highlight the network detaching from the global mode, blue links are plotted between brain areas with values <-0.1, as negative elements of V_1, represented as blue-to-cyan spheres, are the brain regions going in the opposite direction of the global mode. Finally, the dFC states can be represented back into matrix format (NxN) by computing the outer product $V_1 V_1^T$, resulting in a matrix with positive values (red) between pairs of brain areas with the same sign, meaning two brain areas with synchronized BOLD signals, negative values (blue) between areas with different signs in the eigenvector. [34, 42]

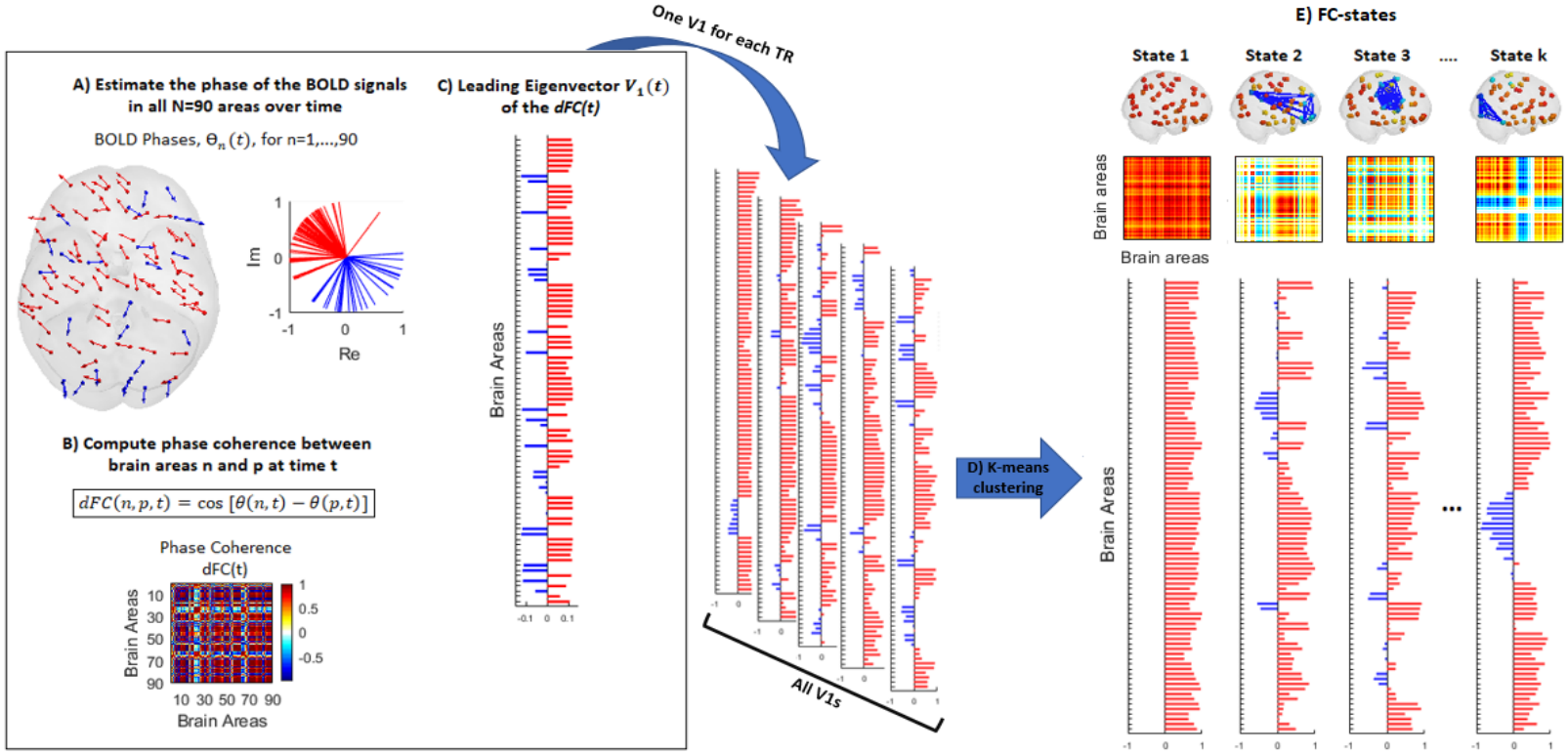

Figure 2.3 Illustration of recurrent dynamic functional connectivity (dFC) states obtained with Leading Eigenvector Dynamics Analysis (LEiDA). (A) Representation of the BOLD phases in all N=90 brain areas, at a single time point, both in AAL space (arrows centered at the center of gravity of each brain area) and in the complex plane (i.e., the unit circle with real and imaginary axes, where all phases are centered at the same origin). The arrows are coloured according to their direction when projected into the leading eigenvector of phase coherence. (B) The NxN phase coherence matrix, dynamic-FC dFC(t), which captures the BOLD phase alignment between each pair of brain areas, indicating for each pair of areas how coherent they are, where 1 (red) means full synchrony and -1 (blue) indicates a phase difference of 180°. (C) The leading eigenvector $V_1(t)$ of the dFC(t) matrix is a Nx1 vector that best captures the main orientation of all BOLD phases, where each element in $V_1(t)$ corresponds to the projection of the BOLD phase in each area into $V_1(t)$. The elements of $V_1(t)$ are colored according to their relative direction with respect to V_1 (red: positive; blue: negative). (D) The leading eigenvectors V_1 are obtained for each time point from all fMRI scans in all subjects, resulting in a large sample of 4437 leading eigenvectors. This sample is partitioned into a pre-defined number of, k. clusters, whereas each cluster is represented by a central vector. (E) These cluster centroid vectors, on bottom, represent recurrent patterns of BOLD phase coherence or dFC states. The signs of the elements in V_1 (red/blue) are used to divide brain areas into communities according to their BOLD phase, which can be visualized in AAL space (right side perspective), on top. Here links between the areas with negative elements in V_1 are plotted in blue. On the middle of (E) is represented the eigenvector's outer product $V_1 V_1^T$, which results in a NxN matrix with positive values (red) that result from the product between elements of V_1 with the same sign (positive or negative) and negative values (blue), between pairs with different signs.

2.2 Neuropsychological evaluation

The neuropsychological evaluation of the patients consisted of a comprehensive battery of cognitive tests. For the purpose of the current investigation, the following four cognitive tests were included in the analysis, in order to reflect the patient's performance in four relevant cognitive domains:

1. Executive function – Stroop Interference (total interference score) and Trail making test part B (time to complete); [66]
2. Processing-speed – Trail making test Part A (time to complete); [66]
3. Working memory - Wechsler Adult Intelligence Scale III (digit span); [67]
4. Long-term memory - Wechsler Memory Scale III (immediate recall learning (delayed recall) and percentage of retention). [68]

Commonly, the most impaired cognitive domains in SVD are executive function which is mainly characterized by defects in set shifting, verbal fluency, abstract problem solving and attention, and decrease speed of information processing. [67] Yet, on this group of SVD patients working-memory and processing speed was the cognitive functions that yielding the worst results. Mental and motor slowing can also be seen in patients with SVD. Tests sensitive to reductions in psychomotor speed, mental flexibility, working memory, and attention, such as the digit symbol or trail making, are useful instruments for detecting early subtle changes in SVD patients. [67]

The z-scores of the cognitive tests were previously calculated by another member of the team, where for each patient, the correspondent percentile score values were converted into z-scores considering normative data for the Portuguese population, except for the trail making test (where an online interface was used for this purpose). [69] Moreover, for both executive function and long-term memory a composite score was computed, combining the z-scores of the corresponding tests. The cognitive profile of SVD patients, as well as their demographic data are displayed on table x. One patient was unable to perform the cognitive evaluation.

Table 2.2 – Demographic data of all patients and their cognitive profile analysis in terms of cognitive scores in executive function, processing speed, working memory and long-term memory domains; mean and standard deviation values are displayed in bold.

	Demographic data			**Cognitive Domains**			
SVD subjects	**Age [yrs]**	**Gender**	**Education (years)**	**Executive Function**	**Processing Speed**	**Working Memory**	**Long-term Memory**
1	48	F	17	-0.3201	-1.36	-0.8965	-0.26300
2	66	F	12	0.6279	0.06	-0.8239	0.18722
3	57	F	17	-0.3322	-1.09	-0.7722	0.39160
4	56	F	4	-0.8850	-1.57	-1.4051	-0.95479
5	61	F	4	-0.9777	-1.32	-1.4051	-0.22764
6	53	F	4	-0.5828	0.13	-1.5141	-0.89410
7	55	F	4	0.7424	-0.29	-0.9346	-0.40946
8	47	M	7	-0.0122	-0.69	-0.9542	-0.17906
9	37	F	19	-0.1191	-1.15	-0.8596	0.47834
10	55	F	4	-0.5172	-0.97	-1.2816	-0.68458
11	44	M	17	-0.4776	-0.12	-0.6903	-0.19392
12	50	M	11	-1.8255	-2.56	-0.9945	-0.67273
13	36	M	12	-0.2274	-1.15	-1.0397	-0.18057
14	52	F	9	-0.0326	-0.94	-1.2816	-0.27780
16	34	F	17	-1.3174	-0.36	-1.0152	0.42724
17	50	F	6	-1.2278	0.09	-1.5141	-0.70136

Mean ± Standard Deviation	**50 ± 9**	**13 F**	**10 ± 6**	**-0.47 ± 0.67**	**-0.83 ± 0.73**	**-1.08 ± 0.27**	**-0.26 ± 0.46**

2.3 Statistical analysis

2.3.1 Between group comparisons

In order to evaluate how the k dFC states found during rest varied between groups, the following metrics were computed for each dFC state and for each subject: probability of occurrence, i.e. the fraction of epochs it occurred throughout the scan duration; mean duration or lifetime, i.e. the mean number of consecutive epochs in the same state; and switching profiles, i.e. the probabilities of switching from a given dFC state to another. [42] All the values were compared between patients and controls using non-parametric permutation-based paired t-test (10,000 permutations). This non-parametric two-sample hypothesis test uses permutations of group labels to estimate the null distribution, which is computed independently. [34] Then, the results over the range of k were analysed by plotting the p-values with respect to different significance thresholds, i.e. the standard $\alpha_1 = 0.05$ or the Bonferroni corrected significance threshold (to correct for the number of independent hypotheses compared in each partition model). [42]

2.3.2 Comparison with resting-state networks

dFC states, which are spatial patterns that replicate across time, exhibit spatial similarities with RSNs defined in the literature, although being referred to as temporal patterns that replicate across space. However, as some dFC states closely resemble RSNs others may reveal sub-parts of specific RSNs or combinations of different RSNs. Correlations of each dFC state with well-established RSNs was performed, with the same method used by Cabral and colleagues [34, 41, 42], in order to find similarities between them. For this purpose, 7 RSNs defined in [70] were transformed into AAL space by counting the number of $2\,mm^3$ MNI voxels in each AAL brain area that belong to each of the 7 networks, obtaining 7 vectors with 90 elements, where each element scales the contribution of each AAL brain area to the corresponding RSN. As the negative values from the centroid vectors are the ones that represent the network contrasting from the global coherence state, the RSN vectors were transformed to its symmetric so that they could be compared with the centroid vector. In addition, the positive values form the centroid vectors were set to zero, keeping only the values of the negative elements, and then correlation between each RSN vector and the centroid vector was computed.

2.3.3 Correlation of dFC features with clinical features

The scores of the cognitive tests, displayed on Table 2.2, which were previously calculated by another member of the project NeuroPhysim, were correlated with the dFC features of SVD patients. However, one of the patients did not performed neurophysiological evaluation and was therefore removed from the analysis. For this purpose, Spearman rank correlation analysis between cognitive scores and probability of occurrence of each dFC state was performed, as well as with lifetimes and switching probabilities, in order to determine whether altered behaviour of patients regarding some dFC states could be related to cognitive impairments evaluated with these neuropsychological tests. For testing the hypothesis of no correlation against the alternative hypothesis of a non-zero correlation, a significance threshold of 5% was applied. All the p-values were Bonferroni corrected by the number of dFC states to find significant correlations.

In order to investigate if the dFC features could be related with the WMLL found on SVD patients, Pearson correlation was computed between the probabilities of occurrences and lifetimes of each dFC state, as well as the switching probabilities from and to the most relevant dFC states, and the lesion probabilities of 11 different WM tracts, obtained from the JHU-ICBM-tracts atlas. These were computed as the fraction of WM tract containing lesion are presented on table 2.3, for each patient. For testing the hypothesis of no correlation against the alternative hypothesis of a non-zero correlation, a significance threshold of 5% was applied. All the p-values were Bonferroni corrected by the number of dFC states and ROIs. The same correlations were performed but between the total WM lesion load obtained for each patient and all the dFC features, mentioned above.

Table 2.3 – Lesion probability of each WM tract obtained from JHU-ICBM-tracts atlas, for each SVD patient. ROIs numeration: 1- Anterior thalamic radiation; 2- Corticospinal tract; 3- Cingulum (cingulate gyrus); 4- Cingulum (hippocampus); 5- Forceps major; 6- Forceps minor; 7 - Inferior fronto-occipital fasciculus; 8- Inferior longitudinal fasciculus; 9- Superior longitudinal fasciculus; 10- Uncinate fasciculus; 11- Superior longitudinal fasciculus (temporal part).

	Lesion probability of each WM tract										
SVD subjects	**ROI 1**	**ROI 2**	**ROI 3**	**ROI 4**	**ROI 5**	**ROI 6**	**ROI 7**	**ROI 8**	**ROI 9**	**ROI 10**	**ROI 11**
1	0.061	0.004	0	0	0.050	0.012	0.026	0.005	0.065	0	0
2	0.033	0.002	0	0	0.095	0.121	0.039	0.004	0.014	0	0
3	0.133	0.012	0	0	0.097	0.054	0.032	0.009	0.152	0	0
4	0.015	0	0	0	0.129	0.024	0.016	0	0.039	0	0
5	0.028	0.006	0	0	0.061	0.032	0.042	0	0.087	0	0
6	0.245	0.174	0	0	0.205	0.039	0.213	0.008	0.119	0.087	0
7	0.149	0.328	0	0	0.297	0.098	0.227	0.055	0.186	0	0
8	0.004	0	0	0	0.118	0.004	0.024	0.001	0.014	0	0
9	0.003	0	0	0	0.011	0	0.004	0	0.007	0	0
10	0.021	0.008	0	0	0.091	0.007	0.048	0.018	0.122	0	0
11	0.088	0.004	0	0	0.174	0.042	0.084	0.021	0.011	0.060	0
12	0.239	0.09	0	0	0.248	0.146	0.213	0.151	0.107	0.027	0
13	0.216	0.041	0	0	0.028	0.090	0.208	0	0.292	0.007	0
14	0.04	0	0	0	0.074	0.004	0.033	0.006	0.017	0	0
16	0.034	0.015	0	0	0.178	0.003	0.049	0.022	0.021	0	0.333
17	0.032	0.001	0	0	0	0,009	0.023	0	0.029	0	0
Mean	**0.081**	**0.041**	**0**	**0**	**0.113**	**0.041**	**0.076**	**0.018**	**0.076**	**0.011**	**0.019**
Standard Deviation	**0.084**	**0.087**	**0**	**0**	**0.083**	**0.046**	**0.082**	**0.037**	**0.079**	**0.025**	**0.081**

Chapter 3

Results and Discussion

3.1 Leading eigenvector explained variance

To reduce the dimensionality of the data, after computing the dFC matrices using the PC method, the leading eigenvector of each matrix was computed and to analyse if it still explains most of the data, the proportion of variance was calculated by dividing the leading eigenvalue by the sum of all eigenvalues. The distribution of the explained variance for each TR and for all subjects is displayed on figure 3.1 (on the right) and for each subject individually (on the left). As we can see, for all subjects the explained variance is always above 50% and occasionally over 90%. The mean value is 69% and the median 71%. At the individual level, the variance explained does not vary much across subjects. These results are in line with previous studies reported in [34, 41, 42], indicating that using only the leading eigenvector can be an appropriate method to reduce the dimensionality of the data, from N(N-1)/2 dimensions (when considering the upper or lower triangular values of the dFC matrix) to only the number of brain regions, N, and still have a high proportion of the data explained with lower dimensions.

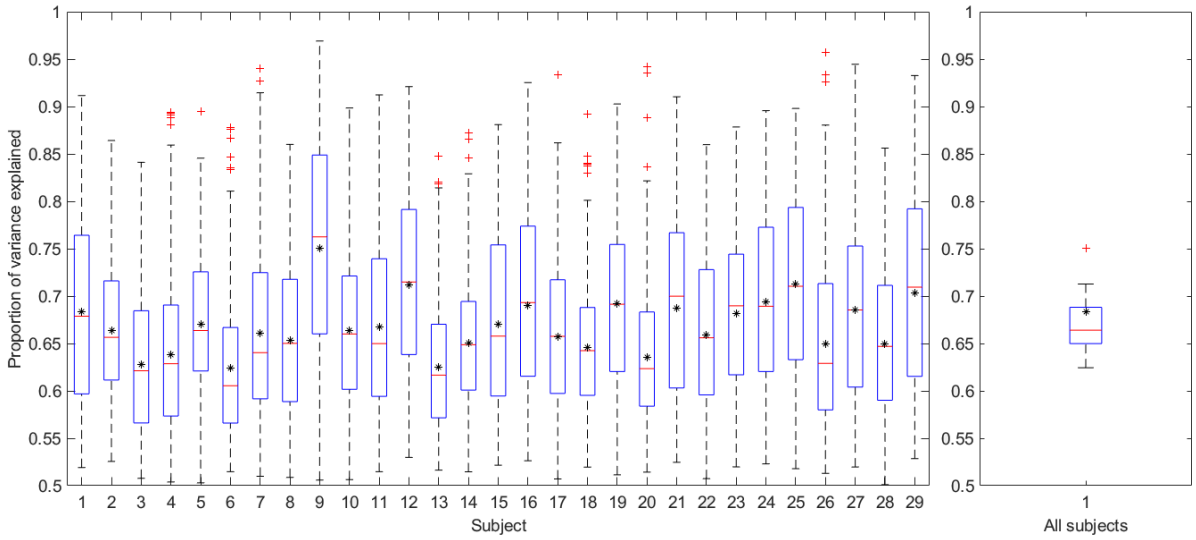

Figure 3.1 - Proportion of variance explained by the leading eigenvector. On the left the results are shown for each subject individually. The median value for each subject is represented by the red horizontal line, the mean value by the star (*) and the outliers are represented by the red plus (+) symbols. On the right is represented the distribution of the explained variance for all subjects.

3.2 Dynamic Functional Connectivity States

In order to evaluate how the dFC states varied upon the number of clusters, k, explored in the k-means clustering algorithm, each dFC state was represented in AAL space (figure 3.2) and it is possible to see that a higher value of k results in more fine-grained networks. Examining the networks formed with the blue links, meaning the brain regions going in the opposite direction of the global mode, we can see that the higher the number of clusters selected some networks reappear, normally with new regions being added to the same network, this way forming extensive networks. However, from a k=12 to 20 it is also clear that some smaller networks are formed, reoccurring in other dFC states with more regions, within the same k.

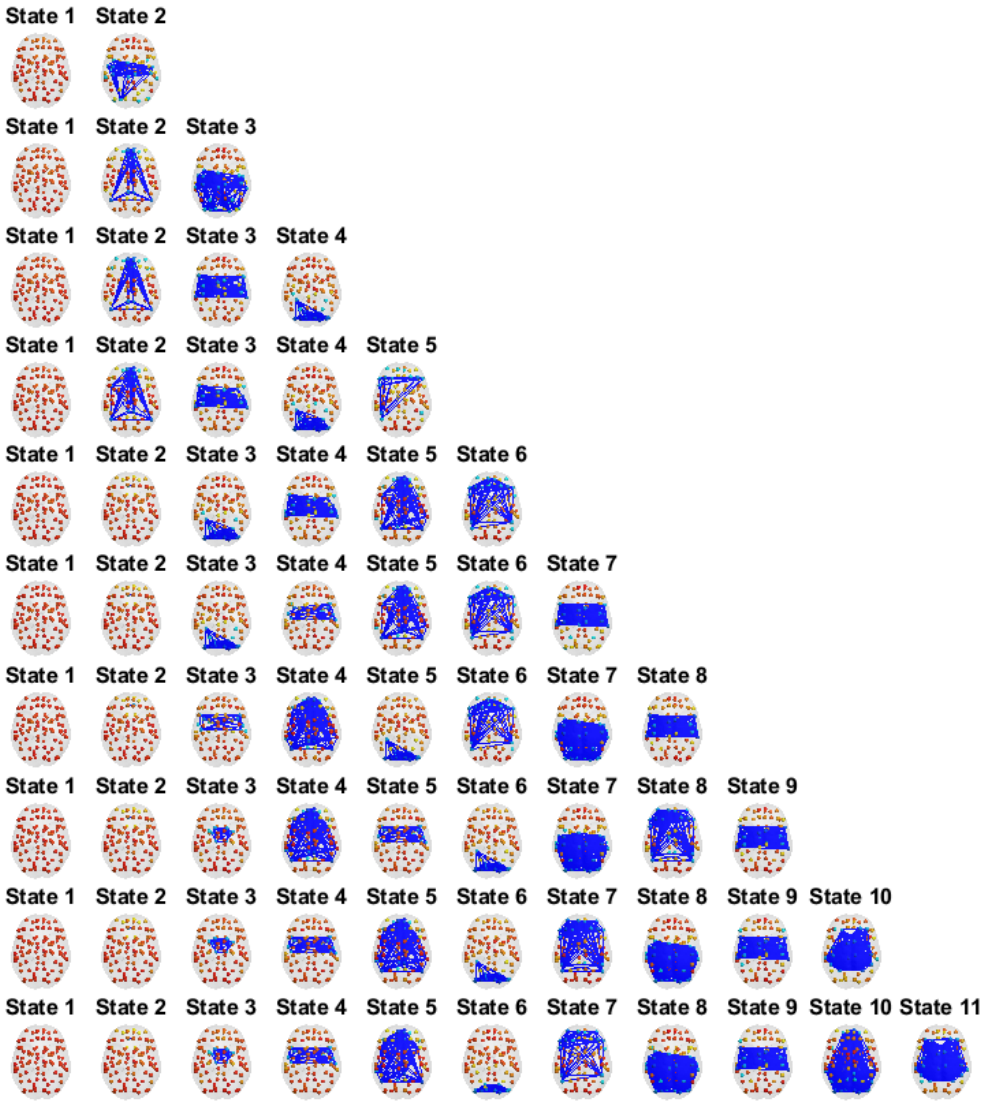

Figure 3.2- Representation of the dFC states obtained by k-means clustering, with k=2, top, to k=11, bottom, in AAL space. The blue links in the cortical representations are plotted between brain regions with a value < −0.1, highlighting the network that contrasts with the global mode.

For example, a dFC state that appears in every k explored is state 1, which is a state of global coherence, aligning with previous studies using this method. [37,38,39] Another state that appears for every k, except k=2, is state 2 (when k=3). This dFC state starts with a small network mainly with regions from the frontal lobe (superior frontal gyrus: orbital part, medial and medial orbital, also gyrus rectus) but including one region from the limbic (posterior cingulate gyrus) and temporal (angular gyrus)

lobes. However, the higher the value of k, the more regions misalign from the rest of the brain and align together forming an extensive network. Therefore, this state appears with additional frontal (inferior frontal gyrus and olfactory cortex), limbic (anterior cingulate, paracingulate gyri and parahippocampal gyrus), parietal (precuneus) and temporal (middle temporal gyrus) areas, for example on state 4 for k=8,9 and on state 5 when k=6,7, 10, 11 and 12.

Additionally, state 3 for k=3, is another example of a network that becomes larger with a higher number of clusters selected. It consists of an extensive network including areas from the frontal, parietal, temporal and occipital lobes, such as precentral gyrus, rolandic operculum, supplementary motor area, insula, cuneus, lingual gyrus, superior, middle and inferior occipital gyrus, postcentral gyrus, superior parietal gyrus, supramarginal gyrus and paracentral lobule. Notably, this state did not appear between k of 4 and 7, though appearing again when k=8 on state 7 and from there reoccurring on every k explored, from 7 to 20, with additional brain regions from the temporal lobe such as fusiform gyrus, heschl gyrus and superior temporal gyrus.

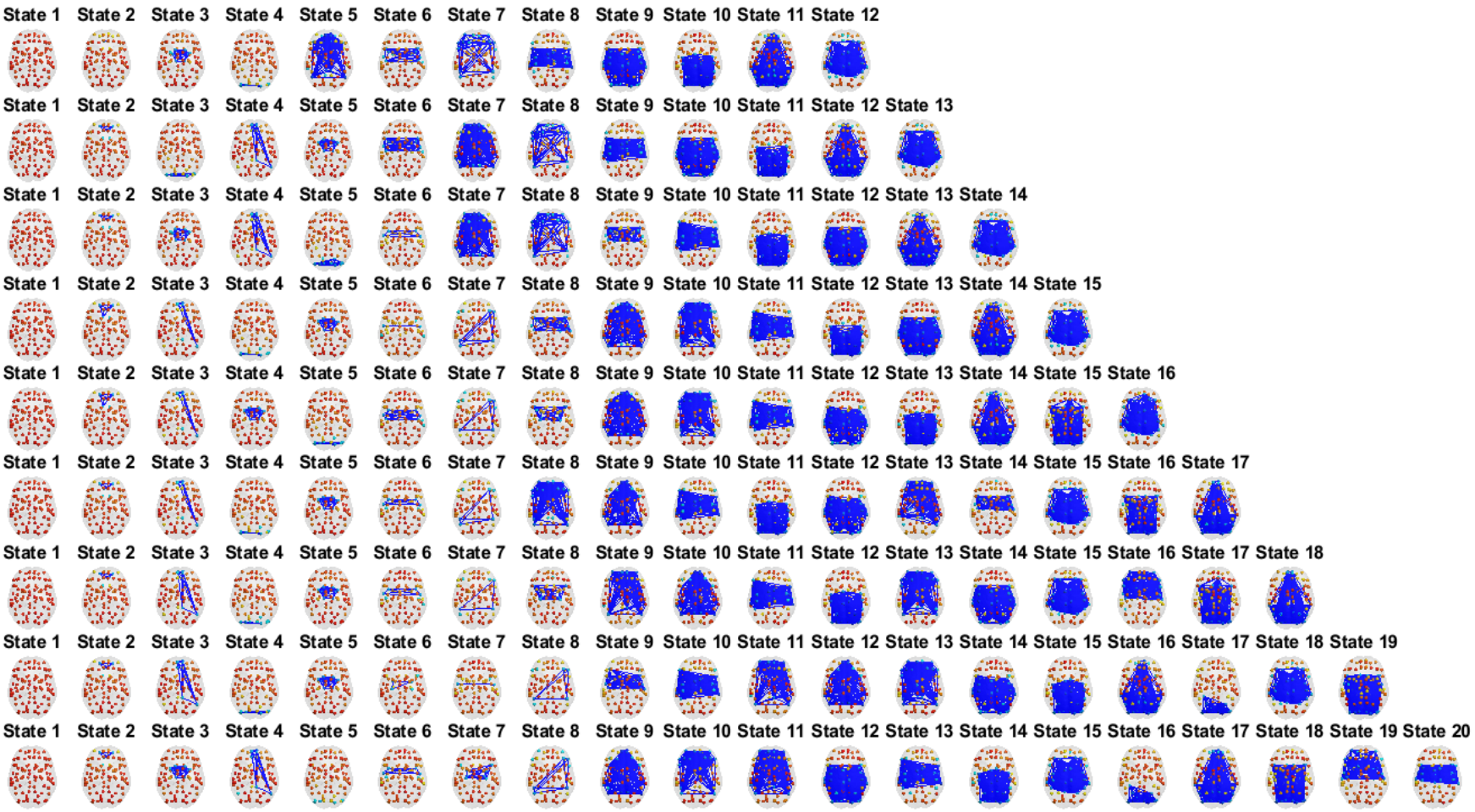

Figure 3.2- (Continued)

3.3 Detection of the most different dFC states

As in this study the aim was to search for dFC states that significantly differentiate SVD patients from healthy controls, the p-values obtained for the between-group comparisons in terms of probability and lifetimes of the k dFC states obtained are presented in figure 3.3. In each model, k hypotheses are tested, therefore, to account for the increased probability of false positives the significance threshold was adjusted to 0.05/k, represented in green dashed line in figure 3.3, using Bonferroni correction.

Most dFC states do not show significant differences between groups, represented in black asterisks falling above the 0.05 threshold (red dashed line), while the p-values marked as red asterisks passed the standard threshold (<0.05) but did not survive the correction for multiple comparisons within each k (>/0.05/k) and are hence considered false positives. In probability, it was found that the clustering returns only one dFC state that significantly differs between SVD patients and controls, falling below the threshold corrected by the number of states within each clustering number, green dashed line. Additionally, in lifetimes it was found two dFC states, within different number of clusters, that showed significant differences between groups ($p<0.05/k$). The blue dashed line refers to the threshold correction if all hypothesis were independent across models, losing statistical power when the hypothesis is not independent, as it is when considering the whole sample of tests performed.

Specifically, for all k, from 2 to 20, dFC state 10 for a k of 10 was the only dFC state that showed significant difference between groups ($p<0.05/k$), occurring more in SVD patients compared to controls. In terms of duration, dFC state 4 for a k of 5 and dFC state 3 for a k of 6 lasted significantly longer ($p<0.05/k$) in SVD patients when compared to controls. Therefore, for the subsequent analysis these dFC states where further explored, whereas for a k of 10 states is in line with previous studies in the resting-state literature. [42, 71]

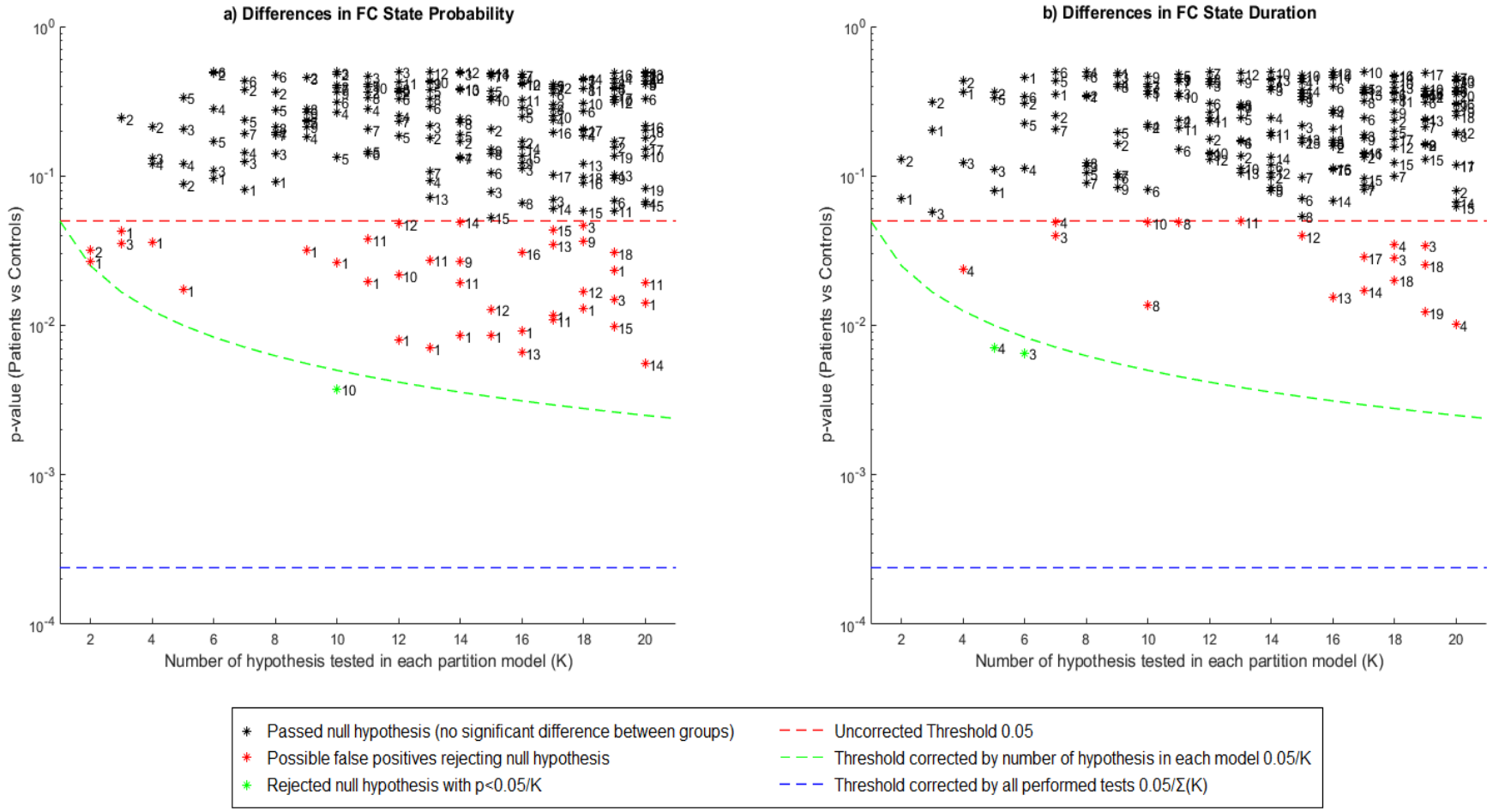

Figure 3.3- Significance of between-group differences in probability of occurrence and lifetime of each dFC state as a function of k. For each k explored (2 to 20), the p-values associated with the between-group comparison between patients and controls in dFC state probability (a) and lifetimes (b) were plotted.

3.4 Relevant dFC states

For k=10, the differences between patients and controls were tested using permutation-based t test and the results are displayed in table 3.1. As we can see on figure 3.4, the only state that showed significant differences in probability between groups ($p<0.05/k$), occurring more in SVD patients (mean probability ± standard error = 0.0415 ± 0.0103) when compared to controls (0.0103 ± 0.0038), was state 10, which consists of a frontal-parietal network. As for lifetime of this state it did not pass the corrected threshold (0.05/k) but did last longer in SVD patients (4.2941 ± 0.5751 seconds) than in controls (2.6042 ± 0.7914 seconds). Another dFC state that fell above the corrected threshold (>0.05/k) but below the standard threshold (<0.05) regarding the state probability was state 1, which occurred more in controls (0.4270 ± 0.0279) when compared to SVD patients (0.3453 ± 0.0289). The same occurred for state 8, in lifetime, where instead patients spent more time (6.4610 ± 0.8334 seconds) than controls (4.2416 ± 0.4324 seconds) in this state.

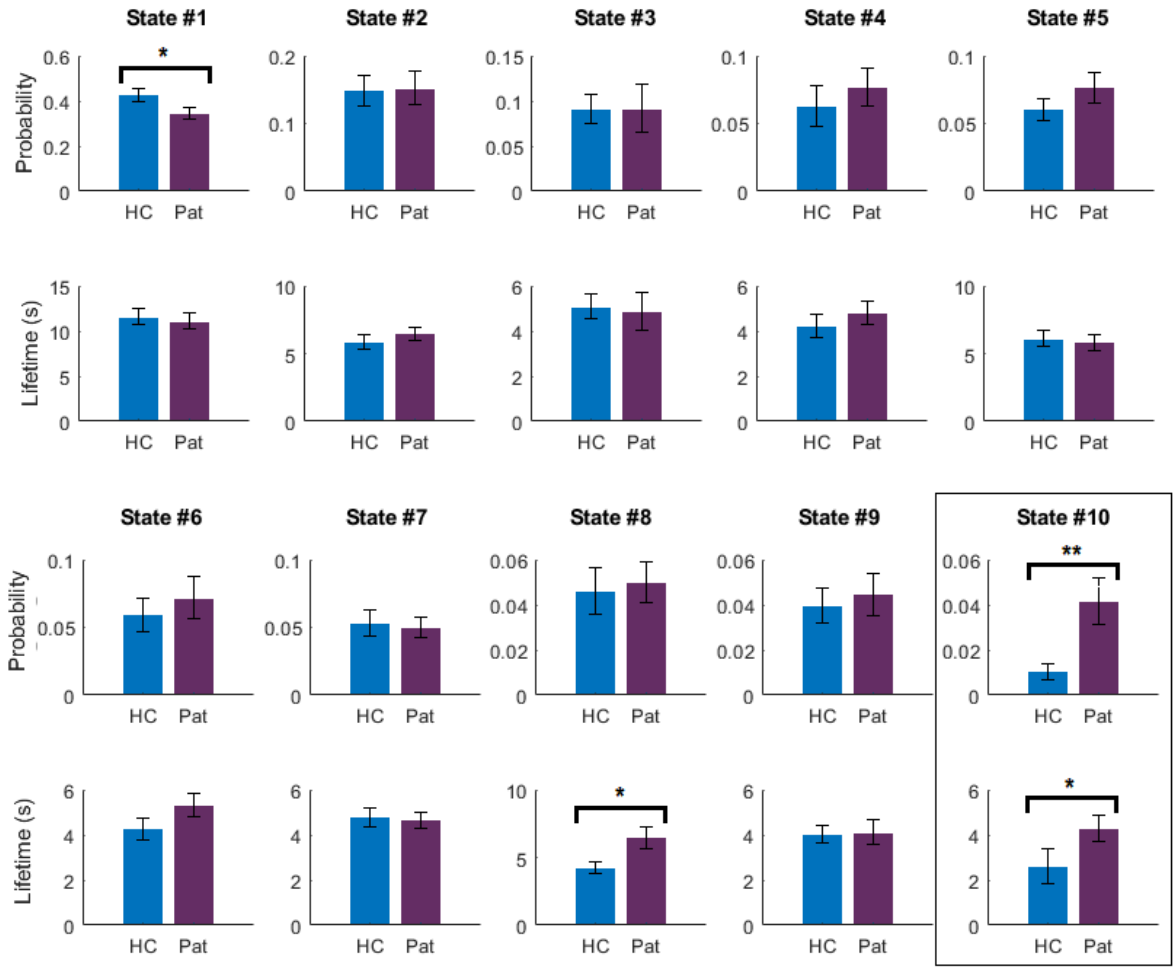

*Figure 3.4 - Probability of occurrence and lifetime of each dFC state, when k=10, for healthy controls and SVD patients. ** Significant group difference after correcting for multiple comparisons. * Significant group difference (only) before correcting for multiple comparisons. Abbreviations: HC = healthy controls; Pat = SVD patients.*

Overall, analysing the mean state probability and lifetimes on a whole-group level, in table 3.1, it was found that subjects spend more time (11.3136 ± 0.6273 seconds) and had more occurrences (0.3791 ± 0.0215) in the state 1, the state of global coherence, and on the other hand state 10 occurred with less probability (0.0286 ± 0.0068) and lower lifetime (3.5948 ± 0.4872) for both patients and controls.

Table 3.1 - Nonparametric permutation-based t tests between groups of the probability of occurrence and the lifetime, for each dFC state when k=10. All p_values are corrected for multiple comparisons. Significant differences are highlighted in bold (p<0.05).

	State 1	State 2	State 3	State 4	State 5	State 6	State 7	State 8	State 9	State 10
Probability (p-values)	0.26	4.80	4.92	2.64	1.33	3.12	3.86	4.03	3.61	**0.03**
Lifetime (p-values)	3.48	2.13	4.08	2.19	3.69	0.81	3.99	0.13	4.64	0.48

The results from figure 3.5, show the representation of the 10 dFC states, when k=10, on AAL space (A), the mean dFC matrix (B) of each FC state obtained by averaging the matrices of all TR's corresponding to each dFC state, the outer product of dFC centroid vector (C), and finally the dFC state centroid vector (D), with indication of the AAL regions. These findings reveal a state of global coherence, state 1, in which the BOLD signals from all brain regions are following the same direction, aligning with previous studies using LEiDA [41, 42, 44].

In addition, as the dFC matrices tells us how coherent paired brain regions are, by analysing the eigenvalues associated to the dFC matrix of each state we can measure the "strength" of each dFC pattern, these values are displayed on table 3.2. We can observe that state 1 has the highest eigenvalue, meaning that its dFC pattern is the strongest from the other 9 states and it represents the state where paired brain areas are the most strongly coherent. Analysing the dFC matrix, on figure 3.5 B, of this global coherence state, it consists of only positive values, represented in red-to-yellow colour, whereas strongly coherent paired regions, with values >0.5, represent ~85.19% of the dFC matrix.

Table 3.2- Mean eigenvalues of each dFC state, representing the "strength" of each dFC pattern, when k=10.

	State 1	State 2	State 3	State 4	State 5	State 6	State 7	State 8	State 9	State 10
Eigenvalues	66.12	60.59	59.68	56.31	55.27	55.82	55.15	55.21	53.61	55.19
std error	0.20	0.26	0.33	0.34	0.30	0.36	0.35	0.36	0.38	0.52

The remaining states, 2 to 10, emerge when the BOLD phases of some brain regions misalign from the rest of the brain and temporarily align together, dividing the brain into two separate functional networks. [34] In fact, when looking to the centroid vectors, on figure 3.5 D, we can see different networks formed on each dFC state and by looking to the negative values, blue bars, and the corresponding brain areas we can evaluate the different regions that belong to these networks. Notably, we can see that they consist of overall symmetric regions and represent different brain subsystems. In state 2 only gyrus rectus opposes the global mode therefore the dFC matrix, with the second higher associated eigenvalue, is mostly composed by positive values (red-to-yellow), meaning that all the regions have temporarily aligned BOLD signals except with the gyrus rectus. In state 3 it is possible to see on its centroid vector a community consisting only of subcortical areas such as caudate nucleus, lenticular nucleus putamen and pallidum and thalamus.

Additionally, state 4 and 9, form similar networks independent from the rest of the brain with regions such as the rolandic operculum, insula, Herschel gyrus, left superior temporal gyrus and temporal pole: superior temporal gyrus. However, state 9 includes extra frontal (precentral gyrus and supplementary motor area), parietal (postcentral gyrus and supramarginal gyrus), temporal (superior temporal gyrus) and subcortical regions (lenticular nucleus putamen and pallidum), forming this way a more extensive network. Interestingly, this state represents the weakest dFC pattern, regarding table 3.2,

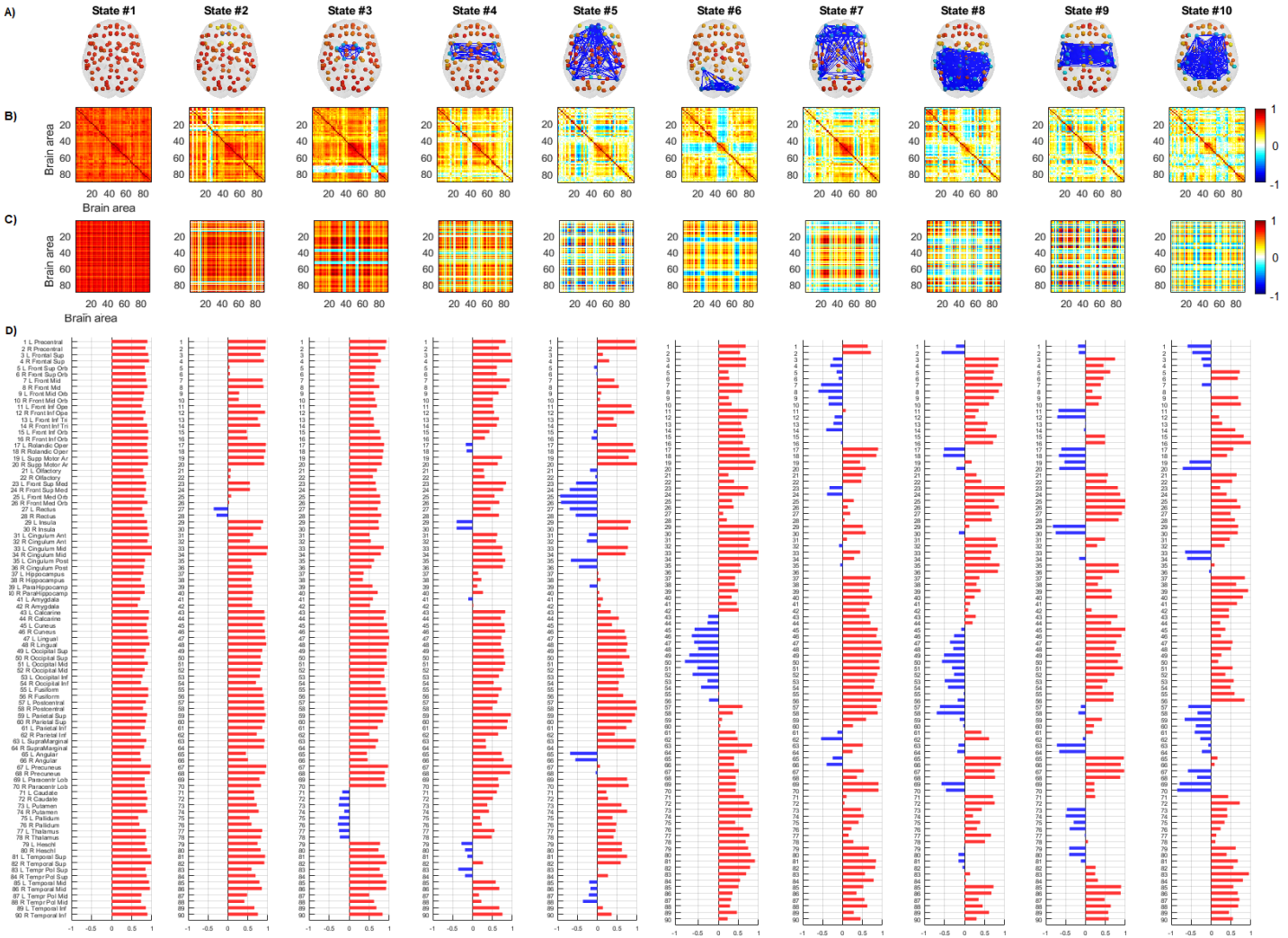

Figure 3.5- dFC states obtained with k-means clustering for k=10. Each state (cluster) is represented in AAL space(A), where functionally connected brain areas (represented as spheres) are colored alike. The spheres colored in cyan/blue spheres, represent areas in the functional network, which are all positively correlated between each other, but negatively correlated with the rest of the brain (yellow, orange, and red). (B) The mean dFC matrix of all TR's correspondent to each state, which reveals for each pair of areas how coherent they are, where 1 (red) means full synchrony and −1 (blue) indicates a phase difference of 180°. (B) The outer product of the centroid vector (C), which reveals the dominant pattern of the dFC matrix, whereas the product of elements with the same sign (positive or negative) is always positive, so negative values in the matrix are between pairs with different signs. (C) The bar plot showing the N elements in the centroid vector (D), representing the projection of the BOLD phase in each brain area into the leading eigenvector. The blue bars represent areas forming the network contrasting from the global mode and bars in red represent the rest of the brain. Further, the magnitude of values indicates the "strength" with which brain areas belong to the dFC state.

and analysing the dFC matrix we can see that it is composed mostly by weakly coherent paired regions, with values >0 and <0.5, representing ~64.26% of the dFC matrix. Additionally, with few regions exhibiting strong coherence between each other, with values >0.5, representing only 3.95% of the dFC matrix.

Regarding dFC state 5, it represents a decoupling mostly of frontal and limbic areas, as well as one region from the parietal lobe and from the temporal lobe. Further, state 6 it is characterized by one functional network comprising occipital areas. In state 7, which is the second weakest dFC pattern, it can be found a network consisting of mainly frontal areas, such as the superior frontal gyrus (dorsolateral, orbital part and medial), middle frontal gyrus and inferior frontal gyrus (opercular and triangular part), but with some regions from the parietal (inferior parietal and angular gyrus) and limbic lobe (anterior cingulate and paracingulate gyri and posterior cingulate gyrus). The dFC matrix of this state is composed mainly by weakly connected brain regions, ~59.67%, still exhibiting paired brain regions with strong coherence between them, with values >0.5 representing ~7.04% of the dFC matrix.

Further, dFC state 8 includes areas mostly from the occipital and parietal lobes. More importantly, state 10 which revealed significant differences between groups, and which first appears when k=10, and from there persist on every k selected, comprises a frontal-parietal network including regions such as precentral gyrus, superior and middle frontal gyrus, supplementary motor area, postcentral gyrus, superior and inferior parietal gyri, supramarginal gyrus and precuneus. From the 10 states this state represents the third weakest dFC pattern, regarding the eigenvalue. Looking to the dFC matrix we can see a pattern mainly composed by weakly synchronized brain regions, with values between 0 and 0.5 representing ~63% of the dFC pattern. Also, we can see that red regions, representing strong coherence between paired brain regions, are scarce. In fact, only ~3.37% of the dFC matrix is composed by strongly coherent BOLD signals, with values >0.5, and this way being the dFC matrix with the lowest number of strongly coherent brain regions, when compared to the other 9 states.

Regarding the dFC states which showed significant differences in lifetimes (displayed on table 3.3 and 3.5): state 4, when k=5, lasted significantly longer in SVD patients (5.9280 ± 0.4144 seconds) that controls (5.0447 ± 0.5397 seconds), as showed on figure 3.6. No other state showed significant differences, only state 1 fell above the corrected threshold (>0.05/k) but below the standard threshold (<0.05) regarding the state probability, occurring with more probability in controls (0.6492 ± 0.0208) than in SVD patients (0.5659 ± 0.0292).

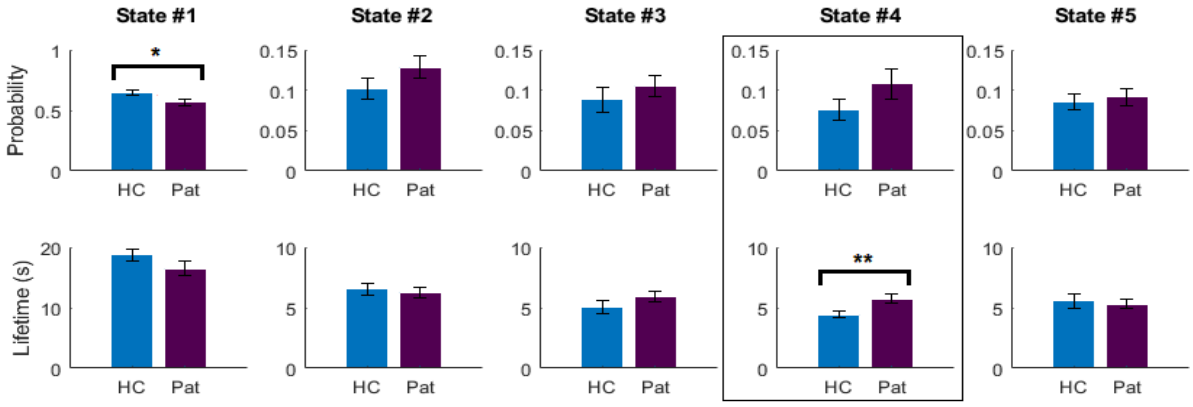

*Figure 3.6- Probability of occurrence and lifetime of each dFC state, when k=5, for healthy controls and SVD patients. ** Significant group difference after correcting for multiple comparisons. * Significant group difference (only) before correcting for multiple comparisons.*

On a whole group level, state 1 continues to be the state with more occurrences (0.6004 ± 0.0204) and with longer duration (17.4184 ± 0.8154 seconds) from all dFC states explored. On contrary, state 5 was the one presenting lowest probability of occurrence (0.0892 ± 0.0074) and state 4 had the lowest lifetime (5.1875 ± 0.2697) regarding all subjects.

Table 3.3 - Nonparametric permutation-based t tests between groups of the probability of occurrence and the lifetime, for each dFC state when k=5. All p_values are corrected for multiple comparisons. Significant differences are highlighted in bold (p<0.05).

	State 1	**State 2**	**State 3**	**State 4**	**State 5**
Probability (p-values)	0.08	0.43	1.02	0.59	1.67
Lifetime (p-values	0.39	1.81	0.55	**0.03**	1.65

In figure 3.7, we can see the representation of the 5 states for k=5. State 4, which showed significant differences between groups in lifetime, is similar to state 6 when k=10. In this state a small network is formed independent from the rest of the brain including regions mainly from the occipital lobe (calcarine fissure and surrounding cortex, cuneus, lingual gyrus, superior, middle and inferior occipital gyrus), with an extra region from parietal lobe (superior parietal gyrus).

This state is represented by an dFC pattern on the middle between the strongest (state 1) and weakest (state 3) of all 5 states, as displayed on table 3.4, and one can highlight that its dFC matrix is the one with more negative values (blue-to-cyan), representing ~25.19% of the dFC matrix, meaning that it is the state with more paired regions with desynchronized BOLD signals when compared to the other 4 states. Yet, is the second dFC pattern, from the other 4 states, with lower number of strongly coherent paired brain regions, whereas values >0.5 represent only 4.54% of the matrix, as state 3 is the dFC pattern with the lowest number of strongly coherent brain regions, ~3.92%, from all the 5 states.

Table 3.4- Mean eigenvalues of each dFC state, representing the "strength" of each dFC pattern, when k=5.

	State 1	State 2	State 3	State 4	State 5
Eigenvalues	64.09	55.72	54.66	55.68	55.48
std error	0.16	0.24	0.26	0.29	0.27

In addition, this state is mostly represented by weakly coherent brain regions, whereas 70.28% of values on the dFC matrix are between >0 and <0.5. Yet, state 5 and 3, which are similar to state 5 and 4, when k=10, respectively, were composed by the weakest coherent dFC patterns, with values of >0 and <0.5 representing 75.90% and 71.83%, respectively, of its dFC matrix.

On figure 3.8 we can see a bar plot representation of the probability of occurrences and lifetimes of the 6 states, when k=6, for healthy controls and patients. Significant differences are noted only for lifetime of state 6, represented inside the black rectangle, exhibiting higher state duration in patients (5.7376 ± 0.3694 seconds) when compared to controls (4.4730 ± 0.2831 seconds). This state has an identical dFC pattern to state 4, when k=5, and to state 6, when k=10, and is composed with the same previously mentioned regions from the occipital lobe that oppose the global mode, except for postcentral gyrus. Moreover, it can also be noted that patients have more occurrences (0.1065 ± 0.0189) in this state than controls (0.0746 ± 0.0121), although significant differences were not found.

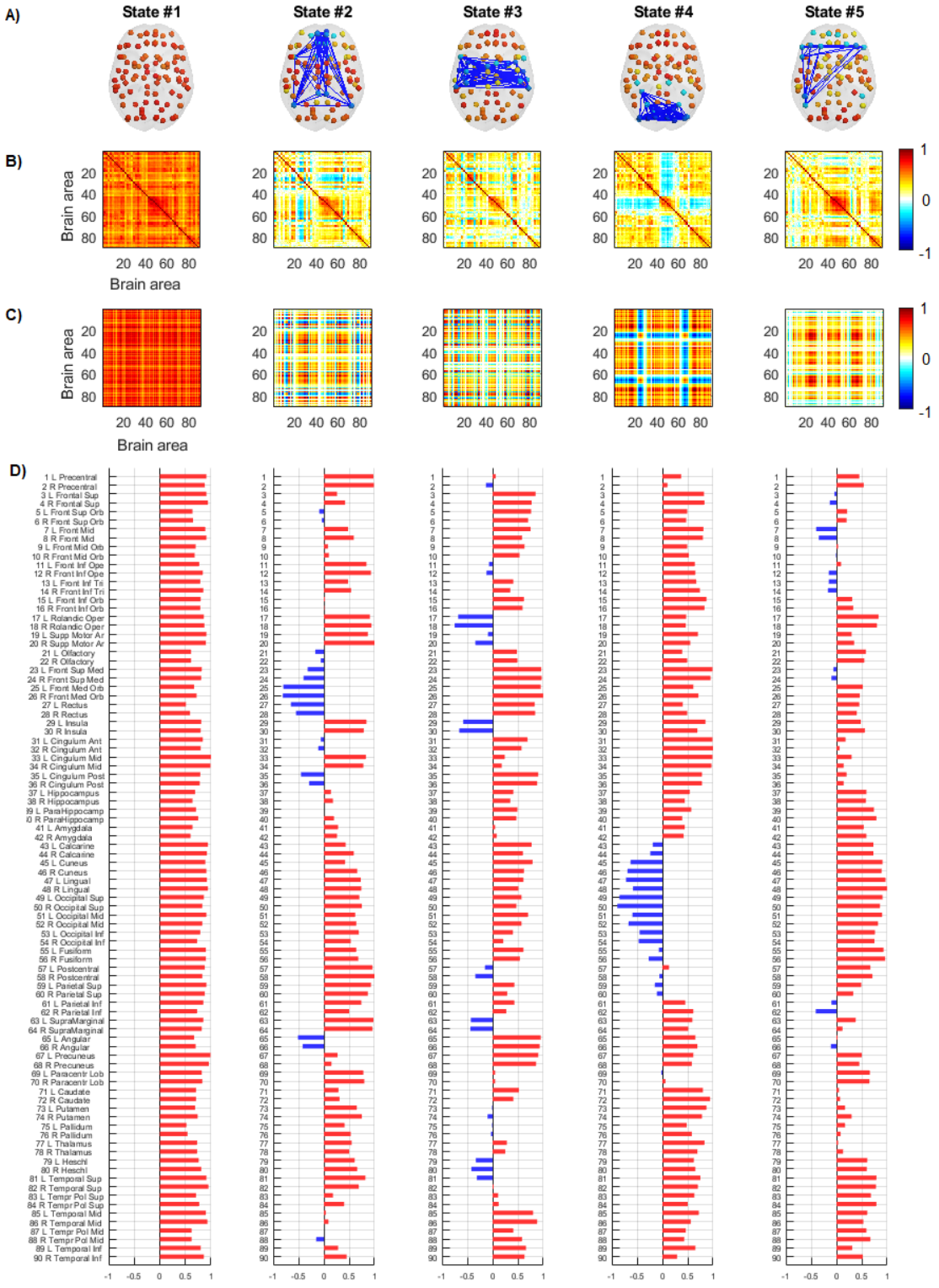

Figure 3.7 - dFC states obtained with K-means clustering for K=5. For each state (cluster) the centroid vector is represented in AAL space (A), the dFC matrix (B), the outer product of the centroid vector (C) and the bar plot of the centroid vector (D).

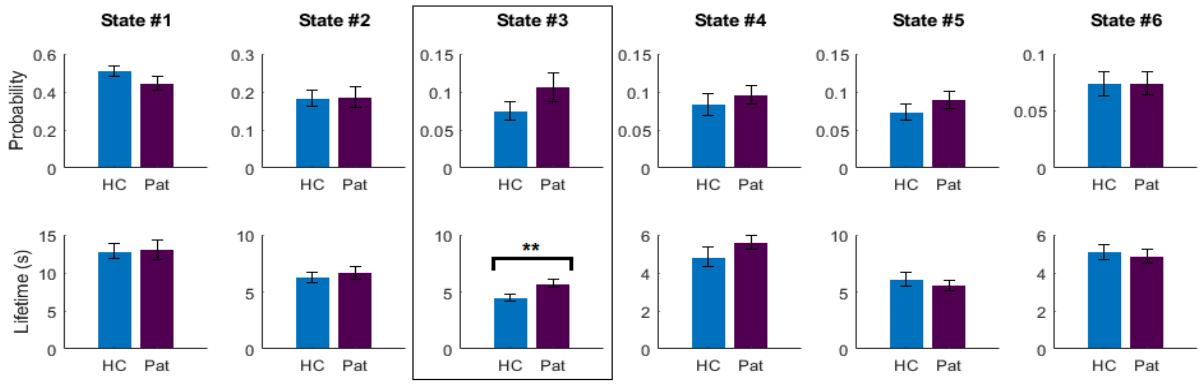

*Figure 3.8 - Probability of occurrence and lifetime of each dFC state, when k=6, for healthy controls and SVD patients. ** Significant group difference after correcting for multiple comparisons. * Significant group difference (only) before correcting for multiple comparisons.*

Analysing on a whole group-level, state 6, which is formed by a small network independent from the rest of the brain, including regions mainly from the frontal lobe, presents the lower probability of occurrence and lifetime for both patients and controls (0.0741 ± 0.0071). On the other hand, state 1 still exhibits the highest probability (0.4731 ± 0.0247) and lifetime (12.9600± 0.8453 seconds) for all subjects.

Table 3.5 - Nonparametric permutation-based t tests between groups of the probability of occurrence and lifetime, for each dFC state when k=6. All p_values are corrected for multiple comparisons. Significant differences are highlighted in bold (p<0.05).

	State 1	**State 2**	**State 3**	**State 4**	**State 5**	**State 6**
Probability (p-values)	0.58	2.92	0.65	1.69	1.02	2.98
Lifetime (p-values	2.75	1.84	**0.03**	0.66	1.34	2.04

Regarding the strength of the dFC patterns, on table 3.6, we can see that state 1 has the strongest dFC pattern, representing a state of global coherence, and also being the preferred state by both groups, whereas state 6, representing the state where both patients and controls had lower occurrences, is the third weakest dFC pattern. When analysing figure 3.9, we can see that the dFC matrix of this state is the one with the higher number of weakly coherent brain regions, with ~72.85% of the values being between >0 and <0.5, whereas strongly coherent brain regions are scares and represent only ~5.42%, with values >0.5.

Table 3.6- Mean eigenvalues of each dFC state, representing the "strength" of each dFC pattern, when k=6.

	State 1	State 2	State 3	State 4	State 5	State 6
Eigenvalues	64.85	59.84	55.71	54.51	55.16	55.36
std error	0.18	0.24	0.29	0.26	0.28	0.29

Still, looking to figure 3.9 one can note that besides state 4, state 2 and 3, when k=5, also reoccur when k=6, as state 5 and 4, respectively, whereas state 4 represents the weakest dFC pattern in line with the results when k=5. It can be noted that, the dFC pattern of state 4 is mostly composed by weakly coherent brain regions (~69.68%) and is the one the less strongly coherent brain regions, with 3.67% of the dFC matrix with values >0.5. As for state 3, that differed between groups, it represented the second state composed with more weakly coherent brain regions, with ~70.46% of the values in the dFC matrix

between >0 and <0.5, whereas strongly coherent brain regions, with values >0.5 represent only 4.49% of the dFC matrix.

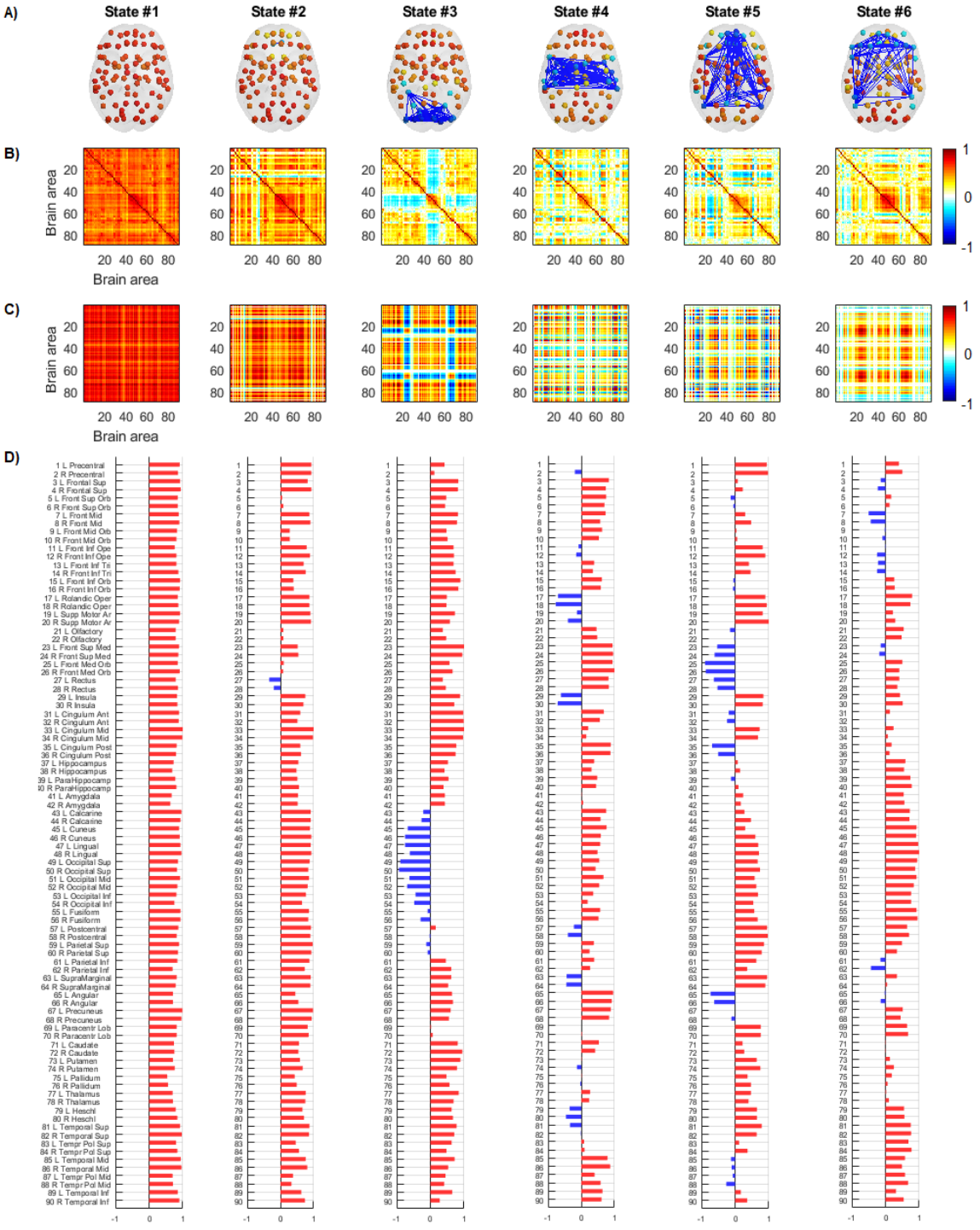

Figure 3.9 - dFC states obtained with k-means clustering for k=6. For each state (cluster) the centroid vector is represented in AAL space (A), the dFC matrix (B), the outer product of the centroid vector (C) and the bar plot of the centroid vector (D).

3.5 Comparison with resting-state networks

As explained before on section 2.3.2, in order to characterize the dFC states that showed significant differences in probability of occurrence and lifetimes between groups, correlation between the centroid vectors from all states, for k=5,6 and 10, and the 7 RSN vectors, represented in figure 3.10, was performed. As previously mentioned, these 7 RSN vectors were obtained by transforming the RSNs defined in [70] by counting the number of $2mm^3$ MNI voxels in each AAL brain area belonging to each of the seven networks. Forming this way, a vector with 90 elements, representing 90 brain regions of the AAL space. Here, as the negative values from the centroid vector, are the ones that represent the network formed independent from the rest of the brain, the RSN vectors were transformed to its symmetric to be compared with the centroid vectors of each state. Moreover, as the global mode, state 1, does not define a brain network, the correlation with the RSNs was not performed for this state.

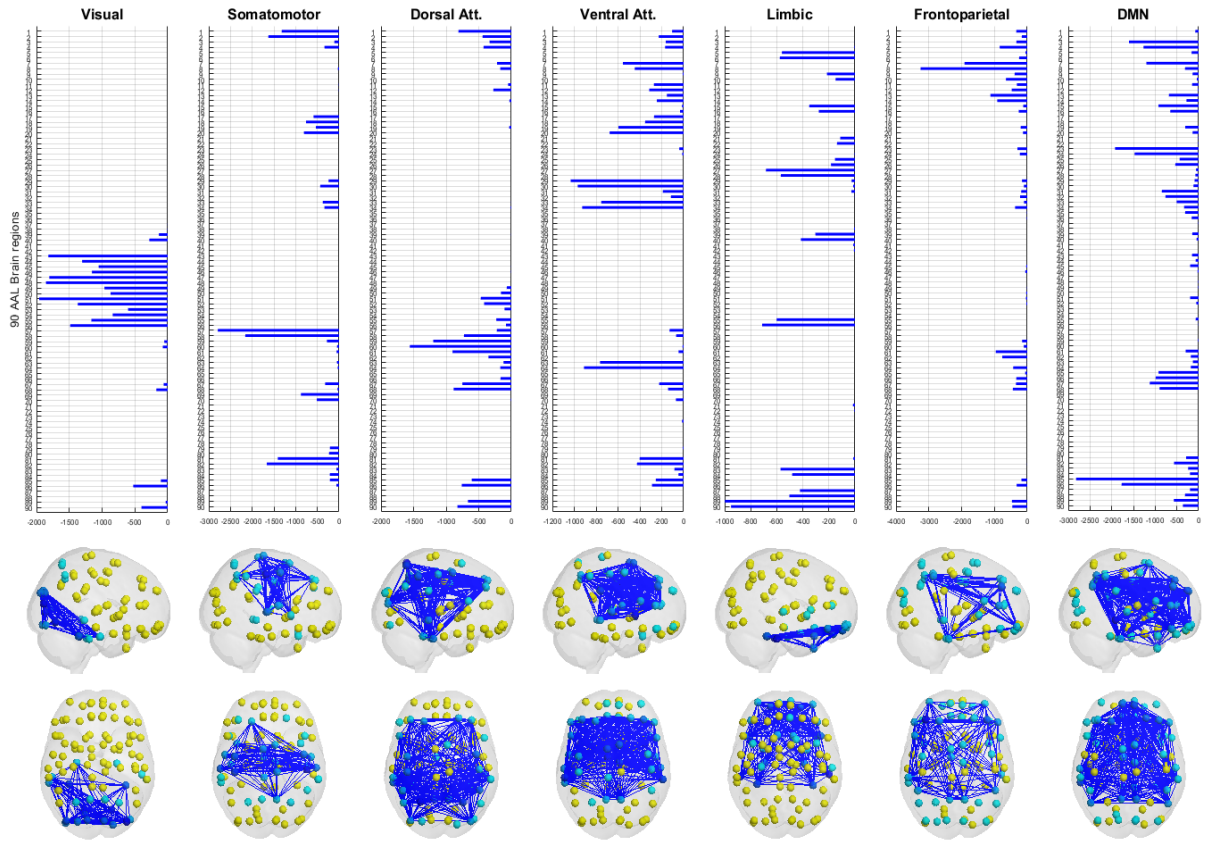

Figure 3.10 – Seven resting-state networks defined in Yeo et al. (2011). On top are represented the vectors of the cortical networks after being transformed into AAL space and on the bottom the representation of each RSN vector in cortical space, from the right (on the top) and frontal (on the bottom) perspective.

On figure 3.11, we can see the representation of state 10, when k=10, which showed significant higher probability of occurrence in SVD when compared to HC. This state, which is mainly formed by regions from the frontal and parietal lobes, significantly overlaps the somatomotor (r=0.49, p-value $=7.6 * 10^{-07}$), the dorsal attention (r=0.39, p-value $=1.2 * 10^{-04}$) and the ventral attention (r=0.30, p-value =0.004) networks. More specifically, analysing the vector of these RSNs, on figure 3.10, it is possible to note that the somatomotor network is mainly composed by regions from the frontal and parietal lobe, yet some regions from the temporal lobe are also present which do not appear on the centroid vector of state 10. Additionally, the dorsal attention network is mainly formed by regions from the frontal, parietal and occipital lobes, although having some regions from the temporal lobe. As for

the ventral attention network, it is mostly composed by regions from the frontal and limbic lobes, including some regions from the parietal and temporal lobe.

Further, analysing the other correlations found on figure 3.11 C), only one state did not show any correlation with the 7 RSNs: state 3, which is composed by subcortical areas such as caudate nucleus, lenticular nucleus putamen and pallidum and thalamus. All these regions belong to the basal ganglia and are not represented in any of the RSNs vectors. Except for this state, every state had at least one significant correlation (p-value<0.01) with one RSN:

- State 2 significantly correlates with the limbic network (r = 0.34, p-value = $9.9 * 10^{-4}$);
- State 4 shows a significant correlation with the ventral attention network (r=0.35, p-value =$6.9 * 10^{-4}$);
- State 5 has a significant correlation with the DMN (r=0.34, p-value = 0.001);
- State 6 significantly correlates with the visual network (r=0.81, p-value =$2.8 * 10^{-22}$);

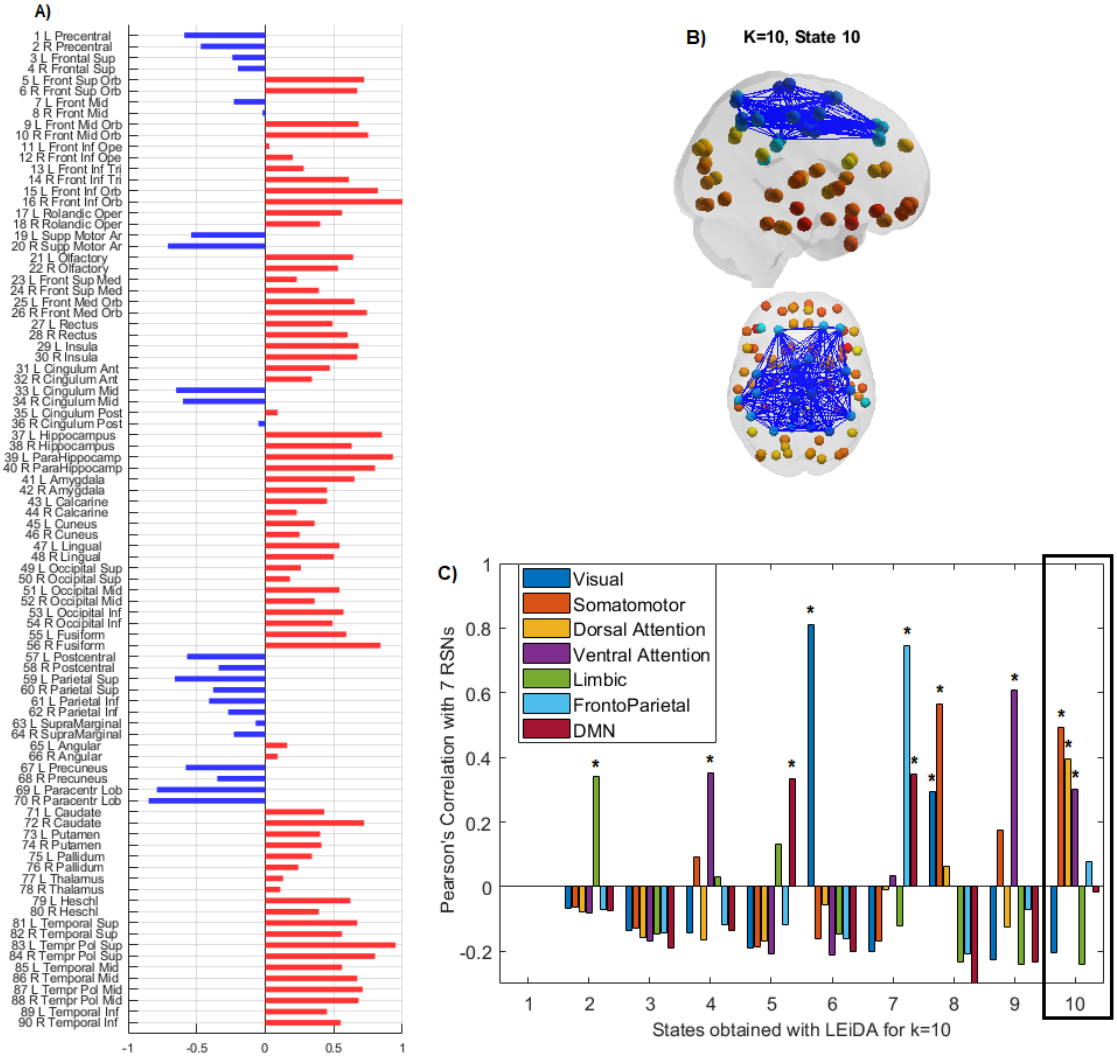

Figure 3.11 – dFC state with a significant higher occurrence probability in SVD vs HC (state 10, for k=10). A) dFC state centroid vector with indication of the AAL regions. B) Representation in AAL space from the right (on the top) and frontal (on the bottom) perspective. C) Pearson Correlation between all centroid vectors obtained with K-means clustering for K=10 and the 7 RSNs defined by Yeo and colleagues [70]. The asterisks indicate significant correlations with p-value < 0.01.

- State 7 shows a significant correlation with the frontoparietal network (r=0.74, p-value $=4.6 * 10^{-17}$) and the DMN (r=0.35, p-value $=8.1 * 10^{-04}$);
- State 8 significantly correlates with the visual (r=0.30, p-value=0.005) and somatomotor (r=0.56, p-value $=7.1 * 10^{-09}$) networks;
- State 9 shows a significant correlation with the ventral attention network (r=0.61, p-value $=1.8 * 10^{-10}$);

When k=5, we can see on figure 3.12 the representation of state 4, which had higher lifetime in patients when compared to healthy controls. This state is composed by regions from the occipital lobe and significantly (p-value<0.01) overlaps the visual network (r=0.81, p-value $=1.27 * 10^{-21}$). In figure 3.11 C), we can note that only state 2 did not show significant correlation with any of the 7 RSNs, yet the limbic network (r=0.16, p-value=0.15) and DMN (r=0.18, p-value=0.08) revealed positive correlations with this state. The other states significantly correlated with at least one RSN: state 3 significantly correlates with the somatomotor (r=0.34, p-value=0.001) and ventral attention (r=0.57, p-value $=4.5 * 10^{-09}$) networks, whereas state 5 shows a significant correlation with the frontoparietal network (r=0.81, p-value $=8.6 * 10^{-22}$).

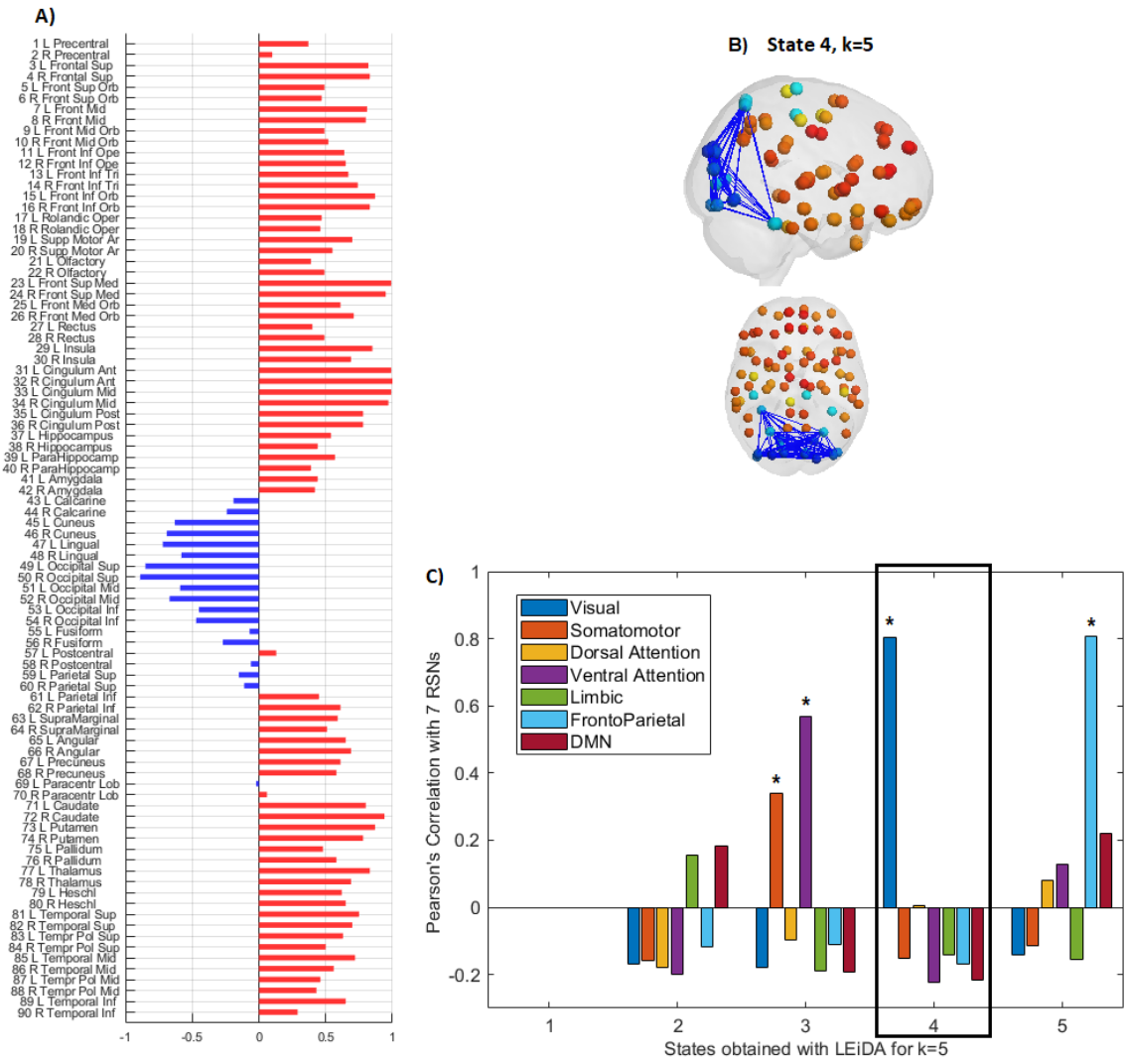

Figure 3.12- dFC state with a significant higher lifetime in SVD vs HC (state 4, for k=5). A) dFC state centroid vector with indication of the AAL regions. B) Representation in AAL space from the right (on the top) and frontal (on the bottom)

perspective. C) Pearson Correlation between all centroid vectors obtained with K-means clustering for K=5 and the 7 RSNs defined by Yeo and colleagues [70]. The asterisks indicate significant correlations with p-value < 0.01.

The representation of state 3, when k=6, can be seen on figure 3.13. This state, which also had a higher lifetime in patients than compared to controls, is the same as the state presented on the previous figure 3.11, and also displayed a significant correlation with the visual network (r=0.81, p-value =$3.43 * 10^{-22}$). The same correlations were also found for states that reappear when k=6, as in case of state 2, when k=5, which appears as state 5 with positive correlation with limbic network (r=0.33, p-value=0.12) and DMN (r=0.31, p-value=0.003). Also, state 3, when k=5, appears on state 4, when k=6, with the same significant correlation with the somatomotor (r=0.38, p-value =$2.02 * 10^{-04}$) and the ventral attention (r=0.57, p-value =$4.22 * 10^{-09}$) networks. Moreover, state 2 has a significant correlation with the limbic network (r=0.34, p-value =0.001) and state 6 significantly correlated with the frontoparietal network r=0.83, p-value =$5.88 * 10^{-24}$).

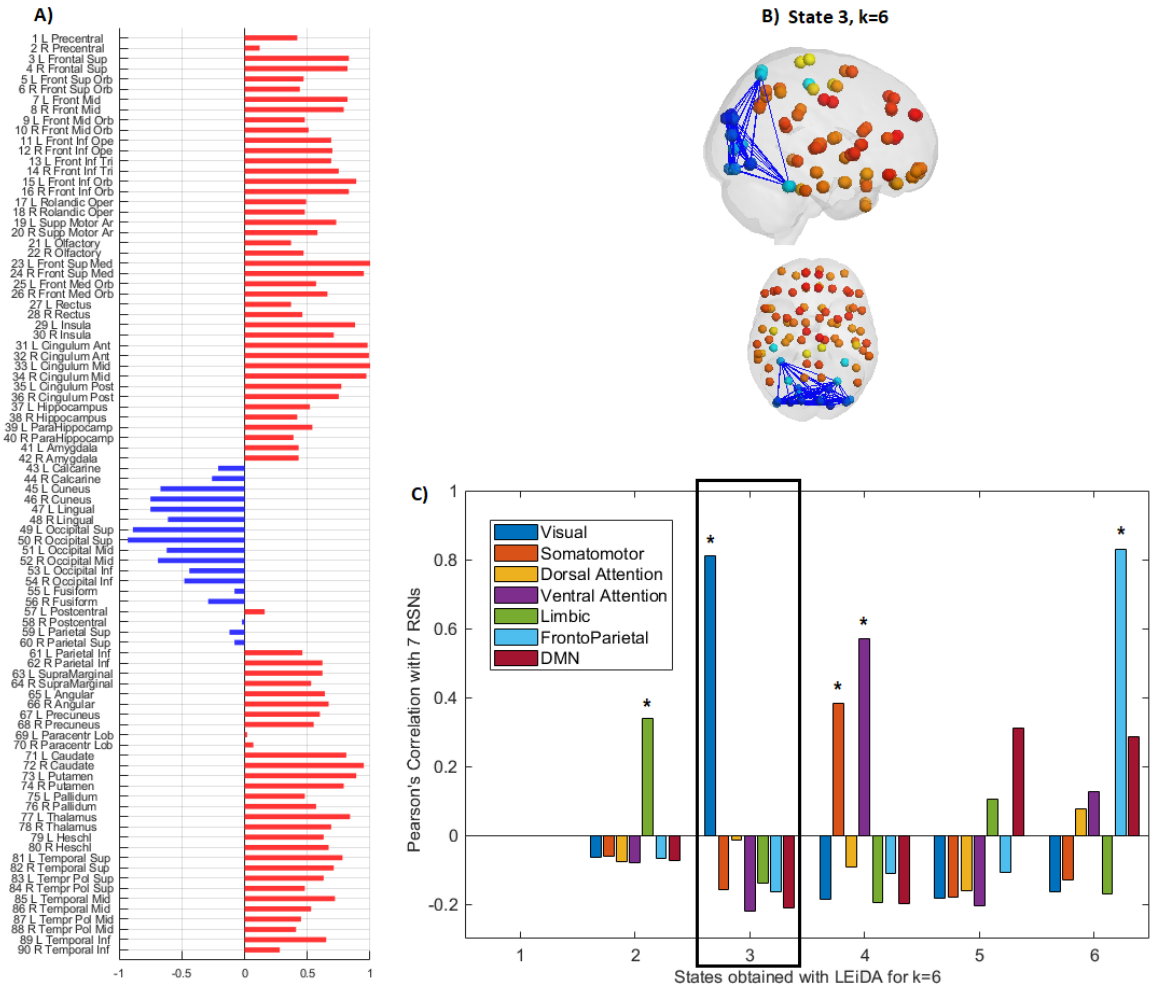

Figure 3.13 - dFC state with a significant higher lifetime in SVD vs HC (state 3, for k=6). A) dFC state centroid vector with indication of the AAL regions. B) Representation in AAL space from the right (on the top) and frontal (on the bottom) perspective. C) Pearson Correlation between all centroid vectors obtained with K-means clustering for K=6 and the 7 RSNs defined by Yeo and colleagues [70]. The asterisks indicate significant correlations with p-value < 0.01.

Importantly, as dynamic functional connectivity is characterized by recurrent connectivity patterns that appear over time and, on the other hand, RSNs are found through static functional connectivity, which analyses the BOLD signal from different regions over a full resting-state scan, it is expected that, although revealing significant overlap with the explored RSNs, the dFC states do not

exactly reproduce these RSNs. Instead the dFC states reveal connectivity between regions of known resting-state networks but also exhibit connectivity with other regions, which may not be found on the static analyse. Moreover, the dFC states can also reproduce sub-portions of common RSNs, as for example, Jones et al. (2012) [72] reported that Alzheimer's disease patients revealed abnormal lifetime in brain functional states with different sub-network configurations of the DMN when compared to healthy controls. Also, [30] identified that a primary node of the default-mode network, posterior cingulate cortex, exhibited variable connectivity with other regions not belonging to the DMN across the scan.

3.6 Switching Probabilities

In figure 3.14, it is represented the switching matrices for patients and controls, containing the mean probabilities of switching from a given state (rows) to any of the other states (columns). In order to easily examine the differences found in the state switching profiles, on the bottom of the figure there is an illustration of the transitions that were significantly different (p-value<0.05) between groups. On a whole-group level, the most common switches were observed from states 2, 4, 5, 8, 9 and 10 toward the global state, first column in the switching matrices. This means that the areas involved in these functional networks realign their BOLD phases with the global signal, returning to the state of global BOLD phase coherence, which is the most prevalent state.

Looking to the significant differences found between groups, it was observed that the probability of transitioning from state 1 to state 10 was significantly higher for patients than controls (6% vs. 0%, p=0.028, uncorrected). This is consistent with the fact that state 10 also had a significantly higher probability of occurrence in patients than controls. The same was found switching from state 2, a state significantly correlated with the limbic network, to state 5, which has a significant correlation with the DMN (15% patients vs. 6% controls, p=0.049, uncorrected). On the contrary, switching from state 1 to state 5 was significantly less frequent in patients than in controls (8% vs. 15%, p=0.026, uncorrected), as well as transitioning from state 2 to state 1 (37% patients vs. 58% controls, p=0.005, uncorrected). Moreover, higher switching probability was observed, transitioning from state 5 to state 7 (16% controls vs. 4% patients, p=0.037, uncorrected), which significantly correlates with the frontalparietal network and DMN, and from state 7 to state 8 (27% controls vs 7% patients, p=0.016, uncorrected), that has a significant correlation with the visual and somatomotor networks. Therefore, the trajectories which had higher probability of switching for controls than patients might suggest that patients have decreased ability to access these states.

The switching probabilities were also calculated for k=5 and 6, where significant differences in lifetimes between patients and controls where found. On a whole-group level, and like in k=10, the most common switches were found from all 5 states, when k=5, and from the 6 states, except for state 5, when k=6, toward the global state, which is the most prevalent state. When k=5, only one significant difference (p>0.05) was found between groups, transitioning from state 2 to state 3, significantly correlated with the somatomotor and ventral attention networks, which was more frequent in patients than controls (29% vs. 13%, p=0.0043, uncorrected). As for when k=6, significant differences were identified switching from state 1 to state 2 (41% controls vs. 35% patients, p=0.04, uncorrected) and from state 2 to state 1 (66% controls vs 49% patients, p=0.03, uncorrected). On the other hand, significant higher switching probabilities in patients when compared to controls were observed transitioning from state 2 to state 4, which significantly correlates with the somatomotor and ventral attention networks, (12% vs. 4%, p=0.02, uncorrected), from state 5 to state 1 (13% vs 5%, p=0.03, uncorrected) and from state 5 to state 3 (31% vs. 16%, p=0.02, uncorrected). This might suggest that patients have an increased ability to switch from a state positively correlated with DMN and the limbic network towards state 3 significantly

correlated with the visual network, which is a state that presented significant higher lifetime for patients when compared to controls.

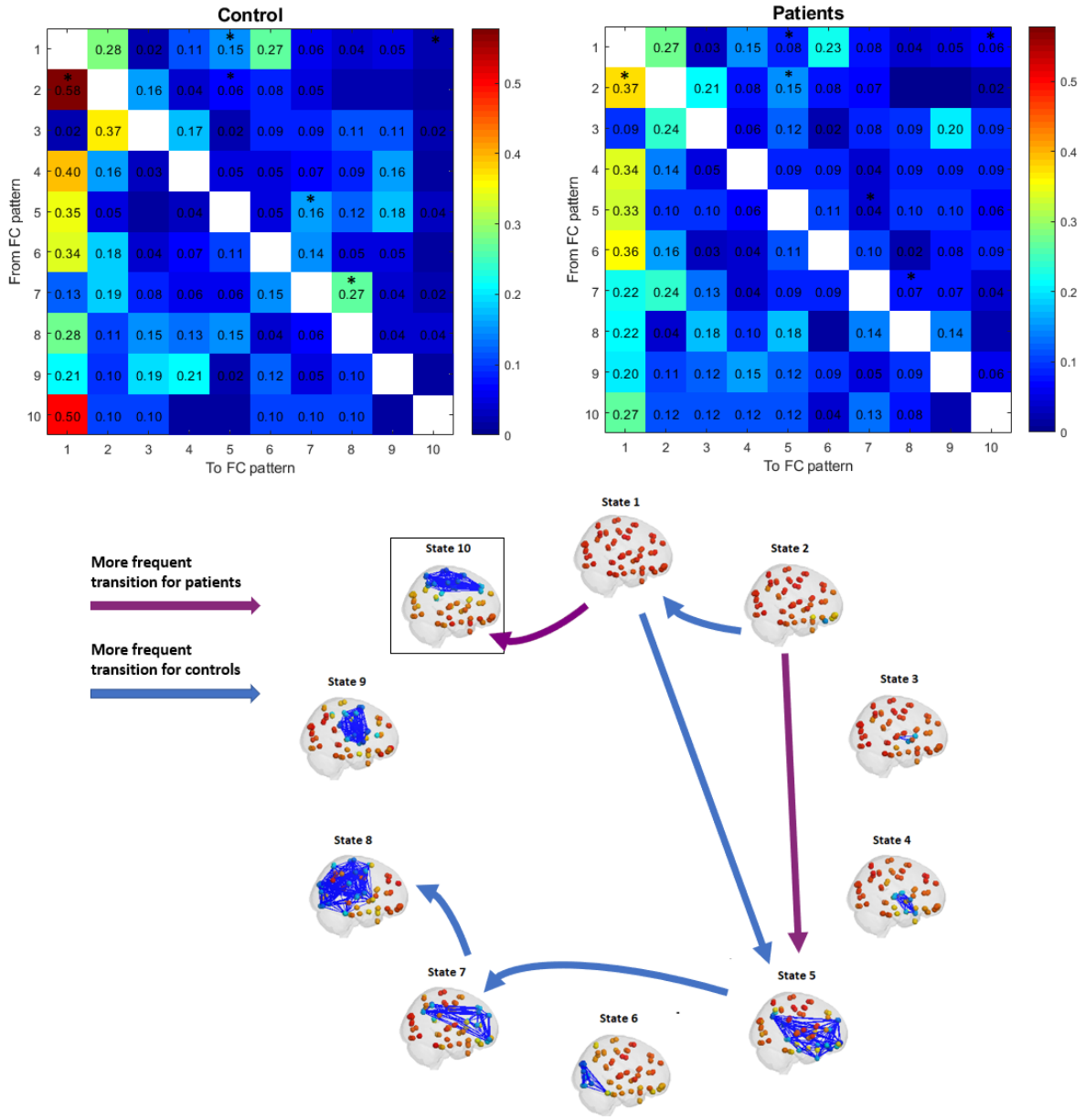

Figure 3.14 – Switching Probabilities for controls and SVD patients, when k=10. Top: Switching matrices showing the probability of transitioning from a given state (rows) to any of the other states (columns). Significant differences between groups assessed via a permutation test are indicated by asterisks (*) for the significance threshold $\alpha_1 = 0.05$*. Bottom: Significant differences (p-value<0.05) found in transition probabilities between groups are represented in arrows, whereas blue arrows represents a state-to-state transition that was significant more frequent in controls than in patients. Inside the black box is state 10, which displayed significant differences between groups in the probability of occurrence.*

3.7 Correlation of dFC features with neurophysiological tests

In order to determine whether the abnormal dFC found on this work could be biomarkers of cognitive decline caused by SVD, Spearman rank correlation analysis between the scores of neuropsychological tests, displayed on table 2.2 on section 2.2, and the probabilities of occurrence of state 10, when k=10, which displayed significant differences between groups, was performed. In figure 3.15 it is represented the correlation's results and we can see that no significant correlation ($p<0.05$) was found, however all cognitive domains showed negative correlations with the probability of occurrence of this weakly connected state, meaning that overall worse performance was associated with more occurrences in this state.

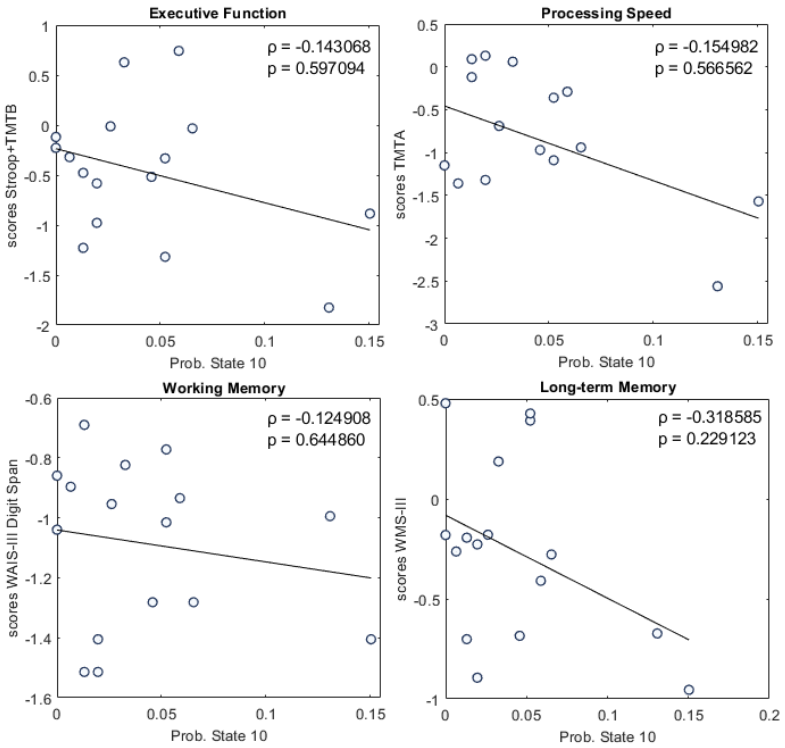

Figure 3.15 – Spearman rank correlation analysis between cognitive scores on the four domains (executive function, processing speed, working memory and long-term memory) and the probabilities of occurrences of state 10 across SVD patients. The associated Spearman's rank correlation coefficients (ρ) and uncorrected p-values (p) are also displayed.

In addition, Spearman rank correlation was also performed between the switching probabilities to and from the state 10, when k=10, and the cognitive scores, in the four domains (executive function, processing speed, working memory and long-term memory) . Significant correlations (p-value<0.05) were found only between for processing speed domain and the probabilities of switching from state 1 to state 10, which showed significant differences between groups (more frequent in patients than in controls), and from state 10 to state 1.

Analysing fig. 3.16, we can see that switching from state 1 to the weakly connected state 10 is negatively correlated with the processing speed domain, meaning that switching more frequently from state 1 to state 10 is significantly associated with worse performance on the processing speed test. On the contrary, higher probability of switching from state 10 to state 1, the state of global coherence, was significantly associated with better performance in this test. Further, no other significant correlation were found, however we can note that overall, except for the executive function domain, positive correlations were found between switching from state 10 to state 1 and the other cognitive scores (second and forth row of figure 3.16) which could mean that switching more from the weakly connected state to

the state of global coherence could be associated with overall better performance. And on the other hand, negative correlations were found between the probability of switching from state 1 to state 10 (first and third row on figure 3.16) and all four domains, meaning that overall worse performance was associated with higher probability of switching from the global coherence state to the weakly connected state which differentiated patients from controls.

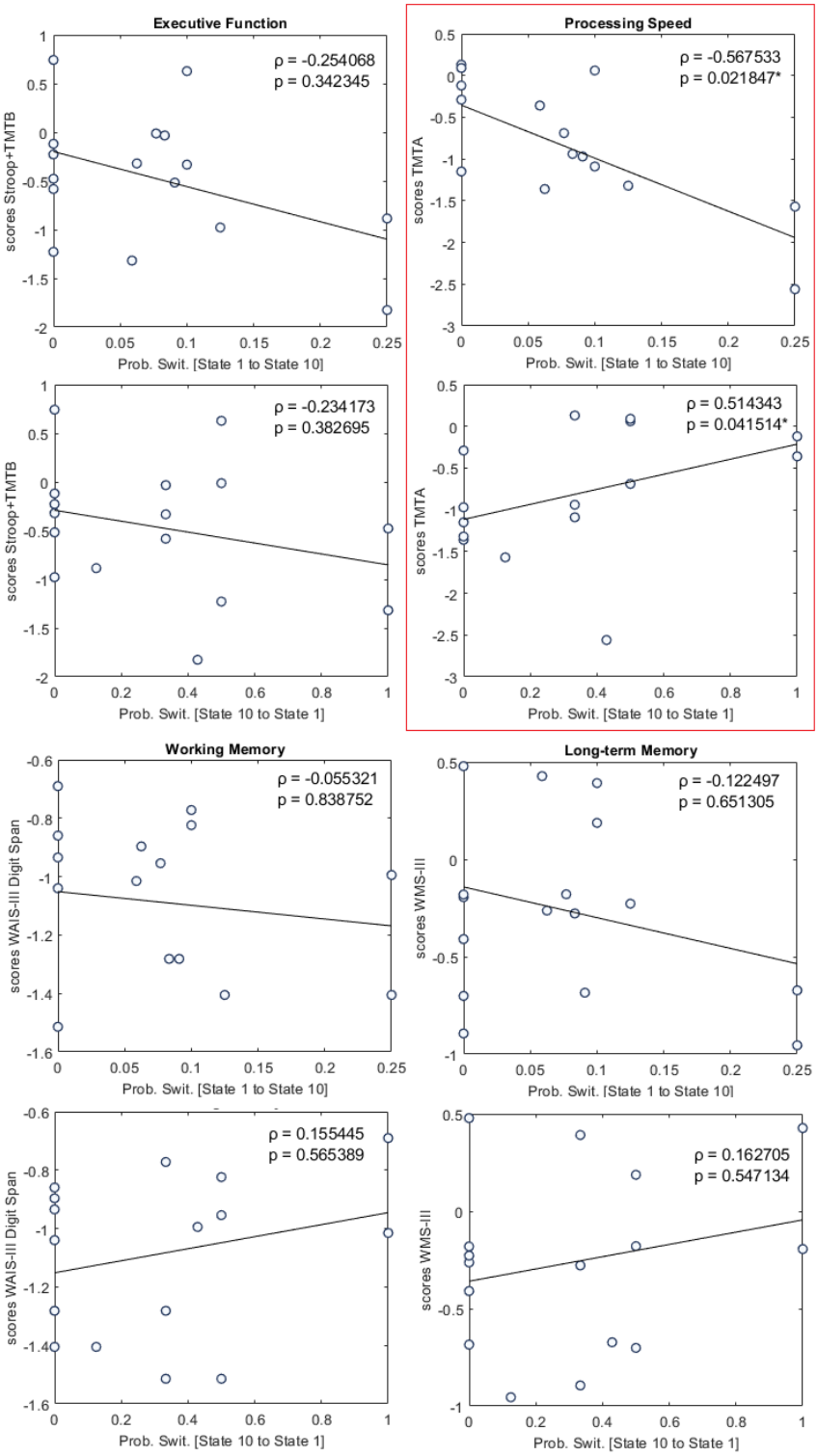

Figure 3.16 – Spearman rank correlation between the cognitive scores on the four domains and the probability of switching from state 1 to state 10 (first and third row) and from state 10 to state 1 (second and forth row), when k=10, across SVD patients. The associated Spearman's rank correlation coefficients (ρ) and uncorrected p-values (p) are also displayed. Significant correlations in a red box.

One can also note that 6 patients did not switch from state 1 to state 10, however all of these patients entered state 10 (mean probability of occurrence ± standard deviation error = 0.0174 ± 0.0089), yet patients with higher probability of switching from state 1 to state 10 had more occurrences on this weakly connected state (0.0582 ± 0.0149). The same was found when switching from state 10 to state 1, with more switches related to more occurrences on this global coherence state. Thus, switching more frequently from state 1 to state 10 and having more occurrences on this weakly connected state could be related to worse cognitive performance on the processing speed test, whereas switching more frequently from state 10 to state 1 and having more occurrences on the state of global coherence could be associated with better performance on this cognitive domain. Moreover, correlations between the probability of occurrences/lifetimes of all dFC states and the cognitive scores in the 4 domains was also performed, but no significant correlations were found.

3.7 Correlation of dFC features with SVD lesion maps

To test if damage to structural connections could predict functional connections, lesions on major WM tracts were explored and correlated with abnormal dFC features found in this work. On fig. 3.17 it is displayed the distribution of the lesion probability, across patients, in each of the 11 ROIs obtained from the JHU-ICBM-tracts atlas. We can see that SVD patients present zero lesion probability on WM tracts such as cingulum (cingulate gyrus) and cingulum (hippocampus). Moreover, only one patient presented lesion in the superior longitudinal fasciculus (temporal part) and lesion in the uncinate fasciculus was found only for four patients. Thus, for this reason these ROIs were not used for further correlations.

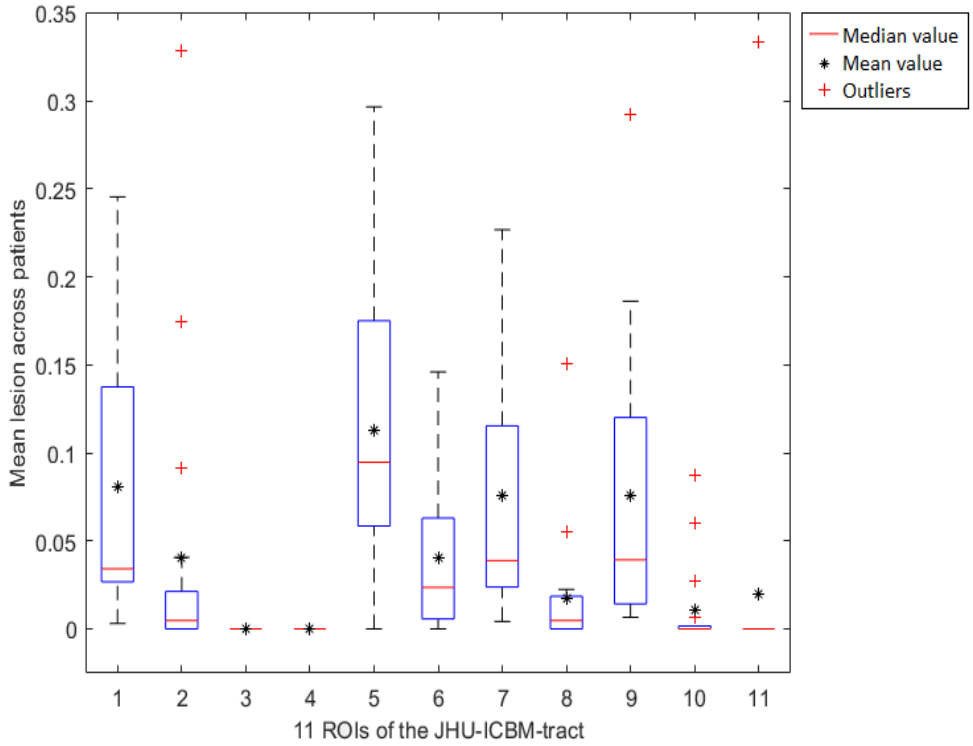

Figure 3.17 - Distribution of the lesion probability in each ROI across all SVD patients. ROIs: 1- Anterior thalamic radiation; 2- Corticospinal tract; 3- Cingulum (cingulate gyrus); 4- Cingulum (hippocampus); 5- Forceps major; 6- Forceps minor; 7 - Inferior fronto-occipital fasciculus; 8- Inferior longitudinal fasciculus; 9- Superior longitudinal fasciculus; 10- Uncinate fasciculus; 11- Superior longitudinal fasciculus (temporal part).

As for the other WM tracts explored, forceps major, which is a white matter fiber bundle providing connections between the occipital lobes [77], was the one that displayed the highest mean lesion probability across patients (mean= 0.1132, standard deviation error= 0.0201, median= 0.0947). This was followed by: anterior thalamic radiation (mean= 0.0810, standard deviation error= 0.0203, median= 0.0341), which connects anterior and mediodorsal thalamic nuclei with frontal and cingulate cortices and runs through the anterior internal capsule [78], and the superior longitudinal fasciculus (mean= 0.0760, standard deviation error= 0.0193, median= 0.0392), a major association pathway that connects frontal, parietal, and temporal association cortices [79].

Then, the longest associative bundle and which connects various parts of the occipital cortex, temporo-basal area and the superior parietal lobule to the frontal lobe [80], the inferior fronto-occipital fasciculus (mean= 0.0758, standard deviation error= 0.0199, median= 0.0388), forceps minor (mean= 0.0407, standard deviation error= 0.0111, median= 0.0235), which is a pathway connecting the bilateral frontal regions and the corticospinal tract (mean= 0.0406, standard deviation error= 0.0211, median= 0.0047) which connects the cortex to the spinal cord and originates primarily from the frontoparietal cortices, including the primary motor cortex, secondary motor area, and somatosensory cortex [81]. Finally, the inferior longitudinal fasciculus (mean= 0.0177, standard deviation error= 0.0090, median= 0.0047), a long-range white matter pathway that primarily connects the occipital lobe of the brain with the anterior temporal lobe. [82] On figure 3.18 we can see the overlap between the sum of the binary WM lesion maps of SVD patients, represented with a hot colormap (red to yellow) with some transparency, with these WM tracts, represented in blue.

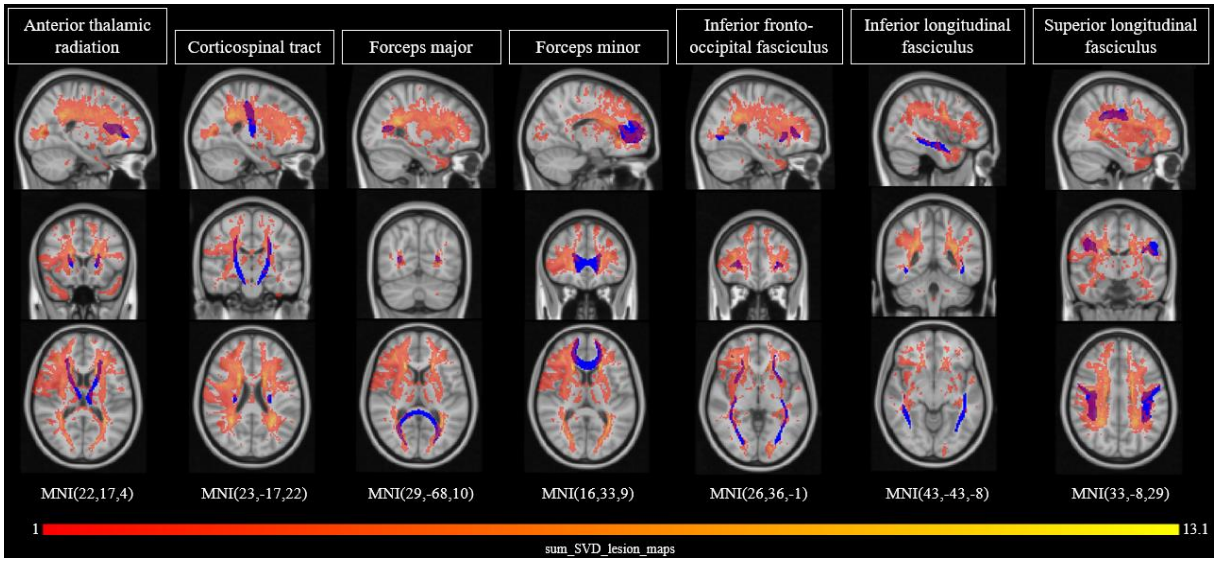

Figure 3.18- Overlap of the sum of the patients WM lesion maps, represented with a hot colormap, with the WM tracts used for further correlation, represented with a blue colormap, along the 3 anatomical planes (sagittal, coronal and axial). On the bottom are shown the coordinates (in mm) corresponding to x,y,z in the standard MNI152 space.

Therefore, major pathways connecting regions within the occipital lobe and between frontal, parietal, and temporal cortices are mostly disrupted on these patients. In figure 3.19, we can see the results of the correlations between the abnormal probability of occurrence of the fronto-parietal state (state 10, for k=10) and the subject's lesion probability on these WM tracts, with the associated Pearson's correlation coefficient and p-value displayed in the figure. Although no significant correlation was found, we can see that WM tracts with the highest lesion probabilities, such as anterior thalamic radiation, inferior fronto-occipital fasciculus and superior longitudinal fasciculus, have a positive correlation with the probability of this state, meaning that more lesions in these WM tracts the greater the presence on this weakly connected state. On the other hand, the forceps major, which is the WM

tract with the highest mean lesion probability across patients, had a negative correlation with this state, which could mean that higher lesion probability in this WM tract was associated with overall lower state probability of this weakly connected state.

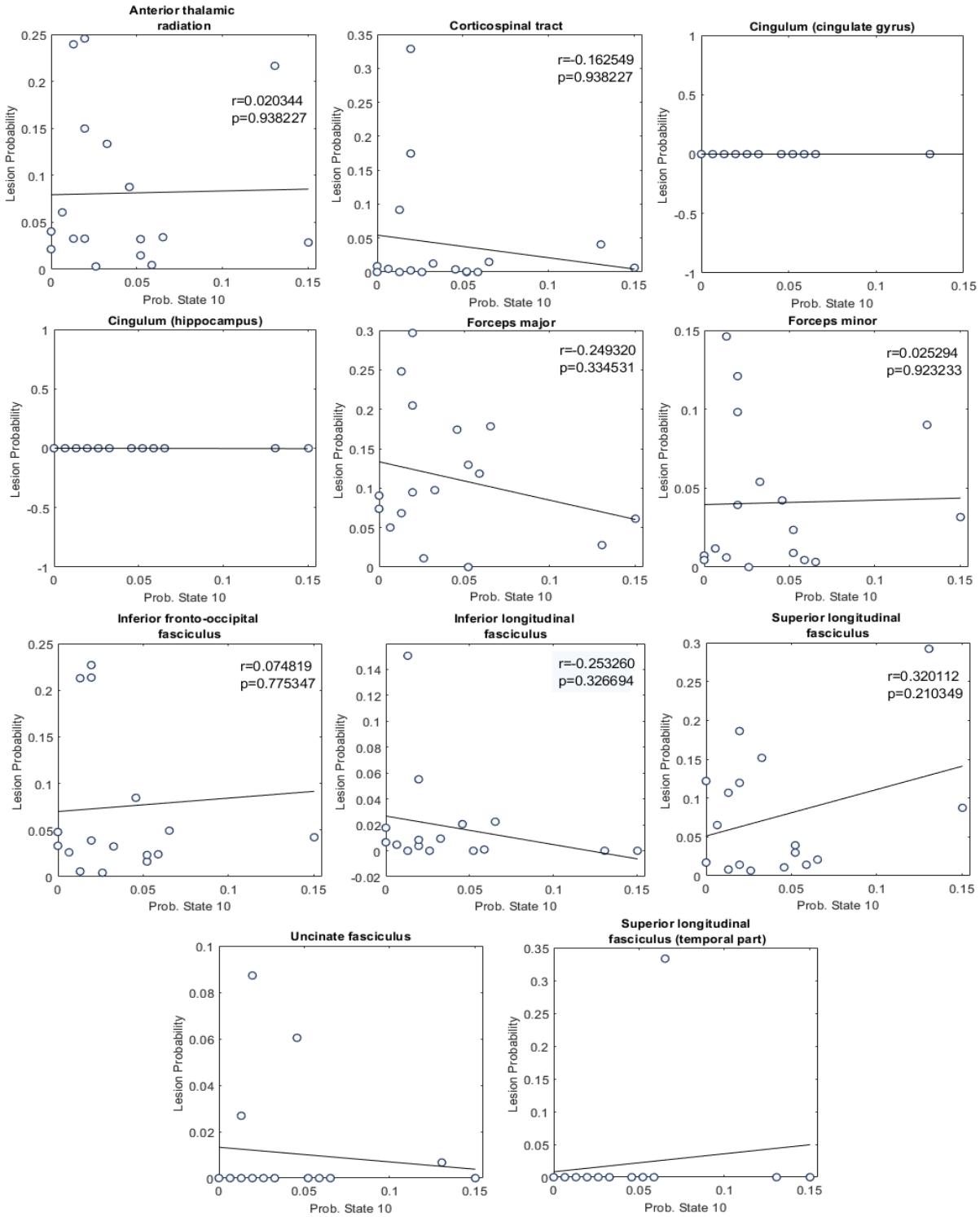

Figure 3.19 – Pearson correlation between the lesion probability of all WM tract, except for those mentioned above, and the probability of occurrence of state 10, which was significantly different between groups. WM tracts which did not enter the correlation are also represented here on a scatter plot with the probability of occurrence of state 10. The associated Pearson's correlation coefficient, r, and p-values, p, are also displayed. P-values displayed here are not corrected for multiple comparisons.

Further, Pearson correlation between all of the other state probabilities from all k explored, as well as with other dFC features, such as lifetimes and switching probability from and to state 10, and the lesion probabilities of the WM tracts mentioned above, was also performed. However, no significant correlations, after correction for multiple comparisons.

Chapter 4
Conclusions

In the present study, we investigated differences in dFC states reoccurring over time during resting-state in 17 SVD patients compared with 11 healthy controls, in order to determine whether these alterations could be associated with the disease and associated cognitive deterioration and hence whether they could provide a valuable clinical biomarker to predict disease progression. We found that patients had an increased probability of occurrence of an dFC state, consisting mainly of frontal and parietal areas, when compared to controls, as well as a significant higher duration in two dFC states, consisting of occipital areas.

This frontal-parietal state, which differed between patients and controls, reveals an extensive network of clinically relevant areas, including key regions from the somatomotor network (precentral gyrus, supplementary motor area, postcentral gyrus and paracentral lobule), dorsal attention network (superior frontal gyrus, dorsolateral; superior parietal gyrus; inferior parietal, but supramarginal and angular gyri and precuneus), and ventral attention network (middle frontal gyrus, median cingulate and paracingulate gyri and supramarginal gyrus). As for the occipital states, exhibiting differences between groups in lifetimes, was significantly correlated with the visual network. Therefore, this study was able to provide a new insight for detecting network abnormalities related to SVD.

4.1 Discussion of the results in relation to the literature

Some of these networks have been identified in FC studies as affected in SVD patients, but also in subjects with cognitive impairments and with Alzheimer's disease (AD), which have been highly associated with cerebral SVD. [83, 84] The dorsal attention network (DAN) [17, 85] and the frontoparietal network [17, 52, 86], which play an important part in goal-directed attention and executive functions, have been reported in neuroimaging studies as two commonly affected networks in SVD. These findings suggest that damage to long association fibres, caused by SVD, can manifest as abnormal FC between major nodes of the attention networks and have been related to an increase degree of cognitive impairments. [3, 85] Further, [87] reported abnormal FC in the somatomotor network, DAN and ventral attention network (VAN) in subjects with mild cognitive impairment and AD.

Converging evidence has suggested that attentional impairment is also an early clinical manifestation of patients with dementia. Even poor initial performance of attention and executive function were better predictors than tests of memory for distinguishing patients with mild AD and normal aging. [88, 89] Optimal attention performance depends on the DAN and VAN, whereas DAN includes dorsal fronto-parietal areas and is responsible for endogenous attention orienting process and the VAN, composed by ventral frontal-parietal areas, is involved in stimuli-driven attention processes. [86] Previous studies regarding attention networks, found that gray matter volume reduction in the frontal cortex contributed to the reduction of effective connectivity in frontal-parietal circuits in attention control for patients with AD. [90] Also, abnormal FC in both DAN and VAN has been found in patients with amnestic mild cognitive impairments [92] and AD [91, 92], which could serve as a sensitive and specific biomarker to distinguish AD from normal controls.

In addition, [93] explored altered functional connectivity based on previously well-defined brain areas that comprise key functional systems, such as the sensorimotor network (SMN) and DAN, in AD

patients with mild cognitive impairment compared with controls. It was found significantly impaired connectivity within the SMN and between DAN-SMN in AD patients. As, the DAN is one of the networks that is related to cognitive functions and the multiple somatosensory integrations of sensory, motor and cognitive systems provide the signals for the organism to perceive and respond to its environment, impairments on any of these components would lead to deficits in function at the clinical level. [93] Moreover, signs of aging usually include decrease attention, sensory and motor declines, which were found to be worse in mild cognitive impairment individuals and in AD patients. [94]

Still, an amount of studies have reported that the functional changes in the olfactory, auditory, visual and motor systems, which are the main components of the SMN, might precede the onset of cognitive impairments and dementia, and aggravate as the disease progresses, being a strong risk factors for AD. [95, 96, 97, 98] So, this impaired functional connectivity, together with the recognition that AD pathology will develop over many years, suggests that declines in specific primary daily functions may be an early non-invasive biomarker for AD. Taken together, our findings might in the same way provide additional evidence that the affected dFC states significantly affecting the somatomotor, dorsal and ventral attention and visual networks should arouse attention when studying SVD. In particular, the functional network in the fronto-parietal state consists of areas typically activated during attention and motor control functions. [99]

Notably, analysing the dFC features which were found to be increased in patients compared with controls, previous studies of dFC in related disorders [49, 50, 51, 52, 53] have reported that patients also had higher occurrences and spent more time in weakly and sparsely connected states, with absence of strong positive and negative connections. Indeed, the frontal-parietal state, that differentiated patients from controls, is a weakly connected state, with low coherence between paired brain regions. In particular, the only study of dFC in SVD [49] also found that SVD patients had more occurrences and spent more time in a weakly connected state when compared to controls. This state presented weak positive and negative connections within regions of the sensorimotor domain (such as postcentral gyrus, paracentral lobule, precentral gyrus, superior parietal lobule and supramarginal gyrus) and the cognitive control domain (such as supplementary motor area, middle frontal gyrus, inferior parietal lobule and superior frontal gyrus). The same regions were present in this fronto-parietal state, which could indicate that dynamic changes in FC in these areas might be particularly important for this disease. Also, the fact that patients had more occurrences in this weakly connected state may imply that the brain prefers switching to a state where information transfer is less efficient, as suggested in [100].

Yet, the occipital states, significantly associated with the visual network, which are composed by relatively strong coherent and desynchronized brain regions, presented higher mean duration in patients than in controls. The previously mentioned study [49] also investigated dFC in AD patients and found that these patients had a mean duration significantly higher than controls, in an strong positive and negative correlated state, exhibiting strong connections with and within the sensorimotor and visual domain. This increase might be explained by an indirect compensatory or adaptive mechanism in SVD patients to regulate brain activity as suggested in [42, 101], or consequences of the underlying disease or even a combination of both, however these hypothesis needs to be tested in future research.

It is also important to note that patients had generally reduced number of transitions between states when compared to controls, besides an increased probability of switching from state 1 to the frontal-parietal state, which may explain why this state occurred more frequently in patients than in controls. On a group level, the switching probability was overall higher when switching from any given state to the state of global BOLD coherence, whereas switching from state 2 to this state was more frequent in controls than in patients. Interestingly, it has been suggested that the more frequently occurring global brain states enable for a greater range of either integration or segregation between

neural networks and brain areas. This means that more flexible switching to different brain states, i.e. this neural flexibility, might facilitate cognitive flexibility. [102] Also, it was found that the patient's switching probability from the strong coherent state 1 to the weakly connected fronto-parietal state was significantly related with worse cognitive performance in the processing speed test. Indeed, deficits in processing speed are among the earliest and most prominent cognitive manifestations of SVD [103], with several studies demonstrating associations with decline in processing speed and quantitative MRI measures. [104, 105, 106] More importantly, cognitive impairments in processing speed of these patients were also significantly correlated with other BOLD rs-fMRI measures explored by different members of the team, such as the amplitude of low-frequency fluctuations [107] and functional connectivity [108].

Importantly, switching probabilities from the weakly connected state to the state of global coherence was significantly correlated with better performance in processing speed. These findings are in line with previous results from [34] which found that better cognitive performers had higher occurrences and switches to this state of global coherence. Hence, the increased switching probability from state 1 to this weakly connected state as well as the reverse, from the weakly connected state to the state of global coherence deserves further prospective studies to determine whether it could be a biomarker of cognitive decline in SVD.

Regarding the WMLs analysis, it has been suggested [73, 74] that these lesions could represent microvascular ischemic and/or demyelinating changes which are widely recognized as commonly seen feature in SVD. Also, WM lesions have been associated with cognitive decline, gait impairment, depression and an increased risk of stroke and dementia. As WM is organized in the brain by tracts, connecting functional brain regions with each other, it is expected that damage to these white matter tracts would lead to deficits in function. Indeed, loss of connections in brain structure (i.e., white matter connections) directly affects brain's functional connectivity (i.e., gray matter activity). Understanding this relationship could help to predict in which brain regions white matter pathology would cause more functional deficits, allowing prevention and early therapy. [75]

Indeed, [75] found that local white matter lesions can decrease tract-specific functional connectivity, both in direct and indirect connections. Also, [76] reported that some dFC coefficients of the connection within the dorsal attention network and the ventral attention network were negatively correlated with the total WMLL, on relapsing-remitting multiple sclerosis (RRMS) patients. Moreover, significant correlations were found [73] between WMLL and DMN connectivity strength, as well as between WMLL and spontaneous neural activity values, in mild cognitive impairment (MCI) patients, suggesting that WM lesions may play an important role in cognitive decline.

Although no significant correlations were found between the lesion probabilities of major WM tracts and the abnormal dFC found on this work, it is interesting to note that several studies have been reporting relationships between lesions on the anterior thalamic radiation and forceps minor, which are major pathways connecting frontal regions, and impaired cognitive performance on processing speed, in SVD and mixed dementia patients. [78] It is therefore tempting to suggest that these WM tracts which were frequently lesioned across patients could have some influence in the impaired processing speed found on this study and which were correlated with higher switching probabilities to the abnormal weakly coherent state, composed by regions mainly from the frontal and parietal lobe. Therefore, pointing to the importance of the role of frontal-subcortical projections in SVD-related impairment.

4.2 Limitations and future work

One of the main limitations in this study concerns the small sample size and the fact that different groups were not equally represented (SVD=11, CADASIL=6 and HC=11). In order to reproduce the results and increase statistical power it is essential to include more subjects in future studies. Also, the selected brain parcellation atlas (AAL) strongly constrains the identification of dFC states. Although commonly being used in studies that employed the methodology used in this work [34, 41, 42], might lead to relatively low BOLD signal homogeneity within its regions compared to other fMRI-based parcellations, due to the anatomical basis of this atlas and the fact that all areas have different and relatively large sizes. [109, 110] Therefore, future work should explore other methods to parcellate the brain based on functional homogeneity and with similar size. This way, subdivisions within the frontal-parietal state could allow to identify specific subsystems driving the activation of this state.

Further, some methodologies choices should be further reviewed, such as the use of Hilbert transform to compute the instantaneous phase, to determine whether other methodologies could be best to estimate the phase of the BOLD signal and the method used to cluster recurrent dFC states, despite the k-means algorithm being mostly used in dFC studies [7, 34, 41, 45, 51, 66], there is not a consensus if it is the most suitable methodology for detecting recurrent dFC patterns.

An important parameter that needs to be defined *a priori* and has a lot of influence in the results is the number of dFC states. Here, the selection of the solutions of k=10, k=5 and k=6 for further analysis was based on the ones that yield group differences in dynamic properties, and thus could be considered a limitation of this work. As the number of states is still an unknown parameter the common approach is to compute the dFC states for different numbers of initial states and then use a criterion (elbow criterion, silhouette method or others) which relies only on the cluster data, to choose the optimal number of states. [17, 34, 41, 50] However, relaying on these standard algorithms for evaluating cluster performance may not necessarily be the appropriate approach for detecting altered patterns in neuroimaging data. [42] Thus, these issues deserver further attention in other studies to confirm if our findings can be reproduced and extendable to patients with SVD.

Moreover, one limitation in studies of dynamic FC is the unclear relationship between the dFC and the real dynamics in the mental activities, as research using high-temporal-resolution imaging techniques, such as EEG or magnetoencephalography (MEG), where reoccurring microstates are identified which are related to spontaneous thoughts and mental processes in a much shorter temporal scale in the order of 200 ms. [111,112, 113] Therefore, measures such as dFC state duration are still a matter of debate. Additional experiments should employ simultaneous EEG-fMRI recordings, in order to tap into the high temporal resolution of EEG to reveal the functional meaning of dFC states.

Additionally, the methods used to correlate dFC features with lesions on the WM tracts explored here deserves further attention in future studies, to determine if other methodologies could be more suitable, and thus to determine whether strategic WM tracts in which WMHs have most impact on cognition would improve our understanding of the functional impact of SVD.

To conclude, as we were able to examine dynamic FC and provided a new insight into abnormalities in dynamic brain network connectivity in SVD patients. In future studies it would be interesting to explore how changes in this dFC state could be related with other neuroimaging and clinical features.

Bibliography

[1] Issac, T. G., Chandra, S. R., Christopher, R., Rajeswaran, J., & Philip, M. (2015). Cerebral Small Vessel Disease Clinical, Neuropsychological, and Radiological Phenotypes, Histopathological Correlates, and Described Genotypes: A Review. *Journal of Geriatrics*, *2015*. doi:10.1177/0963689718795148.

[2] Cuadrado-Godia, E., Dwivedi, P., Sharma, S., Santiago, A. O., Gonzalez, J. R., Balcells, M., ... & Saba, L. (2018). Cerebral small vessel disease: a review focusing on pathophysiology, biomarkers, and machine learning strategies. *Journal of stroke*, *20*(3), 302. doi:10.5853/jos.2017.02922.

[3] ter Telgte, A., van Leijsen, E. M., Wiegertjes, K., Klijn, C. J., Tuladhar, A. M., & de Leeuw, F. E. (2018). Cerebral small vessel disease: from a focal to a global perspective. *Nature Reviews Neurology*, *14*(7), 387.doi: 10.1038/s41582-018-0014-y.

[4] Pantoni, L. (2010). Cerebral small vessel disease: from pathogenesis and clinical characteristics to therapeutic challenges. *The Lancet Neurology*, *9*(7), 689-701. doi: 10.1016/S1474-4422(10)70104-6

[5] Shi, Y., & Wardlaw, J. M. (2016). Update on cerebral small vessel disease: a dynamic whole-brain disease. *Stroke and vascular neurology*, *1*(3), 83-92. doi:10.1136/svn-2016-000035.

[6] Craggs, L. J., Yamamoto, Y., Deramecourt, V., & Kalaria, R. N. (2014). Microvascular pathology and morphometrics of sporadic and hereditary small vessel diseases of the brain. *Brain pathology*, *24*(5), 495-509. doi:10.1111/bpa.12177.

[7] Heiss, W. D. (2018). Neuroimaging in Cerebral Small Vessel Disease. *Neurol Neuromedicine*, 3(2), 1-7. doi: 10.29245/2572.942X/2018/1.1171.

[8] Wardlaw, J. M., Smith, C., & Dichgans, M. (2013). Mechanisms of sporadic cerebral small vessel disease: insights from neuroimaging. *The Lancet Neurology*, *12*(5), 483-497. doi:10.1016/S1474-4422(13)70060-7.

[9] Banerjee, G., Wilson, D., Jäger, H. R., & Werring, D. J. (2016). Novel imaging techniques in cerebral small vessel diseases and vascular cognitive impairment. *Biochimica et Biophysica Acta (BBA)-Molecular Basis of Disease*, *1862*(5), 926-938. doi: 10.1016/j.bbadis.2015.12.010.

[10] Wardlaw, J. M., Smith, E. E., Biessels, G. J., Cordonnier, C., Fazekas, F., Frayne, R., ... & Black, S. E. (2013). Neuroimaging standards for research into small vessel disease and its contribution to ageing and neurodegeneration. *The Lancet Neurology*, *12*(8), 822-838. doi: 10.1016/S1474-4422(13)70124-8.

[11] Smith, E. E., & Beaudin, A. E. (2018). New insights into cerebral small vessel disease and vascular cognitive impairment from MRI. *Current opinion in neurology*, *31*(1), 36-43. doi: 10.1097/WCO.0000000000000513

[12] Soares, J. M., Magalhães, R., Moreira, P. S., Sousa, A., Ganz, E., Sampaio, A., ... & Sousa, N. (2016). A hitchhiker's guide to functional magnetic resonance imaging. *Frontiers in neuroscience*, *10*, 515. doi: 10.3389/fnins.2016.00515.

[13] Buxton, R. B. (2009). Introduction to functional magnetic resonance imaging: principles and techniques. *Cambridge university press.*

[14] Forstmann, B. U., & Wagenmakers, E. J. (2015). Model-based cognitive neuroscience: A conceptual introduction. *An introduction to model-based cognitive neuroscience*, 139-156. Springer, New York, NY.

[15] Murphy, K., Birn, R. M., & Bandettini, P. A. (2013). Resting-state fMRI confounds and cleanup. *Neuroimage*, *80*, 349-359. doi: 10.1016/j.neuroimage.2013.04.001.

[16] Lawrence, A. J., Tozer, D. J., Stamatakis, E. A., & Markus, H. S. (2018). A comparison of functional and tractography based networks in cerebral small vessel disease. *NeuroImage: Clinical*, *18*, 425-432. doi:10.1016/j.nicl.2018.02.013

[17] Liu, R., Wu, W., Ye, Q., Gu, Y., Zou, J., Chen, X., ... & Wang, C. (2019). Distinctive and Pervasive Alterations of Functional Brain Networks in Cerebral Small Vessel Disease with and without Cognitive Impairment. *Dementia and geriatric cognitive disorders*, *47*(1-2), 55-67. doi: 10.1159/000496455.

[18] Smitha, K. A., Akhil Raja, K., Arun, K. M., Rajesh, P. G., Thomas, B., Kapilamoorthy, T. R., & Kesavadas, C. (2017). Resting state fMRI: A review on methods in resting state connectivity analysis and resting state networks. *The neuroradiology journal*, *30*(4), 305-317. doi: 10.1177/1971400917697342.

[19] Fox, M. D., & Greicius, M. (2010). Clinical applications of resting state functional connectivity. *Frontiers in systems neuroscience*, *4*, 19. doi: 10.3389/fnsys.2010.00019

[20] Damoiseaux, J. S., & Greicius, M. D. (2009). Greater than the sum of its parts: a review of studies combining structural connectivity and resting-state functional connectivity. *Brain Structure and Function*, *213*(6), 525-533. doi: 10.1007/s00429-009-0208-6.

[21] Biswal, B., Zerrin Yetkin, F., Haughton, V. M., & Hyde, J. S. (1995). Functional connectivity in the motor cortex of resting human brain using echo-planar MRI. *Magnetic resonance in medicine*, *34*(4), 537-541. doi: 10.1002/mrm.1910340409

[22] Van Den Heuvel, M. P., & Pol, H. E. H. (2010). Exploring the brain network: a review on resting-state fMRI functional connectivity. *European neuropsychopharmacology*, *20*(8), 519-534. doi: 10.1016/j.euroneuro.2010.03.008

[23] Barkhof, F., Haller, S., & Rombouts, S. A. (2014). Resting-state functional MR imaging: a new window to the brain. *Radiology*, *272*(1), 29-49. doi: 10.1148/radiol.14132388.

[24] Smith, S. M., Fox, P. T., Miller, K. L., Glahn, D. C., Fox, P. M., Mackay, C. E., ... & Beckmann, C. F. (2009). Correspondence of the brain's functional architecture during activation and rest. *Proceedings of the national academy of sciences*, *106*(31), 13040-13045. doi: 10.1073/pnas.0905267106

[25] Vossel, S., Geng, J. J., & Fink, G. R. (2014). Dorsal and ventral attention systems: distinct neural circuits but collaborative roles. *The Neuroscientist*, *20*(2), 150-159. doi: 10.1177/1073858413494269.

[26] Heine, L., Soddu, A., Gómez, F., Vanhaudenhuyse, A., Tshibanda, L., Thonnard, M., ... & Demertzi, A. (2012). Resting state networks and consciousness. *Frontiers in psychology*, *3*, 295. doi: 10.3389/fpsyg.2012.00295.

[27] Lee, M. H., Smyser, C. D., & Shimony, J. S. (2013). Resting-state fMRI: a review of methods and clinical applications. *American Journal of neuroradiology*, 34(10), 1866-1872. doi: 10.3174/ajnr.A3263

[28] Zang, Y., Jiang, T., Lu, Y., He, Y., & Tian, L. (2004). Regional homogeneity approach to fMRI data analysis. *Neuroimage*, *22*(1), 394-400. doi: 10.1016/j.neuroimage.2003.12.030.

[29] Li, K., Guo, L., Nie, J., Li, G., & Liu, T. (2009). Review of methods for functional brain connectivity detection using fMRI. *Computerized medical imaging and graphics*, *33*(2), 131-139. doi: 10.1016/j.compmedimag.2008.10.011.

[30] Chang, C., & Glover, G. H. (2010). Time–frequency dynamics of resting-state brain connectivity measured with fMRI. *Neuroimage*, *50*(1), 81-98. doi: 10.1016/j.neuroimage.2009.

[31] Hutchison, R. M., Womelsdorf, T., Allen, E. A., Bandettini, P. A., Calhoun, V. D., Corbetta, M., ... & Handwerker, D. A. (2013). Dynamic functional connectivity: promise, issues, and interpretations. *Neuroimage*, *80*, 360-378. doi: 10.1016/j.neuroimage.2013.05.079.

[32] Savva, A. D., Mitsis, G. D., & Matsopoulos, G. K. (2019). Assessment of dynamic functional connectivity in resting-state fMRI using the sliding window technique. *Brain and behavior*, *9*(4), e01255. doi: 10.1002/brb3.1255.

[33] Hindriks, R., Adhikari, M. H., Murayama, Y., Ganzetti, M., Mantini, D., Logothetis, N. K., et al. (2016). Can sliding-window correlations reveal dynamic functional connectivity in resting-state fMRI? *Neuroimage*, 127, 242–256. doi: 10.1016/j.neuroimage.2015.11.055.

[34] Cabral, J., Vidaurre, D., Marques, P., Magalhães, R., Moreira, P. S., Soares, J. M., ... & Kringelbach, M. L. (2017). Cognitive performance in healthy older adults relates to spontaneous switching between states of functional connectivity during rest. *Scientific reports*, *7*(1), 5135. doi: 10.1038/s41598-017-05425-7.

[35] Deng, L., Sun, J., Cheng, L., & Tong, S. (2016). Characterizing dynamic local functional connectivity in the human brain. *Scientific reports*, *6*, 26976. doi: 10.1038/srep26976.

[36] Filippi, M., Spinelli, E. G., Cividini, C., & Agosta, F. (2019). Resting state dynamic functional connectivity in neurodegenerative conditions: a review of magnetic resonance imaging findings. *Frontiers in neuroscience*, *13*. doi: 10.3389/fnins.2019.00657.

[37] Tagliazucchi, E., & Laufs, H. (2015). Multimodal imaging of dynamic functional connectivity. *Frontiers in neurology*, *6*, 10. doi: 10.3389/fneur.2015.00010.

[38] Thompson, G. J. (2018). Neural and metabolic basis of dynamic resting state fMRI. *Neuroimage*, *180*, 448-462. doi: 10.1016/j.neuroimage.2017.09.010.

[39] Preti, M. G., Bolton, T. A., & Van De Ville, D. (2017). The dynamic functional connectome: State-of-the-art and perspectives. *Neuroimage*, *160*, 41-54. doi: 10.1016/j.neuroimage.2016.12.061.

[40] Kiviniemi, V., Vire, T., Remes, J., Elseoud, A. A., Starck, T., Tervonen, O., & Nikkinen, J. (2011). A sliding time-window ICA reveals spatial variability of the default mode network in time. *Brain connectivity*, *1*(4), 339-347. doi: 10.1089/brain.2011.0036.

[41] Lord, L. D., Expert, P., Atasoy, S., Roseman, L., Rapuano, K., Lambiotte, R., ... & Cabral, J. (2019). Dynamical exploration of the repertoire of brain networks at rest is modulated by psilocybin. *NeuroImage*, *199*, 127-142. doi: 10.1016/j.neuroimage.

[42] Figueroa, C. A., Cabral, J., Mocking, R. J., Rapuano, K. M., van Hartevelt, T. J., Deco, G., ... & Ruhé, H. G. (2019). Altered ability to access a clinically relevant control network in patients remitted from major depressive disorder. *Human brain mapping*, *40*(9), 2771-2786. doi: 10.1002/hbm.24559.

[43] Allen, E. A., Damaraju, E., Plis, S. M., Erhardt, E. B., Eichele, T., & Calhoun, V. D. (2014). Tracking whole-brain connectivity dynamics in the resting state. *Cerebral cortex*, *24*(3), 663-676. doi: 10.1093/cercor/bhs352.

[44] Leonardi, N., Richiardi, J., Gschwind, M., Simioni, S., Annoni, J. M., Schluep, M., ... & Van De Ville, D. (2013). Principal components of functional connectivity: a new approach to study dynamic brain connectivity during rest. *NeuroImage*, *83*, 937-950. doi: 10.1016/j.neuroimage.2013.07.019.

[45] Abreu, R., Leal, A., & Figueiredo, P. (2019). Identification of epileptic brain states by dynamic functional connectivity analysis of simultaneous EEG-fMRI: a dictionary learning approach. *Scientific reports*, *9*(1), 638. doi: 10.1038/s41598-018-36976-y.

[46] Sun, Y. W., Zhou, Y., Xu, Q., Qian, L. J., Tao, J., & Xu, J. R. (2011). Abnormal functional connectivity in patients with vascular cognitive impairment, no dementia: a resting-state functional magnetic resonance imaging study. *Behavioural brain research*, *223*(2), 388-394. doi: 10.1016/j.bbr.2011.05.006.

[47] Kim, H. J., Cha, J., Lee, J. M., Shin, J. S., Jung, N. Y., Kim, Y. J., ... & Lee, J. H. (2016). Distinctive resting state network disruptions among Alzheimer's disease, subcortical vascular dementia, and mixed dementia patients. *Journal of Alzheimer's Disease*, *50*(3), 709-718. doi: 10.3233/JAD-150637.

[48] Schaefer, A., Quinque, E. M., Kipping, J. A., Arélin, K., Roggenhofer, E., Frisch, S., ... & Schroeter, M. L. (2014). Early small vessel disease affects frontoparietal and cerebellar hubs in close correlation with clinical symptoms—a resting-state fMRI study. *Journal of Cerebral Blood Flow & Metabolism*, *34*(7), 1091-1095. doi: 10.1038/jcbfm.2014.70.

[49] Fu, Z., Caprihan, A., Chen, J., Du, Y., Adair, J. C., Sui, J., ... & Calhoun, V. D. (2019). Altered static and dynamic functional network connectivity in Alzheimer's disease and subcortical ischemic vascular disease: shared and specific brain connectivity abnormalities. *Human Brain Mapping*. doi: 10.1002/hbm.24591.

[50] Schumacher, J., Peraza, L. R., Firbank, M., Thomas, A. J., Kaiser, M., Gallagher, P., ... & Taylor, J. P. (2019). Dynamic functional connectivity changes in dementia with Lewy bodies and Alzheimer's disease. *NeuroImage: Clinical*, *22*, 101812. doi: 10.1016/j.nicl.2019.101812.

[51] Díez-Cirarda, M., Strafella, A. P., Kim, J., Peña, J., Ojeda, N., Cabrera-Zubizarreta, A., & Ibarretxe-Bilbao, N. (2018). Dynamic functional connectivity in Parkinson's disease patients with mild cognitive impairment and normal cognition. *NeuroImage: Clinical*, *17*, 847-855. doi: 10.1016/j.nicl.2017.12.013.

[52] Fiorenzato, E., Strafella, A. P., Kim, J., Schifano, R., Weis, L., Antonini, A., & Biundo, R. (2019). Dynamic functional connectivity changes associated with dementia in Parkinson's disease. *Brain*, *142*(9), 2860-2872. doi: 10.1093/brain/awz192.

[53] Rabany, L., Brocke, S., Calhoun, V. D., Pittman, B., Corbera, S., Wexler, B. E., ... & Assaf, M. (2019). Dynamic functional connectivity in schizophrenia and autism spectrum disorder: Convergence, divergence and classification. *NeuroImage: Clinical*, *24*, 101966. doi: 10.1016/j.nicl.2019.101966.

[54] Beckmann, C. F., DeLuca, M., Devlin, J. T., & Smith, S. M. (2005). Investigations into resting-state connectivity using independent component analysis. *Philosophical Transactions of the Royal Society B: Biological Sciences*, *360*(1457), 1001-1013. doi: 10.1098/rstb.2005.1634

[55] Smith, S. M. (2002). Fast robust automated brain extraction. *Human brain mapping*, *17*(3), 143-155. doi: 10.1002/hbm.10062

[56] Jenkinson, M., Bannister, P., Brady, M., & Smith, S. (2002). Improved optimization for the robust and accurate linear registration and motion correction of brain images. *Neuroimage*, *17*(2), 825-841. doi: 10.1016/s1053-8119(02)91132-8

[57] Woolrich, M. W., Ripley, B. D., Brady, M., & Smith, S. M. (2001). Temporal autocorrelation in univariate linear modeling of FMRI data. *Neuroimage*, *14*(6), 1370-1386. doi: 10.1006/nimg.2001.0931.

[58] Griffanti, L., Salimi-Khorshidi, G., Beckmann, C. F., Auerbach, E. J., Douaud, G., Sexton, C. E., ... & Moeller, S. (2014). ICA-based artefact removal and accelerated fMRI acquisition for improved resting state network imaging. *Neuroimage*, *95*, 232-247. doi: 10.1016/j.neuroimage.2014.03.034

[59] Beckmann, C. F., & Smith, S. M. (2004). Probabilistic independent component analysis for functional magnetic resonance imaging. *IEEE transactions on medical imaging*, 23(2), 137-152. doi: 10.1109/TMI.2003.822821

[60] Salimi-Khorshidi, G., Douaud, G., Beckmann, C. F., Glasser, M. F., Griffanti, L., & Smith, S. M. (2014). Automatic denoising of functional MRI data: combining independent component analysis and hierarchical fusion of classifiers. *Neuroimage*, *90*, 449-468. doi: 10.1016/j.neuroimage.2013.11.046

[61] Griffanti, L., Douaud, G., Bijsterbosch, J., Evangelisti, S., Alfaro-Almagro, F., Glasser, M. F., ... & Beckmann, C. F. (2017). Hand classification of fMRI ICA noise components. *Neuroimage*, *154*, 188-205. doi: 10.1016/j.neuroimage.2016.12.036

[62] Tzourio-Mazoyer, N., Landeau, B., Papathanassiou, D., Crivello, F., Etard, O., Delcroix, N., ... & Joliot, M. (2002). Automated anatomical labeling of activations in SPM using a macroscopic anatomical parcellation of the MNI MRI single-subject brain. *Neuroimage*, *15*(1), 273-289. doi: 10.1006/nimg.2001.0978

[63] A. Graça,. (2016). Segmentation of white matter lesions from multimodal MRI in small vessel disease. Tese de Mestrado. Instituto Superior Técnico.

[64] Hua, K., Zhang, J., Wakana, S., Jiang, H., Li, X., Reich, D. S., ... & Mori, S. (2008). Tract probability maps in stereotaxic spaces: analyses of white matter anatomy and tract-specific quantification. *Neuroimage*, *39*(1), 336-347. doi: 10.1016/j.neuroimage.2007.07.053

[65] Newman, M. E. (2006). Finding community structure in networks using the eigenvectors of matrices. *Physical review E*, *74*(3), 036104. doi: 10.1103/PhysRevE.74.036104.

[66] Cavaco, S., Gonçalves, A., Pinto, C., Almeida, E., Gomes, F., Moreira, I., ... & Teixeira-Pinto, A. (2013). Trail Making Test: Regression-based norms for the Portuguese population. *Archives of Clinical Neuropsychology*, *28*(2), 189-198. doi: 10.1093/arclin/acs115

[67] Wechsler, D. (2008). WAIS-III: Manual da Escala de Inteligência de Wechsler para Adultos - 3ª edição, Lisboa: CEGOC-TEA.

[68] Wechsler, D. (2008). WMS-III: Escala de Memória de Wechsler–3. ª Edição.

[69] Cavaco, S., Goncalves, A., Pinto, C., Almeida, E., Gomes, F., Moreira, I., Fernandes, J., and Teixeira-Pinto, A. Trail Making Test: Regression-based Norms for the Portuguese Population. *Archives of Clinical Neuropsychology*, 28(2):189–198, 2013.

[70] Yeo, B. T., Krienen, F. M., Sepulcre, J., Sabuncu, M. R., Lashkari, D., Hollinshead, M., ... & Fischl, B. (2011). The organization of the human cerebral cortex estimated by intrinsic functional connectivity. *Journal of neurophysiology*. doi: 10.1152/jn.00338.2011

[71] Damoiseaux, J. S., Rombouts, S. A. R. B., Barkhof, F., Scheltens, P., Stam, C. J., Smith, S. M., & Beckmann, C. F. (2006). Consistent resting-state networks across healthy subjects. *Proceedings of the national academy of sciences*, *103*(37), 13848-13853. doi: 10.1073/pnas.0601417103.

[72] Jones, D. T., Vemuri, P., Murphy, M. C., Gunter, J. L., Senjem, M. L., Machulda, M. M., ... & Boeve, B. F. (2012). Non-stationarity in the "resting brain's" modular architecture. *PloS one*, *7*(6), e39731. doi: 10.1371/journal.pone.0039731.

[73] Zhou, Y., Yu, F., Duong, T. Q., & Alzheimer's Disease Neuroimaging Initiative. (2015). White matter lesion load is associated with resting state functional MRI activity and amyloid PET but not FDG in mild cognitive impairment and early Alzheimer's disease patients. *Journal of Magnetic Resonance Imaging*, *41*(1), 102-109. doi: 10.1002/jmri.24550

[74] Liang, Y., Sun, X., Xu, S., Liu, Y., Huang, R., Jia, J., & Zhang, Z. (2016). Preclinical Cerebral Network Connectivity Evidence of Deficits in Mild White Matter Lesions. *Frontiers in aging neuroscience*, 8, 27. doi: 10.3389/fnagi.2016.00027

[75] Langen, C. D., Zonneveld, H. I., White, T., Huizinga, W., Cremers, L. G., de Groot, M., ... & Vernooij, M. W. (2017). White matter lesions relate to tract-specific reductions in functional connectivity. *Neurobiology of aging*, *51*, 97-103. doi: 10.1016/j.neurobiolaging.2016.12.004

[76] Huang, M., Zhou, F., Wu, L., Wang, B., Guo, L., Zhao, Y., ... & Gong, H. (2019). White matter lesion loads associated with dynamic functional connectivity within attention network in patients with relapsing-remitting multiple sclerosis. *Journal of Clinical Neuroscience*, *65*, 59-65. doi: 10.1016/j.jocn.2019.03.034

[77] Musiek, F. E. (1986). Neuroanatomy, neurophysiology, and central auditory assessment. Part III: Corpus callosum and efferent pathways. *Ear and hearing*, 7(6), 349-358. doi: 10.1097/00003446-198612000-00001.

[78] Biesbroek, J. M., Weaver, N. A., & Biessels, G. J. (2017). Lesion location and cognitive impact of cerebral small vessel disease. *Clinical Science*, 131(8), 715-728. doi: 10.1042/CS20160452.

[79] Makris, N., Kennedy, D. N., McInerney, S., Sorensen, A. G., Wang, R., Caviness Jr, V. S., & Pandya, D. N. (2005). Segmentation of subcomponents within the superior longitudinal fascicle in humans: a quantitative, in vivo, DT-MRI study. *Cerebral cortex*, 15(6), 854-869. doi: 10.1093/cercor/bhh186.

[80] Martino, J., Brogna, C., Robles, S. G., Vergani, F., & Duffau, H. (2010). Anatomic dissection of the inferior fronto-occipital fasciculus revisited in the lights of brain stimulation data. *Cerebral cortex*, 46(5), 691-699. doi: 10.1016/j.cortex.2009.07.015.

[81] Jang, S. H. (2014). The corticospinal tract from the viewpoint of brain rehabilitation. *Journal of rehabilitation medicine*, 46(3), 193-199. doi: 10.2340/16501977-1782.

[82] Herbet, G., Zemmoura, I., & Duffau, H. (2018). Functional anatomy of the inferior longitudinal fasciculus: from historical reports to current hypotheses. *Frontiers in neuroanatomy*, *12*, 77. doi: 10.3389/fnana.2018.00077.

[83] Cai, Z., Wang, C., He, W., Tu, H., Tang, Z., Xiao, M., & Yan, L. J. (2015). Cerebral small vessel disease and Alzheimer's disease. *Clinical interventions in aging*, 10, 1695. doi: 10.3389/fneur.2020.00927.

[84] Sun, Y. W., Zhou, Y., Xu, Q., Qian, L. J., Tao, J., & Xu, J. R. (2011). Abnormal functional connectivity in patients with vascular cognitive impairment, no dementia: a resting-state functional magnetic resonance imaging study. *Behavioural brain research*, 223(2), 388-394. doi: 10.1016/j.bbr.2011.05.006.

[85] Dey, A. K., Stamenova, V., Turner, G., Black, S. E., & Levine, B. (2016). Pathoconnectomics of cognitive impairment in small vessel disease: A systematic review. *Alzheimer's & Dementia*, 12(7), 831-845. doi: 10.1016/j.jalz.2016.01.007.

[86] Fox, M. D., Corbetta, M., Snyder, A. Z., Vincent, J. L., & Raichle, M. E. (2006). Spontaneous neuronal activity distinguishes human dorsal and ventral attention systems. *Proceedings of the National Academy of Sciences*, 103(26), 10046-10051. doi: 10.1073/pnas.0604187103.

[87] Wang, Z., Qiao, K., Chen, G., Sui, D., Dong, H. M., Wang, Y. S., ... & Han, Y. (2019). Functional connectivity changes across the spectrum of subjective cognitive decline, amnestic mild cognitive impairment and Alzheimer's disease. *Frontiers in neuroinformatics*, 13, 26. doi: 10.3389/fninf.2019.00026.

[88] Finke, K., Myers, N., Bublak, P., & Sorg, C. (2013). A biased competition account of attention and memory in Alzheimer's disease. *Philosophical Transactions of the Royal Society B: Biological Sciences*, 368(1628), 20130062. doi:10.1098/rstb.2013.0062.

[89] Perry, R. J., Watson, P., & Hodges, J. R. (2000). The nature and staging of attention dysfunction in early (minimal and mild) Alzheimer's disease: relationship to episodic and semantic memory impairment. *Neuropsychologia*, *38*(3), 252-271. doi: 10.1016/s0028-3932(99)00079-2.

[90] Neufang, S., Akhrif, A., Riedl, V., Förstl, H., Kurz, A., Zimmer, C., ... & Wohlschläger, A. M. (2011). Disconnection of frontal and parietal areas contributes to impaired attention in very early Alzheimer's disease. *Journal of Alzheimer's Disease*, 25(2), 309-321. doi: 10.3233/JAD-2011-102154.

[91] Li, R., Wu, X., Fleisher, A. S., Reiman, E. M., Chen, K., & Yao, L. (2012). Attention-related networks in Alzheimer's disease: A resting functional MRI study. *Human brain mapping*, 33(5), 1076-1088. doi: 10.1002/hbm.21269.

[92] Qian, S., Zhang, Z., Li, B., & Sun, G. (2015). Functional-structural degeneration in dorsal and ventral attention systems for Alzheimer's disease, amnestic mild cognitive impairment. *Brain imaging and behavior*, 9(4), 790-800. doi: 10.1007/s11682-014-9336-6.

[93] Wang, P., Zhou, B., Yao, H., Zhan, Y., Zhang, Z., Cui, Y., ... & Zhang, X. (2015). Aberrant intra- and inter-network connectivity architectures in Alzheimer's disease and mild cognitive impairment. *Scientific reports*, 5, 14824. doi: 10.1038/srep14824.

[94] Albers, M. W., Gilmore, G. C., Kaye, J., Murphy, C., Wingfield, A., Bennett, D. A., ... & Duffy, C. J. (2015). At the interface of sensory and motor dysfunctions and Alzheimer's disease. *Alzheimer's & Dementia*, 11(1), 70-98. doi: 10.1016/j.jalz.2014.04.514.

[95] Devanand, D. P., Liu, X., Tabert, M. H., Pradhaban, G., Cuasay, K., Bell, K., ... & Pelton, G. H. (2008). Combining early markers strongly predicts conversion from mild cognitive impairment to Alzheimer's disease. *Biological psychiatry*, 64(10), 871-879. doi: 10.1016/j.biopsych.2008.06.020.

[96] Lin, F. R., Metter, E. J., O'Brien, R. J., Resnick, S. M., Zonderman, A. B., & Ferrucci, L. (2011). Hearing loss and incident dementia. *Archives of neurology*, 68(2), 214-220. doi:10.1001/archneurol.2010.362.

[97] Li, W., Howard, J. D., & Gottfried, J. A. (2010). Disruption of odour quality coding in piriform cortex mediates olfactory deficits in Alzheimer's disease. *Brain*, 133(9), 2714-2726. doi: 10.1093/brain/awq209.

[98] Verghese, J., Wang, C., Lipton, R. B., Holtzer, R., & Xue, X. (2007). Quantitative gait dysfunction and risk of cognitive decline and dementia. *Journal of Neurology, Neurosurgery & Psychiatry*, 78(9), 929-935. doi: 10.1136/jnnp.2006.106914.

[99] Carter, A. R., Astafiev, S. V., Lang, C. E., Connor, L. T., Rengachary, J., Strube, M. J., ... & Corbetta, M. (2010). Resting interhemispheric functional magnetic resonance imaging connectivity predicts performance after stroke. *Annals of neurology*, 67(3), 365-375. doi: 10.1002/ana.21905.

[100] Gu, Y., Lin, Y., Huang, L., Ma, J., Zhang, J., Xiao, Y., ... & Alzheimer's Disease Neuroimaging Initiative. (2020). Abnormal dynamic functional connectivity in Alzheimer's disease. *CNS Neuroscience & Therapeutics*. doi: 10.1111/cns.13387.

[101] Bondi, M. W., Houston, W. S., Eyler, L. T., & Brown, G. G. (2005). fMRI evidence of compensatory mechanisms in older adults at genetic risk for Alzheimer disease. *Neurology*, 64(3), 501-508. doi: 10.1212/01.WNL.0000150885.00929.7E.

[102] Nomi, J. S., Vij, S. G., Dajani, D. R., Steimke, R., Damaraju, E., Rachakonda, S., ... & Uddin, L. Q. (2017). Chronnectomic patterns and neural flexibility underlie executive function. *NeuroImage*, 147, 861-871. doi: 10.1016/j.neuroimage.2016.10.026.

[103] Duering, M., Gesierich, B., Seiler, S., Pirpamer, L., Gonik, M., Hofer, E., Jouvent, E., Duchesnay, E., Chabriat, H., Ropele, S., Schmidt, R., & Dichgans, M. (2014). Strategic white matter tracts for processing speed deficits in age-related small vessel disease. *Neurology*, *82*(22), 1946–1950. doi: 10.1212/WNL.0000000000000475

[104] Prins, N. D., van Dijk, E. J., den Heijer, T., Vermeer, S. E., Jolles, J., Koudstaal, P. J., ... & Breteler, M. M. (2005). Cerebral small-vessel disease and decline in information processing speed, executive function and memory. *Brain*, 128(9), 2034-2041. doi: 10.1093/brain/awh553.

[105] Righart, R., Duering, M., Gonik, M., Jouvent, E., Reyes, S., Hervé, D., ... & Dichgans, M. (2013). Impact of regional cortical and subcortical changes on processing speed in cerebral small vessel disease. *NeuroImage: Clinical*, 2, 854-861. doi: 10.1016/j.nicl.2013.06.006.

[106] Chen, H., Huang, L., Yang, D., Ye, Q., Guo, M., Qin, R., Luo, C., Li, M., Ye, L., Zhang, B., & Xu, Y. (2019). Nodal Global Efficiency in Front-Parietal Lobe Mediated Periventricular White Matter

Hyperintensity (PWMH)-Related Cognitive Impairment. *Frontiers in aging neuroscience*, 11, 347. doi: 10.3389/fnagi.2019.00347.

[107] J. Moreira (2018). Investigation of physiologic fluctuations in resting-state fMRI as biomarkers of cerebral small vessel disease. Tese de Mestrado. Instituto Superior Técnico.

[108] M. Carmo (2017). Investigation of brain functional connectivity by resting- state fMRI in cerebral small vessel diseases. Tese de Mestrado. Instituto Superior Técnico.

[109] Craddock, R. C., Jbabdi, S., Yan, C.-G., Vogelstein, J., Castellanos, F. X., Di Martino, A., … Milham, M. P. (2013). Imaging human connectomes at the macroscale. *Nature Methods*, 10(6), 524–539. https://doi.org/10.1038/ nmeth.2482.

[110] Glasser, M. F., Coalson, T. S., Robinson, E. C., Hacker, C. D., Harwell, J., Yacoub, E., … Van Essen, D. C. (2016). A multi-modal parcellation of human cerebral cortex. *Nature*, 536,171–178. doi:10.1002/mrm.24623.

[111] Lehmann, D., Strik, W., Henggeler, B., König, T., & Koukkou, M. (1998). Brain electric microstates and momentary conscious mind states as building blocks of spontaneous thinking: I. Visual imagery and abstract thoughts. *International Journal of Psychophysiology*, 29,1–11. doi: 10.1016/s0167-8760(97)00098-6.

[112] Baker, A. P.,Brookes,M.J., Rezek, I. A.,Smith,S.M., Behrens, T.,Probert Smith, P. J., &Woolrich, M. (2014). Fast transient networks in spontaneous human brain activity. *eLife*, 3, e01867. doi: 10.7554/eLife.01867.

[113] Vidaurre, D., Quinn, A. J., Baker, A. P., Dupret, D., Tejero-Cantero, A., & Woolrich, M. W. (2016). Spectrally resolved fast transient brain states in electrophysiological data. *NeuroImage*, 126,81–95. doi: 10.1016/j.neuroimage.2015.11.047